The
PHILOSOPHICAL MAGAZINE

UNIVERSITY OF HAWAII
LIBRARY

FIRST PUBLISHED IN 1798

2 Eighth Series No. 15 March 1957

A Journal of Theoretical Experimental and Applied Physics

EDITOR
PROFESSOR N. F. MOTT, M.A., D.Sc., F.R.S.

EDITORIAL BOARD
SIR LAWRENCE BRAGG, O.B.E., M.C., M.A., D.Sc., F.R.S.
SIR GEORGE THOMSON, M.A., D.Sc., F.R.S.
PROFESSOR A. M. TYNDALL, C.B.E., D.Sc., F.R.S.

PRICE £1 0s. 0d.
Annual Subscription £10 10s. 0d. payable in advance

ALERE FLAMMAM.
Printed and Published by
TAYLOR & FRANCIS LTD.
RED LION COURT, FLEET STREET, LONDON, E.C.4

The Scientific Work of René Descartes

(1596–1650)

By

J. F. SCOTT, B.A., M.Sc., Ph.D.

With a foreword by H. W. TURNBULL, M.A., F.R.S.

This book puts the chief mathematical and physical discoveries of Descartes in an accessible form, and fills an outstanding gap upon the shelf devoted to the history of philosophy and science.

There is to be found in this volume the considerable contribution that Descartes made to the physical sciences, which involved much accurate work in geometrical optics and its bearing upon the practical problem of fashioning lenses, as also the deeper problems of light and sight and colour. The careful treatment that Dr. Scott has accorded to this work of Descartes is welcome, is well worth reading and will be an asset to all libraries. Publication is recommended and approved by the Publication Fund Committee of the University of London

212 *pages*, 7″ × 10″, *amply illustrated*

Price £1 - 0 - 0 net **First published July 1952**

Printed & Published by

TAYLOR & FRANCIS, LTD.

RED LION COURT, FLEET STREET, LONDON, E.C.4

Interactions of the Heavy Nuclei of the Cosmic Radiation †

By P. H. Fowler, R. R. Hillier and C. J. Waddington
H. H. Wills Physical Laboratory, Bristol

[Received August 10, 1956]

Abstract

We have observed in a systematic manner 317 nuclear interactions produced by the heavy nuclei of the primary cosmic radiation in nuclear emulsions. From a study of these interactions we have found the interaction mean free paths and fragmentation probabilities. The interaction mean free paths are in good agreement with those reported previously. The fragmentation probabilities, particularly those for the production of light nuclei, are considerably smaller than those currently accepted. In addition, from a study of the angular distribution of the nuclei emitted from the interactions we have shown that the energies of emission in the C-system of the incident nucleus are greater than those previously accepted and depend on the charge of the primary nucleus.

§ 1. Introduction

The heavy nuclei in the cosmic radiation, those with charges equal to or greater than that of lithium, are rapidly absorbed in the atmosphere by nuclear interactions. As a result, in order to study these nuclei it is necessary to place the detecting equipment as high in the atmosphere as possible. However, with present day techniques it is impossible to keep such equipment above the atmosphere for any length of time. It is therefore necessary to make measurements with matter above the detectors, and to correct for the effects produced by this residual matter. These effects are threefold :

(i) Nuclei with comparatively low primary energies may be brought to rest by ionization energy losses. The correction introduced in this manner may be calculated.

(ii) Nuclei may be broken up into nucleons and singly charged particles in nuclear interactions above the detectors, and thus not be observed.

(iii) Nuclei may arrive at the detectors with reduced charge due to nuclear interactions in which they were broken into one or more heavy fragments.

In this paper we are concerned with effects (ii) and (iii) ; i.e. with determining the interaction mean free paths and fragmentation probabilities.

---

† Communicated by the Authors.

In the primary radiation there appear to be nuclei with all charges between those of lithium and iron. It is not, as yet, possible to determine these quantities for individual elements. Indeed it has been customary to separate these nuclei into only three charge groups. However, due to the somewhat greater statistical weight of our results, and because we intend to increase this weight later, we have separated our data into four groups. These we have defined as : light nuclei, L, $3 \leqslant Z \leqslant 5$; medium nuclei, M, $6 \leqslant Z \leqslant 9$; heavy nuclei, H, $10 \leqslant Z \leqslant 19$; and very heavy nuclei, VH, $Z \leqslant 20$.

We have determined the mean free paths and fragmentation probabilities of these charge groups in nuclear emulsion. An estimate of the corresponding values in air has then been deduced from these experimental values. In addition, from the angular distribution of the fragments produced in these interactions we have been able to estimate the r.m.s. transverse momentum for emission of α-particles in the C-system of the incident nucleus.

§ 2. EXPERIMENTAL PROCEDURE

We have used a stack of 80, 20×15 cm, 600 μ Ilford G5 stripped photographic nuclear emulsions. This stack was flown on the 14th of October 1954 over Northern Italy, at a mean altitude of 105 000 feet. The cut-off energy at the top of the atmosphere for multiply charged nuclei has been determined previously as $1{\cdot}55 \pm 0{\cdot}06$ BeV per nucleon (Fowler and Waddington 1956). We have therefore assumed that all the nuclei arriving at the emulsions had energies greater than 1 BeV per nucleon.

In order to detect the tracks of the heavy nuclei a line 1 cm below the top edge of the emulsions was scanned for tracks longer than a certain minimum length per emulsion. This length ranged between 2 and 6 mm. The track of every nucleus found in this manner was followed through the stack until the nucleus either interacted or left the stack. If a heavy fragment emerged from an interaction, this fragment was also followed.

The charges of the nuclei were measured in two ways. For those nuclei with charges between those of lithium and oxygen inclusive a measurement was made of the δ-ray density by counting the number of δ-rays with four or more grains. For those nuclei with charges greater than or equal to that of oxygen the δ-ray density was measured by a photoelectric method. It is estimated that these charge determinations each had a probable error of about a charge. Fuller details of these measurements will be given in a later paper.

Each interaction was classified in terms of the charge of the incident nucleus, the number of black and grey prongs emitted, N_h, the number of minimum ($g < 1{\cdot}4 g_0$) tracks emitted, n_s, the number of fast α-particles emitted, n_α, and the number and type of heavy nuclei emitted. In each interaction where helium or heavy nuclei were emitted we have measured the space angles between their directions of motion and that of the primary nucleus.

§ 3. EXPERIMENTAL RESULTS

3.1. *Interaction Mean Free Paths*

The interaction mean free paths for the four different charge groups are shown in table 1. The results are given in g/cm^2, assuming that the density of emulsion was 3·83 g/cm^3. Also shown in this table are the values found by Noon and Kaplon (1955) for two groups of nuclei defined by them as medium, M', $6 \leqslant Z \leqslant 10$; and heavy H', $Z > 10$. The mean charge of the nuclei in the M' group of these authors is the same as that observed by us in our M group.

It can be seen from this table that our results are in good agreement with those of Noon and Kaplon. However, we believe that our values can represent only upper limits to the true values, since some interactions may have been missed. For example, interactions of the type where one evaporation track only is formed, and the incident nucleus emerges apparently unchanged, are difficult to detect, as are those where no evaporation tracks are formed, but the incident nucleus loses a few charges in the form of minimum tracks. The detection of this last type of interaction will be very dependent on the relative change of charge. The values found for fragmentation probabilities involving only a small change in charge are therefore dependent on the efficiency of detection of these interactions. For this reason we have not included anywhere in the analysis of our results interactions of the first type. The exclusion of these events is supported by the fact that they may be examples of the diffraction scattering of the hydrogen in emulsions by the incident nuclei, and thus represent a different physical process to the other interactions.

In order to extrapolate the values found in emulsion to those in air we have used a method originally due to Bradt and Peters (1950), which was also used by Noon and Kaplon. The reader is referred to this last paper for details. Essentially this method requires that some overlap of the nuclear volumes has to occur before an interaction takes place, so that the interaction cross section σ, is given by

$$\sigma = \pi(R_t + R_i - 2\Delta R)^2 \text{ and } R = r_0 A^{1/3} (r_0 = 1{\cdot}45 \times 10^{-13} \text{ cm})$$

where R_t and R_i are the radii of the target and incoming nuclei respectively, A is the atomic weight, and ΔR has the empirical value of $0{\cdot}85 \times 10^{-13}$cm. Using this expression, and the known composition of emulsion, a mean free path can be calculated for the various groups of nuclei. The values found by us and by Noon and Kaplon are shown in table 1. It can be seen that they are in good agreement with the experimental values. Therefore, we have used the above expression to calculate the mean free path in dry air, and the values found are also shown in table 1. In order to make these calculations we have had to determine the mean charge of each group of nuclei. These mean charges were determined from the number of nuclei found capable of producing interactions rather than from the number that actually produced interactions, and are shown in table 1.

Table 1. The interaction mean free paths in emulsion found in the present work and by Noon and Kaplon (1955), together with calculated values in emulsion and air

Present work				Noon and Kaplon			
$\bar{Z}$			g/cm^2	$\bar{Z}$			g/cm^2
		emul. (exp.)	51·6±6·1				
L nuclei	4·2	emul. (cal.)	60·1	*L* nuclei	—	emul. (exp.)	61·7±19·4
		air (cal.)	34·2			air (cal.)	31·5
		emul. (exp.)	51·9±3·8			emul. (exp.)	59·6±6·0
M nuclei	7·0	emul. (cal.)	49·7	*M′* nuclei	7·0	emul. (cal.)	56·5 (?)
		air (cal.)	27·6			air (cal.)	26·5
		emul. (exp.)	37·8±5·0				
H nuclei	12·8	emul. (cal.)	38·3				
		air (cal.)	20·6			emul. (exp.)	36·5±4·8
				H′ nuclei	15	emul. (cal.)	36·5
		emul. (exp.)	45·1±9·5			air (cal.)	18·0
VH nuclei	23·6	emul. (cal.)	28·7				
		air (cal.)	14·8				

3.2. *Angular Distribution of Secondary Nuclei*

In those interactions where the geometrical conditions were suitable, the space angle was measured between the directions of the primary nucleus and those of the emitted helium and heavy nuclei. The angular distributions for various classes of interaction are shown in the figure.

From the data shown in this figure we have estimated the root mean square (r.m.s.) transverse momentum of the emitted α-particles in the C-system of the incident heavy nuclei. In order to make these estimations we have used the results of a previous experiment made in these emulsions, (Fowler and Waddington 1956) which showed that the integral energy spectrum was proportional to $E_t^{-1\cdot5}$, where E_t was the total energy; and that the cut-off energy at the top of the atmosphere was 1·55 Bev per nucleon. In addition, we have assumed that the fragmentation probabilities and characteristics of the interactions in the C-system are independent of the energy of the primary nucleus. In order to allow for the loss of energy by ionization in air and emulsion above the interactions we have calculated the 'typical' depth at which interactions produced by the nuclei of different charge groups occur. We find this typical depth for *L* nuclei to be equivalent to 11·5 cm of emulsion, for *M* nuclei 11 cm of emulsion, and for *H* and *VH* nuclei 10 cm of emulsion. These values have been calculated from the observed positions of the interactions, allowing for the effects of production of secondary nuclei in the overlying atmosphere, and for the slightly differing cut-off energies of those nuclei for which $A/Z \neq 2$.

From the above data we have calculated numerically 'effective' values for the incident momentum p_{eff}, which would result in the same r.m.s. angles as those observed experimentally. The values of this 'effective'

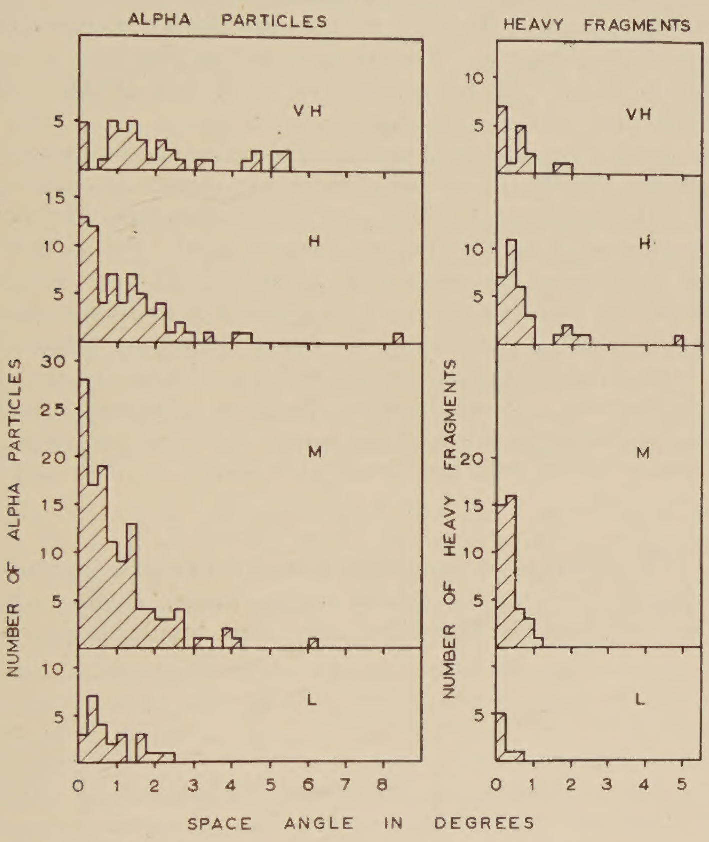

The angular distribution of the α-particles and heavy fragments emitted from interactions of *VH*, *H*, *M* and *L* nuclei.

Table 2. The transverse momenta of the α-particles emitted from interactions. For explanation see text

	α-particles				Heavy fragments	
	L	*M*	*H*	*VH*	*M*	*H**
p_{eff} (MeV/c)	3310	3220	3010	2740		2920
n_α	25	121	67	43	37	50
$\sqrt{\vartheta^2}$ degrees	1·1±0·14	1·47±0·11	1·83±0·18	2·52±0·26	0·48±0·06	1·14±0·13
p_t (MeV/c)	64±8	83±6	96±10	120±13		
E_i (MeV)	13	22	30	47		

momentum are shown in table 2. In this table we have separated the interactions producing α-particles into those produced by L, M, H, and VH nuclei. In each case we give the number of α-particles n_α, the r.m.s. angle $\sqrt{\vartheta^2}$, in degrees, the r.m.s. transverse momentum p_t, in MeV/c per nucleon, and the kinetic energy in the C-system of the incident nucleus E_i, in MeV, assuming isotropy of emission in this system. The errors shown on the values of $\sqrt{\vartheta^2}$ and p_t are standard deviations calculated from the observed distributions. For the sake of completeness we also give the values of n and $\sqrt{\vartheta^2}$ for interactions of M and H^* ($H^*=H+VH$) nuclei which produce secondary heavy nuclei.

Within the limited statistical weight of these results two main features are apparent. Firstly the values of the mean energy of emission in the C-system appear to be considerably greater than those assumed previously for such interactions, see for example, Peters (1952). Secondly the r.m.s. transverse momentum increases with increasing primary charge. As a consequence it appears that primary energies estimated from the opening angles of α-particles produced in such interactions have frequently been underestimated, and that these energy estimates depend on the charge of the primary particle. It may be noted that these experimentally observed transverse momenta are in good agreement with the results of Perkins (1950) for interactions with large excitation energy on silver and bromine nuclei.

Table 3. The effect on the transverse momenta of separating the emitted α-particles into those which are emitted alone, ' single α ', and those produced together with other α-particles, ' multiple α '

	M		H^*	
	Single α	Multiple α	Single α	Multiple α
n_a	45	76	22	67
$\sqrt{\vartheta^2}$ degrees	$1{\cdot}82 \pm 0{\cdot}20$	$1{\cdot}18 \pm 0{\cdot}12$	$1{\cdot}50 \pm 0{\cdot}20$	$2{\cdot}50 \pm 0{\cdot}03$
p_t (MeV/c)	102 ± 11	66 ± 7	77 ± 10	127 ± 15
E_i (MeV)	35	14	20	54

We have also separated the interactions producing α-particles into those with one α-particle, and those with more than one. The results for M and H^* nuclei are shown in table 3. It can be seen that for M nuclei the r.m.s. transverse momenta when only one α-particle is removed is considerably greater than when more than one is produced ; whereas for H^* nuclei the situation is reversed. It appears, therefore, that considerable care must be taken in assuming what transverse momentum is appropriate to a given case.

3.3. *Fragmentation Probabilities*

The characteristics of each of the 317 nuclear interactions observed so far are shown in table 4. These interactions are listed according to the charge of the primary nucleus. It should be noted that the distribution in charge in this table does not represent the charge distribution observed to enter the emulsions, even allowing for the differing mean free paths, since a number of the interactions have been produced by fragments from other interactions. In addition, in order to increase the statistical weight on the higher charge nuclei, the length criterion was sometimes reduced for these, although never below 2 mm per emulsion.

In table 5 are shown the fragmentation probabilities obtained in this experiment, together with those obtained by Noon and Kaplon, and by Gottstein (1954). The errors shown on these values are standard deviations assuming a normal distribution for the fragments, and using the observed distributions for α-particles. Noon and Kaplon found their interactions in stripped emulsion stacks by following the tracks of heavy nuclei having lengths, in 400 μ emulsions, of greater than 750 μ, or, in one stack, of greater than 450 μ. Gottstein detected his disintegrations by making a direct scan for them in glass backed emulsions 400 μ thick. The maximum inclination to the plane of the emulsion accepted in this experiment is not specified.

The results shown in table 5 suggest that the fragmentation probabilities into H or M nuclei found in the various experiments are not significantly different. However, those for fragmentation into L nuclei or α-particles appear to differ widely, with the values found in the present experiment being considerably less than those found previously. In addition, the probability that no nuclei should emerge from an interaction is found to be considerably higher than suggested previously. The divergence between our results and those of Noon and Kaplon is exemplified by the frequency of occurrence of interactions in which two or more heavy fragments are emitted. Noon and Kaplon, in 214 interactions, found 11 where two fragments were emitted, and 3 with three fragments. We, on the other hand, in 249 comparable interactions find only 2 where two fragments were emitted. We have never in this laboratory seen an interaction from which three fragments emerge.

This discrepancy between our results and those of the earlier workers can be explained in two ways. Either we have failed to detect a considerable proportion of the L nuclei and α-particles emitted from these interactions, or the earlier workers have wrongly identified evaporation particles from the target nuclei as energetic fragments. It cannot be explained by assuming that the charge determinations on the primary nuclei were seriously in error in any of the experiments. For example, if we make the extreme assumption that in the present experiment the fragments identified as carbon nuclei are, in fact, boron, and that all the boron primaries producing fragments are carbon, then the fragmentation probability for M, H and VH nuclei into L nuclei is still only

Table 4 (*a*). The characteristics of each of the 317 nuclear interactions observed in emulsion. Each interaction is classified in terms of the type of heavy fragment n_Δ, the number of α-particle n_α, the number of 'shower' tracks n_s, and the number of black and grey tracks N_h.

Lithium			
n_Δ	n_α	n_s	N_h
Li		2	11
	1	2	14
	1	1	0
	1	1	0
		22	39
		18	18
		15	15
		11	20
		10	5
		6	9
		6	5
		4	2
		3	5
		3	0
		2	2

Beryllium			
n_Δ	n_α	n_s	N_h
	2	0	9
	1	4	11
	1	4	9
	1	4	5
	1	3	0
	1	2	0
		22	24
		18	30
		14	22
		13	37
		13	7
		11	11
		10	24
		9	14
		7	4
		7	3
		6	5
		5	16
		5	1

Boron			
n_Δ	n_α	n_s	N_h
B		5	8
B		4	0
B		2	5
B		1	1
Li	1	1	1
Li	1	1	0
	2	8	12
	2	5	0
	2	3	11
	2	1	12
	2	1	0
	1	8	3
	1	7	5
	1	5	2
	1	4	14
	1	3	4
		26	11
		23	14
		22	30
		22	23
		19	34
		19	23
		19	20
		18	5
		14	19
		14	6
		12	11
		10	29
		10	20
		10	19
		7	5
		7	5
		?	11
		?	6

Carbon							
n_Δ	n_α	n_s	N_h	n_Δ	n_α	n_s	N_h
C		1	10		1	5	0
C		1	6		1	4	5
C		0	5		1	4	1
C		0	5			80	17
C		0	3			46	25
C		0	1			44	19
B		1	5			40	17
Be	1	2	3			37	22
Be		4	5			30	33
Li	1	1	2			24	18
Li	1	0	7			24	11
	3	3	3			23	3
	3	0	4			23	3
	3	0	2			20	13
	3	0	1			19	12
	2	15	1			18	22
	2	11	13			17	3
	2	4	0			16	23
	2	3	0			16	10
	2	2	6			16	0
	2	2	5			15	37
	2	2	0			15	22
	2	2	0			15	21
	1	22	22			14	19
	1	17	6			14	17
	1	13	5			14	5
	1	12	11			12	16
	1	12	5			12	11
	1	11	6			12	2
	1	9	12			11	23
	1	8	20			11	16
	1	8	6			11	16
	1	7	1			9	34
	1	6	13			8	17
	1	6	5			8	8
	1	5	1			8	2
						8	0
						6	8
						6	6

Nitrogen			
n_Δ	n_α	n_s	N_h
N		0	4
N		0	4
N		0	3
N		0	1
C		8	6
C		5	3
B	1	0	4
B		3	5
B		1	4
B		1	4
Be	1	1	1
Be		2	3
Li		8	5
Li		5	0
	3	6	5
	3	6	3
	2	9	6
	2	5	3
	2	3	4
	2	2	2
	1	14	4
	1	12	5
	1	10	4
	1	8	7
	1	7	5
	1	6	3
	1	5	3
		44	42
		27	26
		18	30
		17	5
		15	27
		12	30
		9	4
		7	29

Oxygen							
n_Δ	n_α	n_s	N_h	n_Δ	n_α	n_s	N_h
O		2	2			16	21
O		0	3			14	23
N		4	11			14	15
C	1	0	0			14	7
B	1	4	6			13	26
B		23	15			13	27
Be	1	2	0			12	35
Li	1	2	1			11	3
Li		19	9			10	15
Li		7	0			8	10
	3	35	4				
	3	4	11				
	3	4	5				
	3	3	5				
	3	3	0				
	3	2	0				
	2	11	11				
	2	11	6				
	2	9	5				
	2	7	5				
	2	5	8				
	2	5	0				
	2	4	1				
	2	4	1				
	1	22	6				
	1	13	5				
	1	12	14				
	1	12	6				
	1	10	11				
	1	8	13				
		48	26				
		19	28				
		19	6				
		19	1				
		18	2				

Fluorine			
n_Δ	n_α	n_s	N_h
F		0	2
C	1	2	2
C	1	1	1
Be		6	0
	1	14	9
	1	13	4
	1	9	6
		6	29

Table 4 (*b*). The characteristics of each of the 317 nuclear interactions observed in emulsion. Each interaction is classified in terms of the type of heavy fragment n_Δ, the number of α-particles n_α, the number of 'shower' tracks n_s, and the number of black and grey tracks N_h.

Neon			
n_Δ	n_α	n_s	N_h
O		8	4
O		7	2
N	1	3	3
N	1	1	0
C		4	9
	4	5	0
	2	11	8
	2	10	15
	1	21	12
		14	14

Sodium			
n_Δ	n_α	n_s	N_h
Na		0	1
Be		10	10
Li+Li		4	7
Li	1	7	2
	5	2	7
	4	16	4
	3	8	14
	2	8	16
		41	24
		34	17
		26	31
		20	18
		20	5

Magnesium			
n_Δ	n_α	n_s	N_h
F	1	1	0
O	2	2	1
O	2	0	0
O		8	6
N	1	5	5
Be	2	7	23
	3	17	11
	1	11	4
		30	22
		25	22
		22	19

Aluminium			
n_Δ	n_α	n_s	N_h
Al		0	1
Al		0	1
	4	22	12
	1	30	9
	1	20	20
	1	19	17
		70	17

Silicon			
n_Δ	n_α	n_s	N_h
Ne	2	0	0
Ne		6	1
F	2	3	0
O	1	8	0
C	1	5	8
	2	19	29
	1	17	2
		24	29

Phosphorus			
n_Δ	n_α	n_s	N_h
Na	1	1	3
N	2	12	0
Li		13	6

Sulphur			
n_Δ	n_α	n_s	N_h
S		0	1
Na	1	4	0
Ne		6	7
C	2	14	2
	2	150	20
		28	19

Chlorine			
n_Δ	n_α	n_s	N_h

Argon			
n_Δ	n_α	n_s	N_h
Na	1	7	5
C+Li	3	4	4

Potassium			
n_Δ	n_α	n_s	N_h
	1	28	27

Calcium			
n_Δ	n_α	n_s	N_h
Ca		0	1
O	2	7	0
N	3	21	17
Be		31	36
	1	44	0

Scandium			
n_Δ	n_α	n_s	N_h
Si		10	3

Titanium			
n_Δ	n_α	n_s	N_h
	5	19	19
	5	19	6
		30	21

Vanadium			
n_Δ	n_α	n_s	N_h
N	2	22	17
Li		20	14
	2	30	10

Chromium			
n_Δ	n_α	n_s	N_h
V		3	4
Ca	1	1	0
Mg	2	20	21

Manganese			
n_Δ	n_α	n_s	N_h
Ca		6	0

Iron			
n_Δ	n_α	n_s	N_h
Fe		0	1
A	1	?	5
S	3	5	3
Si	1	11	9
C	5	6	4
C	4	14	4
		50	18

Table 5. The fragmentation probabilities observed in emulsion by Gottstein (1954) G, Noon and Kaplon (1955) N, and in the present work P

Prim.	Sec.	No. of stars	*VH*	*n*	*H*	*n*	*M*	*n*	*L*	*n*	α	*n*	n_s only	*n*
VH	(G)	3	0·00	0	0·33±0·33	1	0·33±0·33	1	1·33±0·67	4	1·66±0·75	5	0·00	0
	(N)	19	0·11±0·07	2	0·26±0·12	5	0·21±0·11	4	0·31±0·13	6	2·95±0·39	56	0·00	0
	(P)	21	0·14±0·08	3	0·24±0·10	5	0·19±0·09	4	0·09±0·06	2	1·52±0·39	32	0·09±0·06	2
H	(G)	28			0·07±0·05	2	0·25±0·09	7	0·14±0·07	4	1·82±0·25	51	0·04±0·04	1
	(N)	74			0·14±0·04	10	0·22±0·05	16	0·46±0·08	34	2·10±0·17	155	0·00	0
	(P)	58			0·09±0·04	5	0·28±0·07	16	0·12±0·05	7	1·15±0·17	67	0·21±0·06	12
M	(G)	36					0·06±0·04	2	0·31±0·09	11	1·22±0·18	44	0·14±0·06	5
	(N)	111					0·08±0·03	9	0·32±0·05	36	1·31±0·11	145	0·06±0·02	7
	(P)	161					0·11±0·03	19	0·12±0·03	20	0·73±0·07	119	0·37±0·04	60
L	(G)	27							0·15±0·07	4	0·85±0·18	27	0·33±0·11	9
	(P)	62							0·10±0·04	7	0·40±0·08	27	0·62±0·10	42
VH +*H* +*M*	(G)		0·00	0	0·10±0·05	3/31	0·15±0·04	10/67	0·28±0·05	19/67	1·49±0·15	100/67	0·09±0·04	6/67
	(N)		0·11±0·07	2/19	0·16±0·04	15/73	0·14±0·03	29/204	0·37±0·04	76/204	1·74±0·09	356/204	0·06±0·02	7/204
	(P)		0·14±0·08	3/21	0·13±0·04	10/79	0·15±0·03	37/240	0·12±0·02	29/240	0·98±0·07	238/240	0·30±0·04	74/240

Table 6. The fragmentation probabilities from interactions with $N \leqslant 7$ in emulsion. Values shown are those of Noon and Kaplon (1955) N, and of the present work P

Prim.	Sec.	No of. stars	*VH*	*n*	*H*	*n*	*M*	*n*	*L*	*n*	α	*n*	n_s only	*n*
VH	(N)	9	0·00	0	0·33±0·16	3	0·44±0·16	4	0·33±0·16	3	3·12±0·72	28	0·00	0
	(P)	12	0·25±0·14	3	0·25±0·14	3	0·33±0·17	4	0·00	0	2·08±0·68	25	0·00	0
H	(N)	44			0·18±0·06	8	0·23±0·06	10	0·52±0·08	23	2·00±0·20	88	0·00	0
	(P)	30			0·20±0·08	6	0·50±0·13	15	0·17±0·07	5	1·33±0·26	40	0·03±0·03	1
M	(N)	74					0·09±0·03	7	0·38±0·06	28	1·33±0·12	98	0·04±0·02	3
	(P)	100					0·16±0·04	16	0·18±0·04	18	0·98±0·11	98	0·17±0·04	17
L	(P)	31							0·16±0·07	5	0·45±0·13	14	0·52±0·13	16
VH +*M* +*H*	(N)	—	0·00	0	0·21±0·06	11/53	0·17±0·03	21/127	0·42±0·04	54/127	1·68±0·10	214/127	0·02±0·01	3/127
	(P)	—	0·25±0·14	3/12	0·21±0·07	9/42	0·25±0·04	35/142	0·16±0·04	23/142	1·15±0·09	163/142	0·13±0·03	18/142

$0{\cdot}21 \pm 0{\cdot}03$ as compared with the value of $0{\cdot}37 \pm 0{\cdot}04$ found by Noon and Kaplon.

We believe that it is extremely unlikely that we could have missed an appreciable proportion of the fragments, since we have examined all possible tracks emitted within a *projected* angle of 10° to the direction of the primary nucleus, and we have not found *any* fragments with a *solid* angle of more than 9°, see the figure. All our primary particles had lengths per emulsion of more than 2 mm, and the majority had more than 4 mm, whereas previous workers have used considerably steeper tracks, and under these conditions the identification of the secondary fragments might well be subject to considerable uncertainties. In addition, the fact that the interaction mean free paths which we observe are in good agreement with those found by Noon and Kaplon suggests that the efficiencies of detection of interactions were comparable in the two experiments. We therefore suggest that the fragmentation probabilities found by Gottstein and by Noon and Kaplon for the production of L nuclei and α-particles are too high.

In order to obtain an estimate of the fragmentation probabilities in air from those observed in emulsion we have adopted the following procedure. Nuclear emulsion consists of hydrogen; carbon, nitrogen and oxygen; and silver and bromine; while air consists of nitrogen and oxygen. Unfortunately, except in special cases, it is not possible to identify the target nucleus involved in an interaction. However, we may divide the observed interactions into two classes on a basis of the number of black and grey prongs emitted. We have assumed that those interactions characterized by $N_h > 7$ are due to moderately central collisions with silver or bromine nuclei, while those with $N_h \leq 7$ are interactions with light nuclei and hydrogen or peripherial collisions with heavy nuclei. It appears likely to us that these interactions will result in somewhat larger fragmentation probabilities than typical interactions with nitrogen and oxygen. Therefore, the fragmentation probabilities found for interactions with $N_h \leq 7$ will presumably be upper limits to those in air. These probabilities are shown in table 6 for both our and Noon and Kaplon's data.

While interactions with hydrogen can sometimes be identified from their appearance we have not attempted to give the fragmentation probabilities, as the present statistical weight does not justify our doing so. We hope that further work will enable us to obtain these important figures.

§ 4. CONCLUSIONS

Our main conclusion from this work is that the probability of a heavy nucleus fragmenting into a L nucleus is considerably less than has been claimed previously on the basis of similar experiments. If so, then those workers who have used the earlier fragmentation probabilities will have underestimated the abundance of L nuclei at the top of the atmosphere. For example, in an experiment by Kaplon *et al.* (1954) these workers obtained a value of 0·46 for the ratio of the fluxes of L nuclei to M nuclei at the top of the atmosphere. Using our figures for the fragmentation probabilities this ratio is increased to about 0·80.

ACKNOWLEDGMENTS

We are grateful to Professor C. F. Powell for the hospitality of his laboratory. We wish to thank Miss B. Bolt and Miss P. Curry for careful and consistent scanning. C.J.W. thanks the Royal Society for the award of a Mackinnon Research Studentship, and R.R.H. thanks the Department of Scientific and Industrial Research for a maintenance grant.

REFERENCES

BRADT, H. L., and PETERS, B., 1950, *Phys. Rev.*, **77,** 54.
FOWLER, P. H., and WADDINGTON, C. J., 1956, *Phil. Mag.*, **1,** 637.
GOTTSTEIN, K., 1954, *Phil. Mag.*, **45,** 347.
KAPLON, M. F., NOON, J. H., and RACETTE, G. W., 1954, *Phys. Rev.*, **96,** 1408.
NOON, J. H., and KAPLON, M. F., 1955, *Phys. Rev.*, **97,** 769.
PERKINS, D. H., 1950, *Phil. Mag.*, **41,** 138.
PETERS, B., 1952, *Progress in Cosmic Ray Physics*, Vol. I, 193.

Stability of Laminar Flow in Curved Channels†

By Chia-Shun Yih‡ and W. M. Sangster§
Iowa Institute of Hydraulic Research, State University of Iowa

[Received July 5, 1956]

Abstract

Occurrence of secondary flow of a viscous fluid flowing under a pressure gradient in curved channels has often been explained by invoking the existence of boundary layers before the primary flow is established. In this paper it is shown that instability can occur even after the full establishment of the primary flow. Chandrasekhar's method is used in the analysis and the relationship between the stability parameter and the wave number of the disturbance for neutral stability is obtained.

§ 1. Introduction

Whereas the occurrence of spirals in fluid flow under a pressure gradient in curved channels is common knowledge, explanations of the phenomenon have been based upon the existence of boundary layers before the primary flow is fully established, and the fully developed two-dimensional flow has generally been believed to be free of such spirals (Goldstein 1938). In the present paper, this phenomenon will be analysed by Chandrasekhar's (1954) method under the assumption that the primary flow is two-dimensional and between two concentric circular cylinders of small spacing, and that it is already fully established. The object is to obtain definite information about the stability of such a flow against the formation of Taylor–Görtler vortices of various transverse wavelengths.

§ 2. Velocity Distribution in the Primary Flow

Cylindrical coordinates (r, ϕ, z) will be used, with the z-axis coinciding with the axis of the cylinders. If the radius of the inner cylinder is a and that of the outer one is b, the distribution of the velocity V of the primary flow can be found by solving the Navier–Stokes equations and is given (Goldstein 1938) by

$$\frac{V}{K}=A\left(\frac{r}{b}-\frac{b}{r}\right)+\frac{r}{b}\ln\frac{r}{b} \qquad (1)$$

in which

$$A=\frac{a^2(\ln a-\ln b)}{b^2-a^2}, \qquad K=\frac{b}{2\mu}\frac{\partial P}{\partial \phi} \qquad (2)$$

μ being the dynamic viscosity and P the pressure for the primary flow.

---

† Communicated by S. Chandrasekhar, F.R.S.
‡ Now at University of Michigan.
§ Now at University of Missouri.

If the spacing d of the cylinders (or $b-a$) is very small compared with the radii of the cylinders it can be shown from eqn. (1) that the velocity distribution of the primary flow is essentially the same as that for plane Poiseuille flow, i.e.

$$V=\frac{d^2}{2\mu a^2}\frac{\partial P}{\partial \phi}(\xi^2-\xi)=\frac{Kd^2}{a^2}(\xi^2-\xi) \quad . \quad . \quad . \quad . \quad (3)$$

in which

$$\xi=\frac{r-a}{b}. \quad . \quad . \quad . \quad . \quad . \quad . \quad . \quad . \quad (4)$$

The mean velocity is, to the same degree of approximation,

$$V_m=-\frac{d^2K}{6a^2}$$

so that the Reynolds number based on V_m and d is

$$R=\frac{V_m d}{\nu}=-\frac{d^3K}{6\nu a^2} \quad . \quad . \quad . \quad . \quad . \quad . \quad . \quad (5)$$

in which ν is the kinematic viscosity. From eqn. (3) it follows that, with terms of higher order in d neglected,

$$\frac{V}{r}=\frac{Kd^2}{a^3}(\xi^2-\xi) \quad . \quad . \quad . \quad . \quad . \quad . \quad . \quad . \quad (6)$$

$$V'+\frac{V}{r}=\frac{Kd}{a^2}(2\xi-1) \quad . \quad . \quad . \quad . \quad . \quad . \quad . \quad (7)$$

in which the prime indicates differentiation with respect to r. These quantities will be useful later in the investigation of stability.

§ 3. FORMULATION OF THE STABILITY PROBLEM

To investigate the stability of the primary flow, one may superpose on it a time-dependent perturbation with (small) velocity components (u, v, w) in the directions of r, ϕ, and z, respectively, and with corresponding pressure p. If it is kept in mind that the primary flow is such that the Navier–Stokes equations and the equation of continuity are satisfied, and if terms of higher order than the first in the perturbation quantities are neglected, the Navier–Stokes equations are

$$\frac{\partial u}{\partial t}-\frac{2Vv}{r}=-\frac{1}{\rho}\frac{\partial p}{\partial r}+\nu\left(\nabla^2 u-\frac{u}{r^2}\right), \quad . \quad . \quad . \quad . \quad (8)$$

$$\frac{\partial v}{\partial t}+uV'+\frac{Vu}{r}=\nu\left(\nabla^2 v-\frac{v}{r^2}\right), \quad . \quad . \quad . \quad . \quad . \quad (9)$$

$$\frac{\partial w}{\partial t}=-\frac{1}{\rho}\frac{\partial p}{\partial z}+\nu\nabla^2 w, \quad . \quad . \quad . \quad . \quad . \quad . \quad (10)$$

in which t and ρ denote time and density respectively, and

$$\nabla^2\equiv\frac{\partial^2}{\partial r^2}+\frac{1}{r}\frac{\partial}{\partial r}+\frac{\partial^2}{\partial z^2}.$$

The equation of continuity is

$$\frac{\partial(ur)}{\partial r}+\frac{\partial(wr)}{\partial z}=0. \qquad (11)$$

Now, following Taylor (1923), one may assume

$$(u, v, w)=\exp\,(\sigma t)[u_1(r)\cos kz,\ v_1(r)\cos kz,\ w_1(r)\sin kz]. \qquad (12)$$

If p is eliminated between eqns. (8) and (10), and if eqn. (12) is used, one has

$$\frac{\nu}{k}D\left(\nabla_1^2-k^2-\frac{\sigma}{\nu}\right)w_1=-\frac{2V}{r}v_1-\nu\left(\nabla_1^2-k^2-\frac{1}{r^2}-\frac{\sigma}{\nu}\right)u_1 \qquad (13)$$

in which

$$D\equiv d/dr, \qquad \nabla_1^2=D^2+\frac{1}{r}D.$$

Furthermore eqn. (9) can now be written as

$$u_1\left(V'+\frac{V}{r}\right)=\nu\left(\nabla_1^2-k^2-\frac{1}{r^2}-\frac{\sigma}{\nu}\right)v_1 \qquad (14)$$

and the equation of continuity is

$$\frac{u_1}{r}+Du_1+kw_1=0. \qquad (15)$$

Although for neutral stability σ may be purely imaginary, one may follow Taylor in taking it to be zero—at any rate if one is looking for the formation of Taylor–Görtler vortices. For neutral stability, therefore, eqn. (14) becomes

$$\nu L_1 v_1=(V'+V/r)u_1 \qquad (16)$$

in which

$$L_1\equiv D^2+\frac{1}{r}D-k^2-\frac{1}{r^2}$$

and it can be readily shown that eqns. (13) and (15) yield

$$\frac{\nu}{k^2}L_1^2u_1=\frac{2V}{r}v_1. \qquad (17)$$

Since the spacing d is much smaller than a or b, and since the perturbation velocities change appreciably as r varies between a and b, and the wavelength $(2\pi/k)$ is comparable with d, the part

$$\frac{1}{r}D-\frac{1}{r^2}$$

in the operator L_1 is small compared with the rest of the terms. If now one denotes kd by α and expresses u_1 and v_1 in terms of V_m, eqns. (16) and (17) become, in virtue of eqns. (5), (6), and (7),

$$Lv_1=\frac{Kd^3}{\nu a^2}u_1=-6R(2\xi-1)u_1, \qquad (18)$$

$$L^2u_1=\frac{2Kk^2d^6}{\nu a^3}(\xi^2-\xi)v_1=-12\alpha^2R\beta(\xi^2-\xi)v_1 \qquad (19)$$

in which

$$L=d^2/d\xi^2-\alpha^2, \qquad \beta=d/a.$$

If one sets

$$u_1=-12\alpha^2R\beta W \quad . \quad . \quad . \quad . \quad . \quad . \quad . \quad . \quad (20)$$

one has finally

$$L^2W=(\xi^2-\xi)v_1 \quad . \quad . \quad . \quad . \quad . \quad . \quad . \quad . \quad (21)$$

$$Lv_1=S\alpha^2(2\xi-1)W \quad . \quad . \quad . \quad . \quad . \quad . \quad . \quad . \quad (22)$$

where

$$S=72R^2\beta \quad . \quad . \quad . \quad . \quad . \quad . \quad . \quad . \quad . \quad (23)$$

is the stability parameter. Equations (21) and (22) are to be solved with the boundary conditions

$$v_1(0)=v_1(1)=0, \qquad W(0)=W(1)=0, \qquad W'(0)=W'(1)=0 \ . \quad (24)$$

the last two being a consequence of eqns. (15) and (20) and of the fact that u_1 and w_1 are zero at $\xi=0$ and $\xi=1$. The primes in the last two of eqns. (24) indicate differentiation with respect to ξ. The differential system consisting of eqns. (21), (22), and (24) represents an eigenvalue problem, the solution of which will result in a functional relationship between S and α for neutral stability since σ has been assumed to be zero to start with.

§ 4. OUTLINE OF THE METHOD OF SOLUTION

Since the method of solution used in this paper is that of Chandrasekhar and is already described in detail elsewhere (Chandrasekhar 1954), only an outline of the essential steps will be presented here. First, one takes

$$v_1=\sum_{n=1}^{\infty} A_n \sin n\pi\xi. \quad . \quad . \quad . \quad . \quad . \quad . \quad . \quad . \quad (25)$$

to satisfy the first two conditions in eqn. (24). Then this expression for v_1 is substituted into eqn. (21) which can be solved to yield the result

$$W=\sum_{m=1}^{\infty}\frac{A_m}{M^2}\Bigg[B_m\cosh\alpha\xi+C_m\sinh\alpha\xi+D_m\xi\cosh\alpha\xi+E_m\xi\sinh\alpha\xi + (\xi^2-\xi)\sin m\pi\xi+\frac{4m\pi(2\xi-1)\cos m\pi\xi}{M}+\frac{4(M-6m^2\pi^2)\sin m\pi\xi}{M^2}\Bigg] \quad . \quad . \quad . \quad . \quad (26)$$

in which $M=m^2\pi^2+\alpha^2$ and the constants B to D can be determined to satisfy the last four conditions in eqns. (24). With these constants so determined, eqn. (26) is then substituted into eqn. (22) and the right-hand side expressed in a Fourier sine series. Then coefficients of the individual harmonics at left and right are equated. This result in an infinite number of homogeneous linear equations involving the A's. Finally the eliminant of these equations (or the condition that the A's are not all zero) furnishes the desired relationship between S and α.

Although the eliminant is a determinant of infinitely many rows and columns, Chandrasekhar (1954) has shown that often it is sufficiently accurate to equate the first element (in the first column and first row) to zero, and that the result of the second approximation (by equating a two-by-two determinant to zero) does not differ much from that of the first. The same was found to be true in a previous calculation (for a slightly different primary flow) by the authors whenever the second approximation was tried for spot checking, so that the relationship between S and α determined by the first approximation is believed to be sufficiently accurate. The ease with which this relationship was obtained is additional proof of the power of Chandrasekhar's method in solving problems of the present type.

§ 5. RESULTS AND CONCLUDING REMARKS

The desired relationship between S and α for neutral stability of the primary flow is given graphically in the figure. It is seen from this figure that established laminar flow under a pressure gradient in a narrow curved channel is unstable for values of the parameter S greater than the approximate critical value 600, which corresponds to a wavelength of the Taylor–Görtler vortices equal to $2\pi/2{\cdot}25$ or $2{\cdot}79$ times the width of the channel. Since the flow tends to be unstable as S is increased, for the same Reynolds number and the same (small) width of the channel it does so as the curvature is increased, as can be seen from the definition of S. Thus centrifugal force is as much a cause of instability for the established flow as it is for the unestablished one, and the occurrence of secondary flow cannot be considered to be exclusively a consequence of boundary-layer development.

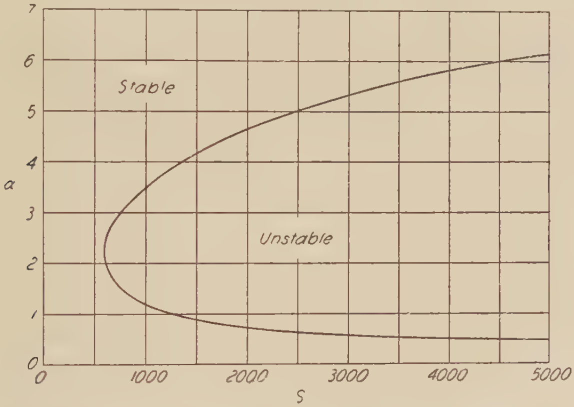

Relationship between the wave number α and the stability parameter S for neutral stability.

Attention might also be called to the fact that, since centrifugal force can be considered as a form of gravitation (Mach, Einstein), the non-uniformity of it is a kind of stratification—a stratification not of density, for the density is homogeneous, but of specific weight in the general sense. Secondary flow occurs if this stratification is not stable, and the mechanics of it is not unlike the falling of a heavier fluid in a lighter one, particularly if the boundary conditions are alike, and diffusion takes place to render the variation of density and that of centrifugal acceleration strictly comparable. This point of view is substantiated elsewhere by the equality of the Rayleigh number for thermal instability and the Taylor number for rotational instability (both being 1708), as first pointed out by Low (1929).

ACKNOWLEDGMENT

This work was jointly sponsored by the Iowa Institute of Hydraulic Research and the Office of Ordnance Research under Contract number DA-11-022-ORD-1729.

REFERENCES

GOLDSTEIN, S. (Editor), 1938, *Modern Developments in Fluid Dynamics* (Oxford), vol. I, pp. 84–87, 315–316.
CHANDRASEKHAR, S., 1954, *Mathematika*, **1**, 5.
TAYLOR, Sir GEOFFREY, 1923, *Phil. Trans. Roy. Soc.* A, **223**, 289.
LOW, A. R., 1929, *Proc. Roy. Soc.* A, **125**, 180.

The Interpretation of the Levels of ^{19}F on the Rotational Model †

By E. B. Paul
Atomic Energy Research Establishment, Harwell

[Received September 14, 1956]

There is considerable experimental evidence that the lower lying levels of nuclei of masses 25, 29 and 31 may be rather well described as overlapping systems of rotational bands (Litherland *et al.* 1956). The moments of inertia required are close to those indicated from a similar interpretation of the levels of neighbouring even–even nuclei. The deformations required are in the range $\beta=0{\cdot}2$–$0{\cdot}3$ which are consistent with the deformations indicated by the few measured quadrupole moments in this region. One would not have thought that the collective model of Bohr and Mottelson (1953) which has had such marked success in the heavy nuclei would be useful for such light nuclei where the zero point oscillation amplitude might be expected to exceed the deformation value. This would prevent the rotational states from being developed to any significant extent. However when the detailed properties of these nuclei such as relative and absolute transition probabilities and level ordering are compared with a model such as that of Nilsson (1955) who has computed the single particle energy levels in a deformed potential, the agreement is remarkably good.

Considerable success has been achieved in the region around ^{16}O in describing the nuclei in terms of configuration mixing in an intermediate coupling shell model; it is of interest therefore to explore the two approaches through a direct comparison for the same nucleus. The shell model calculation becomes impractically laborious in its rigorous form for nuclei above ^{20}Ne having more than four nucleons outside the ^{16}O closed shell. The nucleus ^{19}F has been very successfully treated on the intermediate coupling shell model by Elliott and Flowers (1955). Some modifications arising from collective effects have been considered by Barker (1956). This paper is an attempt to apply the rotational model to this nucleus in a similar way to that used for ^{25}Al. No attempt has been made to introduce refinements to the theory which may be necessary for nuclei in this region. Such refinements are being considered by Rakavy (private communication).

The Even Parity States of ^{19}F

Figure 1 shows the known states of ^{19}F below 6 Mev together with some of their measured properties (Ajzenberg and Lauritsen 1955). Let us consider first the even parity states. Based on the ground state with

---

† Communicated by the Author.

$I=\frac{1}{2}$ we expect a rotational band with $K=\frac{1}{2}$, where K is the projection of the total angular momentum on the nuclear symmetry axis. The level order for bands with $K=\frac{1}{2}$ is given by (Bohr and Mottelson 1954).

$$E_I=E_0+\hbar^2/2\mathfrak{J}[I(I+1)+a(-)^{I+1/2}(I+\tfrac{1}{2})]$$

where $\mathfrak{J}$ is the moment of inertia and a depends on the configuration mixing of the last odd particle. For reasonable values of a given by Nilsson's model and of the moment of inertia, the level spacing is much greater than that observed, as shown for example on the left-hand side of fig. 2, although the level order is correct.

Fig. 1

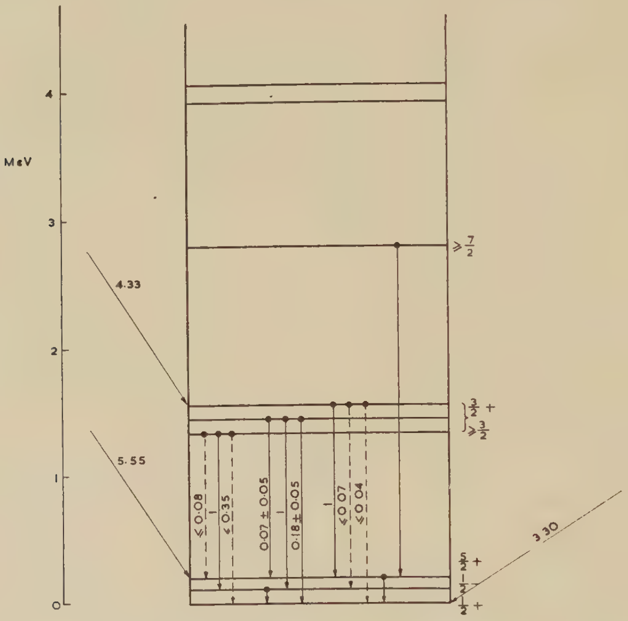

The known states of ^{19}F below 6 MeV. The arrows from the left represent β-transitions from ^{19}O, that from the right the β-transition from ^{19}Ne. All three are labelled with the value of log ft.

Let us now consider the next higher rotational band which may occur. According to Nilsson's model this will have $K=\frac{3}{2}$ and will be about 3 MeV higher. Kerman (1956) has shown that through the rotation–particle coupling there is the possibility for K-admixture between bands with K differing by one unit. This means that K is no longer a very good quantum number. The level ordering is affected since states having the same spin in the two series will be pushed apart. In this case the state with $I=\frac{1}{2}$ is not changed since it has no corresponding member in the $K=\frac{3}{2}$ band. The mixing amplitudes and the changed level positions can be calculated using the matrix element for the interaction between the two bands which can be derived from Nilsson's wave functions.

The final fit shown in fig. 2 has been derived by requiring (1) the $\frac{3}{2}$ state with $K=\frac{1}{2}$ to be at 1·55 MeV where it is observed and (2) the $\frac{3}{2}$ state with $K=\frac{3}{2}$ to be at 4 MeV near the first two states one of which could be identified with it. For a value of $\beta=0{\cdot}3$ the agreement shown in the third and fourth columns of fig. 2 is obtained. The rotational energy $\hbar^2/2\mathfrak{J}$ required for both bands is 0·3 MeV. When the first excited states of 2+ of ^{18}O and ^{20}Ne are assumed to be rotational states, values of 0·33 and 0·27 MeV for $\hbar^2/2\mathfrak{J}$ are obtained. The $\frac{5}{2}$ state occurs at 0·24 MeV to be compared with the observed position of 0·197 MeV while a $\frac{9}{2}$ state occurs at 2·9 MeV which may well be identified with the state observed at 2·81 MeV which has spin $\geqslant\frac{7}{2}$. The effect of the K-admixture is to make the $\frac{5}{2}$ state contain 19% in intensity of $K=\frac{3}{2}$ configuration and the $\frac{3}{2}$ state contain 46% of $K=\frac{3}{2}$.

Fig. 2

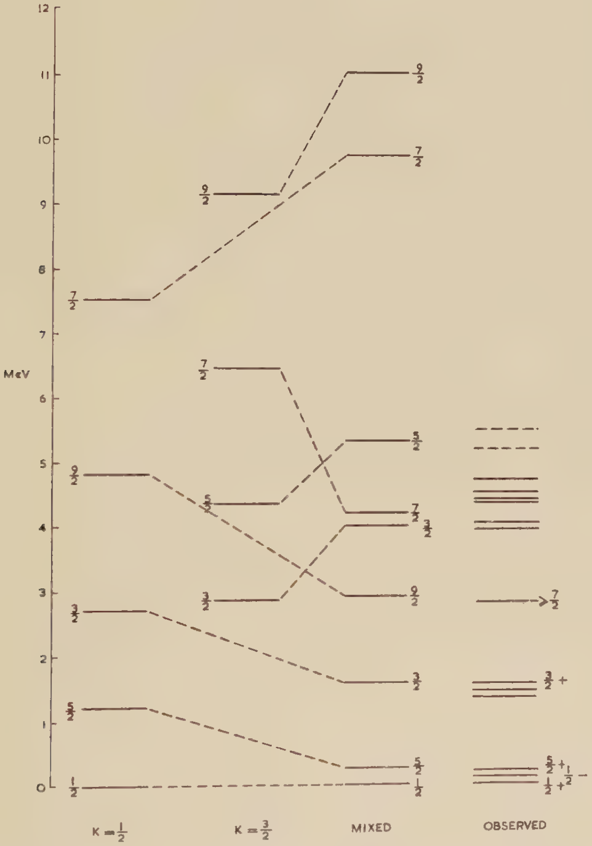

The states predicted for ^{19}F (column 3) resulting from mixture of two bands (columns 1 and 2) compared with the observed states (column 4).

Using this specification for levels, other properties may be derived from the wave functions of Nilsson. These are listed in table 1 along with the experimentally determined values. The corresponding predictions of the shell model calculation of Elliott and Flowers are also listed. In the calculation of the $E2$ lifetime of the $\frac{5}{2}+$state on the rotational model, the collective as well as the particle part of the $E2$ transition probability has been included. For ^{19}F the two parts are of comparable importance, unlike the heavy nuclei where the collective part predominates.

The Beta Decay of ^{19}O

To explain the β-transition probabilities for the decay of ^{19}O to the states of ^{19}F, it is necessary to interpret the states of ^{19}O also on the rotational model. This is difficult because of the meagre experimental information available. The spin of ^{19}O should be $\frac{3}{2}+$, $K=\frac{3}{2}$ on Nilsson's model but experimentally may be $\frac{3}{2}$ or $\frac{5}{2}+$. The spins and positions of other states in ^{19}O need to be determined before an unambiguous description of the β-decay is possible.

Table 1. Predictions of the Two Models compared with the Experimental Values

Property	Rotational model	Shell model	Experimental
γ-ray branching Ratio $\frac{3}{2}\to\frac{1}{2}+$ to $\frac{3}{2}\to\frac{5}{2}+$	0·8%	0·6%	4%[(a)]
Magnetic moments : of $\frac{1}{2}+$ state of $\frac{5}{2}+$ state	 2·75 n.m. 3·70	 2·80 n.m. 3·3	 2·63 n.m.[(b)] $3{\cdot}50 \pm 0{\cdot}24$[(c)]
Lifetime of $\frac{5}{2}+$ state	$0{\cdot}9 \times 10^{-7}$ sec	$5+10^{-7}$ sec[(d)] $1+10^{-7}$ sec	$1{\cdot}25 \pm 0{\cdot}025+10^{-7}$ sec[(e)]
Log ft value for ^{19}Ne decay	3·52	3·2	3·3[(a)]

(*a*) Ajzenberg and Lauritsen (1955).
(*b*) Mack (1950).
(*c*) Phillips and Jones (1956).
(*d*) The first value is that obtained when core vibrations are neglected, the second value is obtained when such vibrations are included.
(*e*) Johnson (1956).

The Odd Parity States of ^{19}F

A state of $\frac{1}{2}-$ has been identified at 0·110 Mev in ^{19}F. In addition two states have been identified (Toppel *et al.* 1956, Freeman 1955) at 1·35 and

1·46 MeV which are not accounted for in the interpretation overleaf of the even parity states. These might be identified as $I=\frac{1}{2}$, $\frac{3}{2}$ and $\frac{5}{2}$ members of a $K=\frac{1}{2}$ band resulting from a hole in the p-shell. From the position of the first excited states of ^{16}O one would expect that 6 or 7 MeV would be required to break up the p-shell. Theoretically, however, it appears that for large enough deformations the rotational energy may be great enough to cancel out this energy for the break-up of the shell and so bring an odd parity particle level down near the ground state. The observed γ-ray branching from the states at 1·35 and 1·46 MeV (assuming them to have odd parity) is characterized by the weakness of the $E1$ transitions compared to the $M1$ or $E2$ transitions. This discouragement of the $E1$ transitions would also result from a large deformation. On the other hand the spacing of the levels indicates a fairly small deformation. This inconsistency makes it difficult to draw further conclusions. However, this model like the shell model requires the two states at 1·35 and 1·46 MeV to have odd parity.

Comparison with the Shell Model

From table 2 we can see that the predictions of the two models are remarkably similar. In table 2 a further comparison is made. The probability of finding the last odd particle in a given configuration j is listed for each even parity state. Those derived from the intermediate shell model calculation are in the coordinate system fixed in space, while those derived from the rotational model are in the coordinate system fixed inside the deformed nucleus. The results are comparable if the period of the rotational motion is slow compared to the particle motion. If this is the case the mixtures of configurations derived from the two approaches show similar trends.

Table 2. Configuration of the Last Odd Particle for the Even Parity States according to the Two Models

State	j	Rotational model	Shell model
		(%)	(%)
$\frac{1}{2}$	$\frac{1}{2}$	29	49
	$\frac{3}{2}$	9	9
	$\frac{5}{2}$	62	42
$\frac{3}{2}$	$\frac{1}{2}$	15	21
	$\frac{3}{2}$	9	19
	$\frac{5}{2}$	76	60
$\frac{5}{2}$	$\frac{1}{2}$	23	19
	$\frac{3}{2}$	9	10
	$\frac{5}{2}$	68	71

ACKNOWLEDGMENTS

I am indebted to Dr. A. M. Lane, Dr. B. H. Flowers and Dr. H. E. Gove for helpful discussions.

REFERENCES

AJZENBERG, F., and LAURITSEN, T., 1955, *Rev. Mod. Phys.*, **27,** 77.
BARKER, F. C., 1956, *Phil. Mag.*, **1,** 329.
BOHR, A., and MOTTELSON, B. R., 1953, *Dan. Mat. Fys. Medd.*, **27,** No. 16.
BOHR, A., and MOTTELSON, B. R., 1954, *Beta and Gamma Ray Spectroscopy*, ed. K. Siegbahn (Amsterdam : North Holland Publishing Co.), Chap. 17.
ELLIOTT, J. P., and FLOWERS, B. H., 1955, *Proc. Roy. Soc.* A, **229,** 536.
FREEMAN, J. M., 1955, *Phys. Rev.*, **99,** 1446 ; and private communication.
JOHNSON, C. M. P., 1956, *Phil. Mag.*, **1,** 573.
KERMAN, A. K., 1956, *Dan. Mat. Fys. Medd.*, **30,** No. 15.
LITHERLAND, A. E., BARTHOLOMEW, C. A., PAUL, E. B., and GOVE, H. E., 1956, *Phys. Rev.*, **102,** 208.
MACK, J. E., 1950, *Rev. Mod. Phys.*, **22,** 64.
NILSSON, S. G., 1955, *Dan. Mat. Fys. Medd.*, **29,** No. 16.
PHILLIPS, W. R., and JONES, G. A., 1956, *Phil. Mag.*, **1,** 576.
TOPPEL, B. J., WILKINSON, D. H., and ALBURGER, D. E., 1956, *Phys. Rev.*, **101,** 1485.

The Growth of Lead Nitrate Crystals from Aqueous Solution†

By Anne P. Williams
Royal Holloway College, Englefield Green, Surrey

[Received November 1, 1956]

Abstract

Natural growth features observed on crystals of lead nitrate when growing from aqueous solution are described in detail. The modes of formation and behaviour of growth layers are discussed. A special feature is the frequent occurrence of stacking fault lines over which the growth layers cannot pass. These often appear at centres of growth. The effect of methylene blue as impurity in solution restricts the growth on the cube faces in a direction parallel to a diagonal in the face. This results in the formation of small striations or tilt faces.

§ 1. Introduction

Following the interest in spiral layer growth as predicted by Burton *et al.* (1951), in their theory of crystal growth, it was decided to re-examine the growth of some of the crystals reported by Bunn and Emmett (1949) as showing layer growth. Bunn and Emmett used cine-photomicrography with an optical microscope, a method by which layer growth can be studied as it occurs and a record of the variations with time made. It is advantageous to use a high magnification, which somewhat restricts the condition of growth of the crystal. It cannot be suspended in a freely stirred medium, and the faces which can be examined depend both on the habit of growth, and on which face the crystal lies. If it is hoped to see any layer growth, the step height and the refractive properties of the solution and crystal will determine whether this is possible. The speed of growth of the layers will also affect visibility. If growth is rapid even statically visible layers will become blurred.

Bunn and Emmett describe the growth of a few crystals in detail and others are just mentioned as either showing or not showing layers. They reported frequent initiation of layers at points inside the crystal faces, which was puzzling in the light of theory at that time. Information on the nature of the centres of growth was not given.

Forty (1951, 1952) examined the growth of cadmium iodide (one of the crystals studied by Bunn and Emmett) in greater detail, showing that it does grow as a result of dislocations in the crystal at later stages of growth. He has made determinations of step heights interferometrically. Korndorffer *et al.* (1952) have shown that spiral growth of layers may result from deformation of previously perfect crystal platelets of cadmium iodide. Both screw and edge dislocations were produced and the growth rate was greatly increased in the deformed crystals.

---

† Communicated by the Author.

Spiral layer growth on crystal faces has now been reported for several crystals and measurement of step height has been carried out using multiple beam interferometry which is well suited to this type of examination of crystal surfaces. This procedure however is only easily done with crystals which have ceased growing. It is mostly on the basal planes of thin plate-like crystals that these features have been seen. Such crystals have grown slowly in the direction normal to the basal plane but rapidly in extension sideways. The initial thin plate formed would be expected to undergo strain and this would give rise to dislocations as suggested by Frank (1951). Such behaviour would not be expected to occur so readily in a cube or octahedral form crystal which tends to grow more uniformly in all directions. Hence a study of the dynamic growth of lead nitrate has been made. Lead nitrate belongs to the cubic system and shows clear layer growth on octahedral faces when growing from pure solution.

§ 2. EXPERIMENTAL DETAILS

A saturated solution of lead nitrate was prepared using Analar materials and distilled water. The solution was warmed above room temperature and then allowed to cool, excess of the salt having been added, so that a supersaturated solution was obtained. A drop was placed on a thin cover slip on the stage of the microscope. The crystals grow as octahedra with one of these faces lying in contact with the cover slip. The face above this was then observed during growth. The crystals appear when the solution has reached a labile condition. If the solution is left untouched, dendritic crystals tend to form from the edge of the drop. Crystals could be nucleated by scratching the cover slip in the centre of the drop when the solution was in the labile state, a crop of small crystals forming. The growth features on crystals nucleated in this way were the same as those on naturally nucleated crystals.

§ 3. METHOD OF OBSERVATION

Using an inverted type microscope, the crystals were studied in transmitted light, with phase contrast illumination. Light traversing a crystal in solution with a layer growing on its upper surface will undergo a differential phase change according to which side of the layer it passes through the crystal, corresponding to the thickness of the layer. The phase difference will depend on the relative refractive indices of the solution and the solid crystal and the thickness of the step. With transmitted light, positive phase contrast takes place and the top of the step appears dark, the lower side appears bright.

§ 4. NATURAL LAYER GROWTH ON LEAD NITRATE CRYSTALS

The natural forms of layer growth on lead nitrate crystals may be described as follows. Immediately after nucleation of the crystal the growth is very rapid due to high supersaturation. On the octahedral face the visible layers are very irregular and optimum illumination and adjustment shows closely spaced smooth layers of very small step height, moving rapidly, sweeping over the face in about one second in the region between the thicker layers, continually building these up and breaking them down. It is unfortunately impossible to photograph these layers. Figures 1, 2 (order of magnification ×600) show successive photographs at an interval of about one second of a face on which this is occurring. The larger layers are visible terminating in the face, constantly altering in length and thickness. The projected film shows the effect clearly. Growth is very rapid at this stage and nucleation of layers occurs apparently at random at different points on the crystal face. The shape of the thick layers is generally dendritic in form. These conditions would probably be normal with faster growth at a higher temperature. The probability for misfits to occur must be high at this stage.

When the growth conditions become steadier, after the first few minutes, thick layers predominate, through the small layers bunching into the thick layers and these are now continuous over the surface. They may be found either to move out from centres of growth, figs. 3, 4 (×600), or they may move inwards forming a pit of encirclement as described by Bunn and Emmett, figs. 5, 6 (×300). The lower side of a step in these photographs is the bright edge, and the dark side is the top of the step. The time taken for a layer to cross the crystal surface was of the order of ten seconds.

From several observations on fresh crops of crystals the natural growth appears to be that of the Kossel–Stranski model of layers nucleating preferentially at the corners and edges and moving inwards. The layers advance more rapidly at the edges of the crystal face, and result in pits of encirclement in the centre. If dislocations were responsible for the nucleation of these layers, the centres would eventually move within the face when the crystal extends further outwards. This did not happen. Bunn suggested that these pits might be related to the trigons observed on the octahedral faces of diamond, but these pits never show a precise orientation with sharp edges as is the required property of a trigon, and their position and shape varies with successive layers. They occur as the natural sequence of the enclosure of layers and have no relation to trigons. However, as described later, some features akin to trigon formation have been observed on the crystals.

Bunn and Emmett attributed growth from the edges of the face to overlapping of a layer from a neighbouring face. A layer reaching an edge might wrap over on to the next face. This effect has been studied in relation to the present work and no justification for this view has been found. An instantaneous photograph might give this impression but it was always seen that in fact there was no relation between layers on neighbouring faces. The initiation of a layer at an edge might at one instant occur at the same time as one was being completed at the same edge on the adjacent face, but this did not always happen.

The growth from centres appears in crystals which are no longer perfect and closed loops or single spiral growth, sometimes from more than one centre, may be seen. Figures 3, 4 (× 600) show a complex spiral system, and fig. 7 (× 300) a single spiral. Fig. 8 (× 300) shows the same spiral after a short time interval when it has changed to a double spiral. Periodic changes of this type were often observed. In fact, the centres of growth were not located precisely at the same point throughout, possibly because of multiple dislocations being present, distributed over a small area. Dissociation and recombination of layers in this region would give rise to these effects. The centre of the multiple spiral illustrates this point. The visible thick layers must build up from smaller layers by the process described by Frank (1949) of the effect of several sources in region. The actual centres of the dislocations where they emerge on to the surface are not revealed by the visible layers, as these are the result of the smaller layers bunching and interfering with one another, the process varying with time, and depending on the relative step heights and the separation of the centres. The origin of the dislocations causing growth from the centres of faces appears to be due to stacking faults occurring during the period of early rapid growth of the crystal, rather than the buckling mechanism which occurs in thin plate crystals.

Figures 9–14 (× 300) show a phenomenon often appearing, that is, of one layer overtaking another which terminates in the face, joining with it as in fig. 10, and passing on leaving part of the joining layer terminating in the face in its place, fig. 11. This then curls around the point of termination as it grows further, showing the behaviour of the layer tied to a dislocation source. This continues until a new layer crosses the region from the dominant growth centre at the top of the crystal face where there is a multiple spiral source. The tied position of the layer is not constant; this again must result from the building up of layers from small sources, existing over small local area as already described.

§ 5. STACKING FAULTS IN GROWTH PHENOMENA

Another feature frequently observed in naturally grown crystals is a crystallographically orientated ledge which acts as a centre of growth often of a spiral nature. Figures 15 (× 770), 16 (× 600) show such ledges with multiple layer growth. The directions of the ledge are always parallel to the edges of the octahedral face. The growth layers move freely over the face until they arrive at these lines, which they cannot cross but pile up against. The ledges must mark the line of a stacking fault in the crystal since the layers cannot cross the line during growth. The fault may have only a single direction, i.e. be seen as a straight line terminating in the face across which growth is impossible, or have two or three joining line sections in the crystallographic directions as seen in the photographs. During growth the layers pile up against the line of the fault forming the visible step, and then travel round to the other side, where they are again held by the fault line and the step is cancelled as they pile up on this side of it. On one side the step is apparently grown in and on the other grown out. The original fault would be some fraction of a unit cell distance of misfit.

Figures 17–22 (×600) illustrate a single layer moving round such a ledge at different stages of growth. When the layer returns to the first side the fault line trace reappears. The inhibition of growth over these lines must be due to misfit along them. As growth proceeds with time the misfits or stacking fault is propagated through the crystal by the growth process described. These faults occasionally traverse the whole face, growth taking place freely on either side, with the layers originating from the fault line. These steps would be indistinguishable from slip lines and it seems feasable that the conjectured ‘ slip ’ lines observed on diamond octahedral faces recently (Emara 1956) are in fact fault traces of this nature which have been propagated through the crystal during growth. Some such propagation of faults might also explain the formation of trigons in diamond. The diamond structure probably gives rise to faulting in three planes of stacking fault arising from a point of original faulting, suggested by Halperin (1954), which would form during the further growth, as each layer would be inhibited at the trigon fault step which would result on the growing surface. This would become larger during the successive passage of growth layers. Growth would also be possible by nucleation inside the pits left on the surface by the holding up of the growth layers, but crossing of the fault planes would be impossible. Faulting could occur at different times and again within trigons already formed, as is often seen on many diamonds.

Another effect observed in connection with the growth of crystallographic fault ledges on the octahedral surfaces of lead nitrate is that these are not always stable at the points joining two directions of the ledge. One layer on passing this point will build up the ledge, and then, starting at the point of junction, break through and ultimately cross over and eliminate the ledge. One would imagine that subsequent layers would then pass freely over this region, the fault no longer impeding the growth, but this is not the case. Restriction occurs again initially with the following layer, with the subsequent breakthrough occurring after a short time delay, always beginning at the point where the two directions of the ledge meet. Each following layer follows the same pattern.

Figures 23–28 (×300) show this kind of breakthrough beginning at the joining point in fig. 24. The step has disappeared in fig. 26 and is being produced again in fig. 28.

§ 6. Effect of Impurity on Layer Growth

The effect of impurity on the growth layers on lead nitrate crystals was studied with methylene blue in solution. As is well known, the habit of the crystal is then changed to the form of slowest growth on the cube faces, as the impurity is presumably preferentially absorbed on these faces, retarding the growth. This is visually confirmed by the figs. 29, 30 (× 600) which show the effect of impurity on the growth layers on the cube faces. With even little impurity present cube faces appear, but the layers on the octahedral faces are unaffected, and growth continues at the same rate and in the same manner as previously described. But the layers on the cube faces are strikingly restricted and growth is much slower than that on the octahedral faces. Cube faces may occasionally be seen in pure solution growth, when the layer form is very much as that of the early rapid growth described for the octahedral faces, with building up and rapid breaking down of the visible layers which are irregular in shape. There is no restriction of the layers. However, with methylene blue in solution the layers become thicker and growth is strongly inhibited in a direction parallel to one of the diagonals of the face, while still free in the direction of the other diagonal. This produces striated growth and a fast rate of layer growth along the direction of the striations and a slow rate perpendicular to them. The surface becomes stepped with small tilts at the striation boundaries, reported by Buckley (1951) as being (451) index faces from measurements on a large crystal. Figures 31, 32 (× 600) show an octahedral face on a crystal growing in solution with methylene blue present. The tilt edges of the striations on the cube faces are shown by the intersection line with the neighbouring face. It is seen that the position of the tilted region has changed in the time between the two photographs moving towards the corner of the cube face as growth proceeds.

Acknowledgment

The author wishes to acknowledge the receipt of a grant from the Department of Scientific and Industrial Research which made this work possible.

References

Buckley, H. E., 1951, *Crystal Growth* (Chapman & Hall).
Bunn, C. W., and Emmett, H., 1949, *Disc. Faraday Soc.*, **5,** 132.
Burton, W. K., Cabrera, N., and Frank, F. C., 1951, *Phil. Trans.*, **234,** 299.
Emara, S. M., 1956, *Thesis* (University of London).
Forty, A. J., 1951, *Phil. Mag.*, **42,** 670 ; 1952, *Ibid.*, **43,** 72.
Frank, F. C., 1949, *Disc. Faraday Soc.*, **5,** 48 ; 1951, *Phil. Mag.*, **42,** 1014.
Halperin, A., 1954, *Proc. Phys. Soc.* B, **67,** 538.
Korndorffer, A., Rahbek, H., and Sultan, F. S. A., 1952, *Phil. Mag.*, **43,** 1301.

Work-Hardening and Work-Softening of Face-Centred Cubic Metal Crystals †

By A. Seeger, J. Diehl, S. Mader and H. Rebstock
Institut für theoretische und angewandte Physik der Technischen Hochschule Stuttgart, and Max-Planck-Institut für Metallforschung, Stuttgart, Germany

(Received August 7, 1956)

Abstract

The present paper investigates by experiment and theory the mechanisms governing work-hardening, work-softening and slipband formation in face-centred cubic metals. The rapid hardening stage (stage II) of the stress–strain curve is investigated by flow–stress measurements at different temperatures, combined tensile and torsion experiments, and by the observation of the length of slip lines as a function of prestrain. Stage III of the stress–strain curve and the work-softening phenomena associated with it are investigated with the electron microscope, showing that the principal surface patterns (slip bands, fragmentation) are due to cross slip. It is argued that in stage II the slip distance is decreased continually by the formation of Lomer–Cottrell dislocations. This also accounts for various observations on the end of the easy glide region. The temperature dependence of work-hardening in stage III is caused by screw dislocations circumventing the sessile Lomer–Cottrell dislocations by cross slip. The mechanisms through which cross slip causes glide band formation and fragmentation are discussed in some detail.

§ 1. Introduction

Recent studies of work-hardening of metals have concentrated on single crystals of face-centred cubic metals. It has proved useful to distinguish three stages of the stress strain curve which may be characterized as follows (fig. 1):

Stage I is the so called 'easy-glide' region. The coefficient of work-hardening $\theta = d\tau/d\epsilon$ is rather small, θ/G (G=shear modulus) being of the same order of magnitude as in typical hexagonal metals (Zn, Cd) at low temperatures. It is probably justified to consider the work-hardening mechanism in stage I as being analogous to the work-hardening in hexagonal metals.

The coefficient of work-hardening of stage II is about one order of magnitude larger than that of stage I and rather independent of the impurity content; stage II seems to be characteristic for all face-centred cubic metals. The observation that the stress strain curves of hexagonal metals do not show a stage with a correspondingly large coefficient of work-hardening suggests that stage II is connected with the capability of face-centred cubic metals to slip on intersecting glide-planes.

---

† Communicated by the Authors.

Stage III is characterized by a decrease of θ with increasing strain. From the temperature dependence of work-hardening it is obvious that in this stage the work-hardening process is partially balanced by a thermally activated process which will be called 'dynamical recovery'. It should be noted that this dynamical recovery proceeds during deformation even at temperatures where no static recovery is observed.

The main object of the present paper is an investigation of the *mechanisms of work-hardening* and *dynamical recovery* going on in stage II and stage III by experiment (work-hardening curves, combined tensile–torsion tests, surface observations by ordinary and electron microscope) and theory. We shall be but little concerned with stage I which is probably best investigated together with hexagonal metals such as zinc and cadmium. The small coefficient of work-hardening, its dependence on the diameter of the crystal (Paterson 1955, Suzuki *et al.* 1956)[†] and the appearance of very long (and rather faint) slip lines are best explained by assuming that in stage I the slip-distance of the dislocations is comparable with the diameter of the specimen (Mott 1952). We mention in passing that contrary to stage II the stress–strain curve in the easy-glide region is rather sensitive to structural irregularities (Diehl 1956 b).

Fig. 1

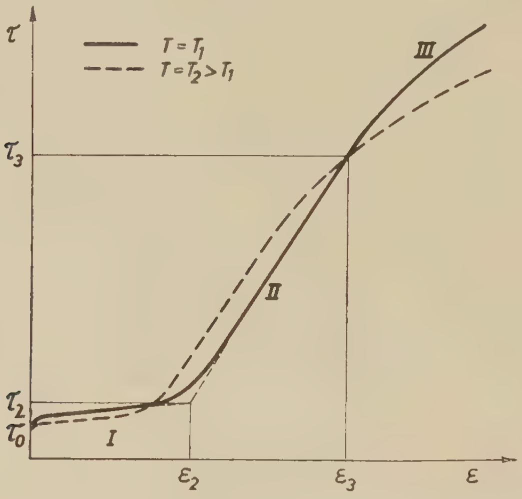

Schematic drawing of the typical shear stress–shear strain curve of a face-centred cubic metal at two different temperatures T_1 and $T_2 > T_1$.

[†] For a comparison of the data obtained by different authors see Diehl (1956 a).

§ 2. THE MECHANISM OF WORK-HARDENING IN STAGE II

2.1. *Survey*

The extent of the easy-glide region and therefore the strain ϵ_2 at which stage II begins depends very markedly on the orientation of the tensile axis with respect to the crystallographic directions of the crystal. ϵ_2 is smallest if the tensile axis is in a symmetric position. Several authors have suggested that the onset of rapid hardening at the beginning of stage II is due to slip in secondary glide-systems† (Masing and Raffelsieper 1950, Röhm and Diehl 1952, Lücke and Lange 1952, Haasen and Leibfried 1952). A rather striking argument in favour of such an explanation is the temperature dependence of ϵ_2 (Seeger 1954 a). We shall return to the theory of this observation later (§ 4.2).

A more detailed consideration of the *mechanism* through which slip in secondary glide-systems is able to increase the coefficient of work-hardening poses the following questions :

(1) Is the increased θ caused by a continuous admixture of slip in secondary glide-systems, or is the action of the secondary systems confined to the beginning of stage II only, as proposed by Friedel (1955)?

(2) Is the main effect of the secondary glide systems due to an increase in density of the dislocation forest which must be cut by the dislocations moving in the primary glide system (Paxton and Cottrell 1954) or is it of a more indirect nature due to the formation of obstacles which cannot be overcome by the dislocations in the primary glide-system with the aid of thermal energy ?

These problems have been attacked experimentally by a combination of tensile and twisting experiments on Cu single crystals. We preferred copper to aluminium because copper shows at room temperature all stages of the stress–strain curve fully developed, and because extensive data on the stress–strain curve of the same material are available (Diehl 1956 a). The main difference between the technique of Paxton and Cottrell (1954) and ours was that we avoided complications due to the elastic core during twisting by using tubular crystals. The external diameter of the crystals was 5·5 mm ; the thickness of the wall was 0·75 mm. For details concerning the preparation of the specimens reference should be made to Rebstock (1956).

Problem (1) was investigated mainly by measurements of work-hardening in tension after twisting (§ 2·2). The basic idea was to introduce by twisting 'artificially' additional dislocations in secondary glide-systems and to simulate thereby the anticipated effect of glide in secondary systems in stage II.

Problem (2) was investigated by measurements of the (reversible) change in flow stress connected with a change in temperature (§ 2.3).

---

† The octahedral glide-system with the largest resolved shear stress τ is called 'primary slip-system' ; all the other ones are denoted as 'secondary' slip-systems.

Both techniques were supplemented by observations of the surface appearance of deformed crystals (§ 2.4).

2.2. *Measurements of Work-Hardening*

Figure 2 gives some selected data on shear stress–shear strain curves, curve *A* corresponding to an ordinary tensile test. Curves *B* and *C* were obtained by tensile tests on crystals with the same crystallographic orientation as crystal *A*. At the strains indicated by arrows the specimens were unloaded, twisted without removal from the apparatus and reloaded in tension. It will be seen that a single twist increases the flow stress. There is no increase in the rate of hardening during the subsequent tensile test. Disregarding the behaviour of the stress–strain curve immediately after reloading in tension, it may be said that the principle effect of an intermediate twist in stage II of the work-hardening curve is a parallel displacement of the stress-strain curve towards higher shear stresses by an amount depending on the shear of the twist (see dashed part of *B* and *C*).

Fig. 2

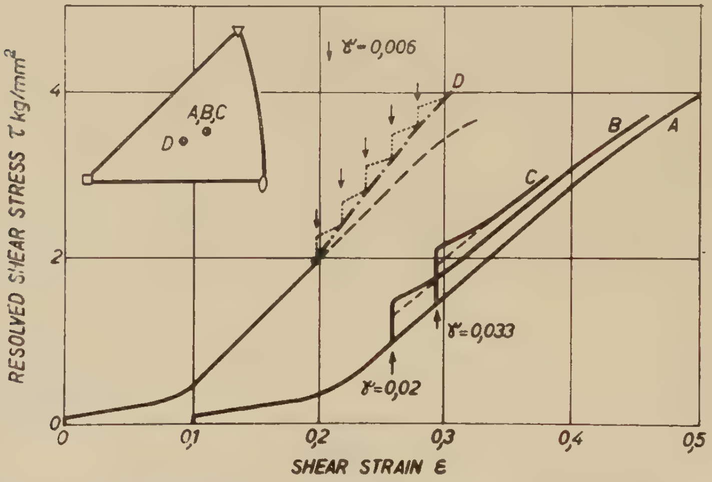

Tensile work-hardening curves of tubular copper crystals at room temperature: The origin of curves A is shifted by $\Delta\epsilon=0{\cdot}1$; *B* and *C* were shifted in addition to this in order to agree at $\epsilon=\epsilon_2$ with *A*. An arrow ↓ or ↑ indicates an interruption of the tensile test and a twist of the crystal, γ being the surface shear of the twist.

Contrary to what should be expected on the basis of Friedel's hypothesis, slip on secondary systems occurring only once does *not* result in an increase of the *rate of hardening*. Since however the *flow stress* is increased by such a procedure it may be expected that repeated twists and therefore repeated action of secondary glide-systems do give an increase in the average rate of hardening. This is verified experimentally by curve *D* in fig. 2. After a shear strain $\epsilon=0{\cdot}2$ in tension crystal D was repeatedly twisted by the same amount γ as indicated in fig. 2. The stress–strain curve obtained by the technique as discussed above does indeed show an increase of its mean slope after $\epsilon = 0{\cdot}2$. We conclude from these experiments that the increased rate of hardening in stage II is due to *continual slip* in secondary glide-systems.

2.3. *Reversible Change of Flow-Stress with Temperature*

The following discussion will be based on the theory of flow-stress given elsewhere (Seeger 1954 a, b, c, 1955 a). The flow-stress of a pure metal can be divided into two contributions τ_G and τ_S according to

$$\tau = \tau_G + \tau_S. \quad . \quad . \quad . \quad . \quad . \quad . \quad . \quad . \quad . \quad . \quad (1)$$

For a given dislocation pattern τ_G depends on temperature only indirectly through the temperature dependence of the shear modulus G (or other elastic constants) and has its main origin in the long range stress fields of the dislocations of the primary glide-system. τ_S is the contribution of the dislocation forest threading the primary glide-plane. Leaving aside certain corrections, τ_S depends linearly on the absolute temperature T. Figure 3 gives the division of τ into τ_S and τ_G as a function of shear strain ϵ for a single-crystal of copper at room temperature. These results were obtained (see Rebstock 1956) by measuring the flow-stress after changing the temperature between $T_1 = 90°\text{K}$ and $T_2 = 293\ \text{K}$.

Fig. 3

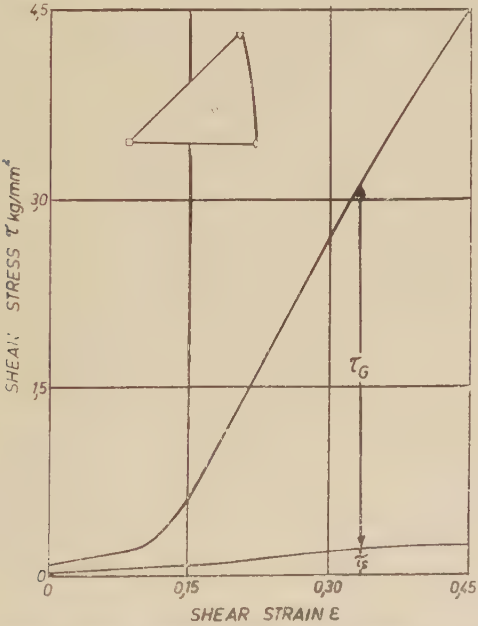

Division of the stress–strain curve of a copper crystal deformed in tension at room temperature into τ_G and τ_S.

and were evaluated using the theory of flow-stress as given for Cu (Seeger 1955 a) and the temperature dependence of the shear modulus as calculated from single crystal elastic constants (Overton and Gaffney 1955). Figure 3 shows that whereas τ_S and τ_G are of comparable magnitude in stage I the relative contribution of τ_S to the flow-stress is substantially reduced in stage II. This difference between stage II and the beginning of plastic deformation is shown even more directly (with hardly any theory intervening) in fig. 4, which gives the difference of the flow-stress τ_{90} at $T_1=90°\text{K}$ and τ_{293} at $T_2=293°\text{K}$ as measured by change-in-temperature tests, plotted against τ_{293}. The data corresponding to the end of stage II agree with those derived from the experimental results of Adams and Cottrell (1955). This is rather satisfactory since these measurements relate mainly to stage III. For small strains we were unable to confirm the assertion of Adams and Cottrell (1955) that the ratio of the temperature dependent part of the flow stress to the total flow stress is independent of the prestrain.

Fig. 4

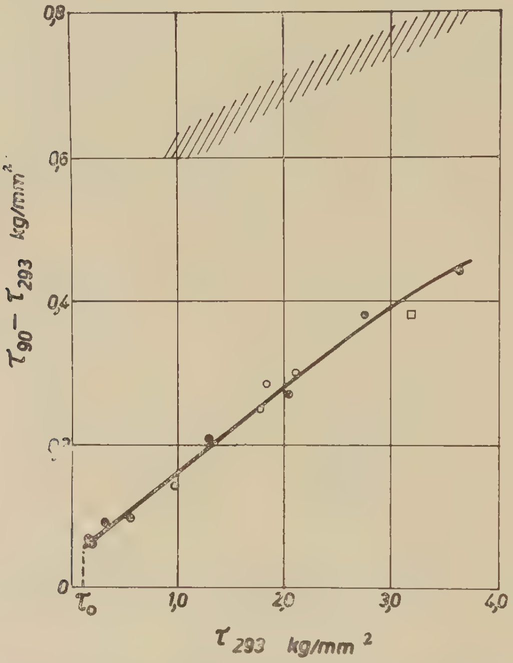

Change in flow-stress accompanying a change in temperature between 90°K and 293°K as a function of the flow-stress at 293°K for copper single crystals. Full circles were obtained in tension alone, empty marks after one or two intermediate twists. The hatched area indicates which experimental points would have been obtained if the increase in flow stress after a twist corresponding to a surface shear $\gamma=0{\cdot}02$ had been due to an increase in τ_S only.

From the results of the tests with change of temperature we conclude that the increased rate of hardening in stage II is *not* due to a substantial increase in the density of the dislocation forest. This is not surprising since the observations on the change in crystal orientation during slip (Taylor and Elam 1925, v. Göler and Sachs 1929, Sachs and Weerts 1930) show that only a rather limited amount of slip in secondary glide systems occurs before the onset of double-slip. If slip in secondary glide systems is at all responsible for the increased hardening of stage II it must cause (indirectly through the formation of obstacles to dislocation movement which cannot be overcome with the aid of thermal energy) an increase in τ_G. Whether this is so or not can be investigated by measuring the temperature dependence of flow-stress after twisting.

Figure 4 contains also those results that were obtained in *tension after twisting*. They do *not* differ from those obtained without twisting. This implies that the division of the total flow-stress into the contributions by τ_G and τ_S remains practically unchanged by an intermediate twist, i.e. that the slip on secondary systems results mainly in an increase of τ_G. This holds even for large twists, since the data at $\tau_{293}=3{\cdot}2$ kg/mm^2 (indicated by a square) was obtained after a twist corresponding to a (surface) shear of $\gamma=0{\cdot}1$. The other data were obtained with twists corresponding to shears between $\gamma=0{\cdot}01$ and $\gamma=0{\cdot}02$. The shaded area in fig. 4 indicates which experimental values would have been obtained if the observed increase of flow-stress by twists of $\gamma=0{\cdot}02$ were due to an increase in τ_S only.

We may summarize the *conclusions* drawn in §§ 2.2 and 2.3 as follows: The rapid hardening in stage II and the increase of flow-stress after intermediate twists are both due mainly to an increase of τ_G. This is explained by the capacity of slip on secondary glide systems to form obstacles which hinder slip in the primary slip systems rather effectively. (The nature of these obstacles will be discussed in § 4.2.) The results presented in §2.2 show that the formation of these obstacles must occur continually during stage II (and not only at the beginning of this stage). We expect therefore a continual reduction of the slip distance during stage II. This can be checked experimentally by surface observations.

2.4 *Length of Slip-Lines*

The discussion of this section will be based on the assumption that the surface markings of deformed face-centred cubic metals correlate with the slip and hardening mechanism in the bulk of the material. This seems to be well justified in view of the results of other investigations in which such a correlation could be established (Diehl *et al.* 1955, Müller and Leibfried 1955, Seeger 1956 a). The following observations were obtained by dark field illumination with an ordinary microscope. Comparison with electron microscopy work showed that the 'slip-lines' visible under these conditions in stage II were arrangements of individual lines, the length of which is about half that visible in the optical microscope.

In order to observe the variation of slip-distance with strain we have to study what we call the 'active length of slip-lines' l. This is the average length of slip-lines *formed* at a certain strain. In the present case where the active length of slip-lines decreases with increasing strain it is rather different from the average of the length of all slip-lines that were formed during the prestrain. For this reason we adopted the method of Blewitt *et al.* (1955) (in its simplest form first employed by Crussard 1945). It consists of polishing electrolytically the crystal after various prestrains ϵ, thereby removing all traces of the previous deformation, and observing the surface pattern after a strain increment $\Delta\epsilon$. Figures 5 (*a*)–(*f*) are photographs obtained by this technique from the same crystal ($\chi_0=49°$; $\lambda_0=52°$ in the notation of Schmid and Boas 1935) after various amounts of prestrain in tension. Figure 5 (*a*) shows the very long slip-lines of stage I (prestrain $\epsilon=0$). Figures 5 (*b*) and 5 (*c*) were taken in stage II with prestrains $\epsilon=0{\cdot}1$ and $\epsilon=0{\cdot}2$. Figures 5 (*d*), 5 (*e*) and 5(*f*) were obtained in stage III with prestrains of $\epsilon=0{\cdot}3$ and $\epsilon=0{\cdot}6$. They show the phenomenon of 'fragmentation' (slip-lines appear to be interrupted, the fragments being displaced sideways), to which we shall return later (§ 3.3).

Fig. 6

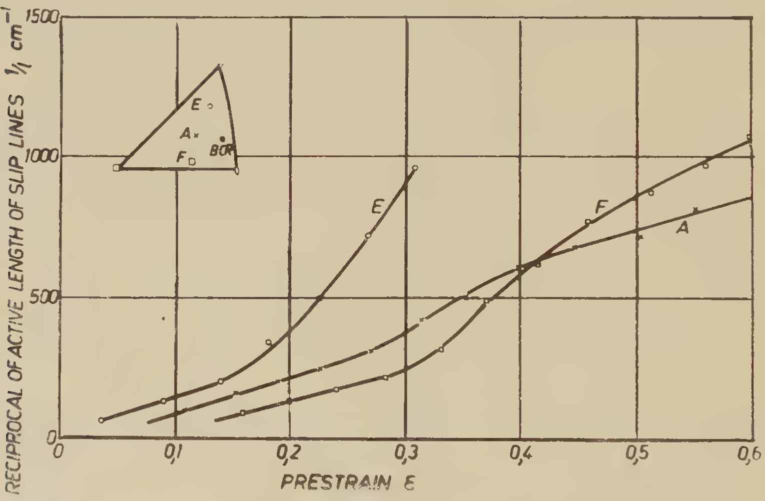

Reciprocal of active length of slip lines l of copper crystals as a function of (shear–) prestrain in tensile tests at room temperature. Additional shear strains after polishing $\Delta\epsilon=0{\cdot}05$. The orientations of the tensile axis of crystals *A*, *E*, and *F* are as indicated in the stereographic triangle.

It can be seen from these photographs that the active length of slip-lines does indeed decrease with increasing prestrain. Following Blewitt *et al.* (1955) we have plotted in fig. 6 $1/l$ (as observed on the top surface of the crystal after $\Delta\epsilon=0{\cdot}05$) versus shear strain. In stage II this results in straight lines, the slope of which does not depend markedly on crystal orientation. At larger prestrains we note a somewhat stronger decrease of the active length of slip-lines with strain, the details depending on the

Fig. 7

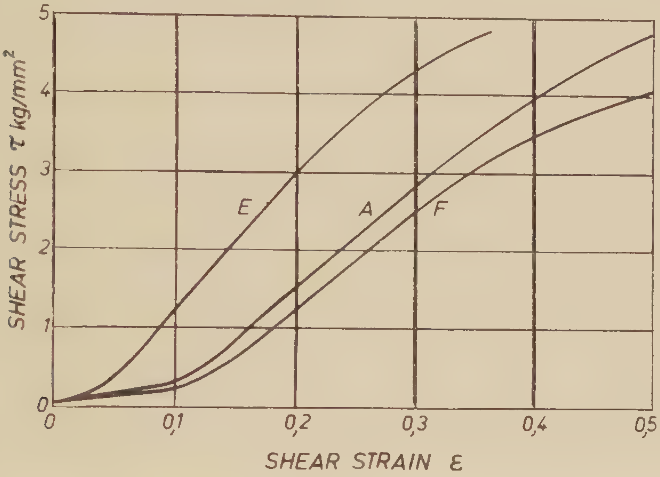

Work-hardening curves of the crystals *A*, *E*, and *F* shown in fig. 6.

Fig. 8

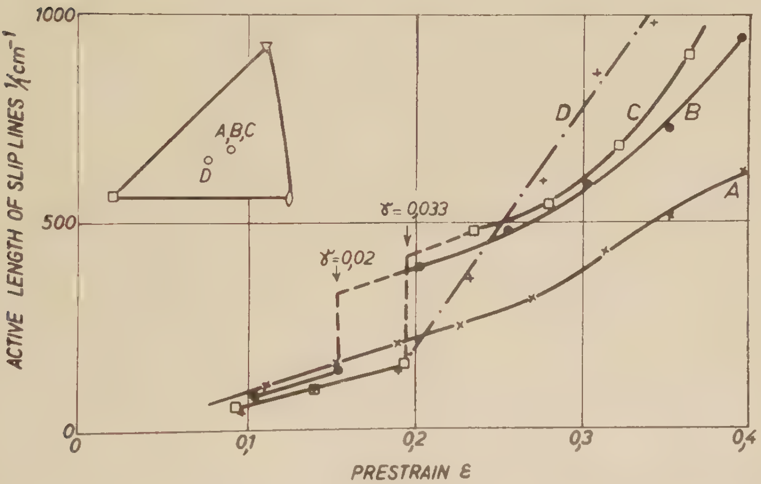

Reciprocal of active length of slip lines of a function of prestrain obtained with an additional strain of $\Delta\epsilon = 0{\cdot}05$ after one twist (*B* and *C*) or with two twists (*D*). The stress-strain curves are given in fig. 2.

orientation of the crystals. A comparison with the stress-strain curves of these crystals (fig. 7) suggests that the deviation from the straight line starts at the beginning of stage III. In stage III fragmentation of slip lines occurs (see § 3.3). In stage III we have taken l equal to the length of the individual fragments (compare figs. 5 (*d*) and 5 (*e*)), following Blewitt *et al.* (1955). The experimental results given by these authors resemble those of crystal (A), although their crystal had a somewhat different crystallographic orientation (indicated by BCR in the stereographic triangle in fig. 6). The rise of $1/l$ with strain is not very marked for these orientations. This may explain why Blewitt *et al.* (1955) described the relationship between $1/l$ and ϵ as being linear over the whole range of stages II and III.

Figure 8 contains the results that were obtained after twisting and refers to the same crystals as the stress–strain curves in fig. 2. It will be seen that the effect of intermediate twists on $1/l$ is analogous to that on the work-hardening curve. A single twist in stage II results in a shift of the graph to larger $1/l$ values; repeated twists however (curve D) give an increased slope of the $1/l$ versus ϵ plot[†]. We may therefore say that the observation of the surface markings have confirmed the conclusions drawn above on the basis of mechanical measurements.

§ 3. DYNAMICAL RECOVERY AND WORK-SOFTENING IN STAGE III

3.1. *Survey*

As was clearly shown by the results of Blewitt *et al.* (1955) on the variation of the stress–strain curve of copper single crystals on temperature, and as may also be derived from the data of Andrade and Henderson (1951) on other face-centred cubic metals if proper allowance is made for the dependence of the shear stress–shear strain curve on orientation, the slightly temperature-dependent stage II is followed by stage III of the stress–strain curve which depends strongly on temperature. Increasing the temperature shifts the shear stress τ_3 (fig. 1), at which stage III replaces stage II, to smaller values. A straightforward interpretation is that in stage II the dislocated structure of face-centred cubic metals varies with plastic deformation but is independent of temperature. This has the consequence that τ_G is also independent of temperature (if we neglect the temperature variation of the elastic constants). A temperature dependence of the slope θ of the stress–strain curve may arise through a variation of the density of the dislocation forest with strain (Seeger 1954 a, 1954 b).

The very small temperature variation of θ in stage II in copper crystals is in full agreement with the experimental result (see § 2.3) that the increase in density of the dislocation forest is rather small†. Since at the transition to stage III no abrupt change in the division of flow-stress into τ_G and τ_S is observed, we conclude that the temperature dependence of stage III is due to the change in the dislocated structure with strain (and thereby also $d\tau_G/d\epsilon$) being temperature dependent. Since unloaded copper crystals do not show mechanical recovery at room temperature, this change in the dislocation pattern during plastic deformation must be due to the combined effects of temperature and applied stress. Such a change is of course irreversible and is thus distinguishable from the reversible change of τ_S accompanying a change in temperature. The irreversible changes manifest themselves clearly in the phenomenon of 'work-softening', studied in some detail on aluminium crystals by Cottrell and Stokes (1955). It seems to be generally agreed that the mechanism responsible for the work-softening phenomenon is the same as that causing the temperature dependence of τ_G in stage III of the work-hardening curve. There are mainly two proposals for this mechanism :

[†] For $\epsilon \gtrsim 0{\cdot}2$ this curve was obtained by polishing after the prestrain indicated in fig. 8, twisting by $\gamma = 0{\cdot}006$, straining by $\Delta\epsilon \sim 0{\cdot}02$ in tension, twisting by $\gamma = 0{\cdot}006$, straining again by $\Delta\epsilon \sim 0{\cdot}02$ in tension and observing the length of the slip lines in dark field illumination. By a suitable choice of the conditions of illumination it was possible to eliminate the effect of the slip-lines formed in torsion thereby retaining the slip-lines formed in tension only. For further details see Rebstock (1956).

1. Diehl *et al.* (1955) have proposed and seconded by observations on the formation of slip bands in face-centred cubic metals that stage III is characterized by screw-dislocations *surmounting* obstacles in the primary glide system by cross slip.

2. Friedel (1955) and Cottrell and Stokes (1955) have proposed that the temperature dependence is caused by dislocations *breaking through* obstacles on their glide-planes.

The main object of this paragraph is to decide experimentally which of these proposals is the correct one. We shall show, mainly by use of the electron microscope, that the empirical results are in agreement with the cross slip hypothesis but not with the breakdown hypothesis.

3.2. *Formation of Slip Bands*

Before attacking the questions outlined in § 3.1 we shall briefly discuss the formation of slip bands. As was first shown by Heidenreich and Shockley (1948) and later studied in detail by other authors (Brown 1952, Wilsdorf and Kuhlmann-Wilsdorf 1952 a, b) the strong 'slip-lines' visible on the surface of polished aluminium crystals deformed at room temperature can be resolved by the electron microscope into a cluster of individual slip-lines. Henceforth we shall refer to these individual lines, whether clustered into slip bands or occurring as isolated lines, as slip lines.

For some time it was believed that these broad slip bands were typical for deformed face-centred cubic metals. Diehl *et al.* (1955) were able to demonstrate that they are typical for stage III only. They showed that aluminium crystals deformed at the temperature of liquid oxygen, and copper and nickel crystals deformed at or below room temperature do not exhibit clustered slip bands but a pattern of rather evenly spaced individual slip-lines of varying depth, provided the plastic deformation was not too extensive (fig. 9 and fig. 10). By polishing and strain-increment experiments slip band formation was shown to be a stage III phenomenon (fig. 11 and fig. 12).

---

† There may be metals (aluminium as a face-centred cubic metal with high stacking-fault energy being possibly one of them) where because of the small latent hardening (Seeger 1956 c) the dislocation forest contributes significantly to the increase of the flow-stress with prestrain. This would give rise to a temperature dependence of the work-hardening coefficient in stage II.

The correlation of the first appearance of slip bands with increasing strain and the beginning of stage III for various metals and different temperatures was so close in these experiments that it was very natural to conclude that the formation of slip bands is caused by the same process that is responsible for the temperature dependence of τ_G as discussed above (Diehl *et al.* 1955). Cross slip had indeed been proposed earlier as a possible basic mechanism for slip band formation (Koehler 1952 a, b. Leibfried and Haasen 1954, Seeger 1955 b).

The reason why on aluminium crystals deformed at room temperature (or above) slip bands form at rather early stages of deformation is as follows: At a given temperature $\tau_3 G$ depends on the stacking-fault energy of a metal (see Seeger 1955 c) in such a way that it is the smaller the higher the stacking-fault energy of the metal under consideration †. The stacking-fault energy of aluminium is so high that τ_3 at room temperature is of the same order of magnitude as τ_2, stage II of the work-hardening curve thereby reducing virtually to an inflexion point in the stress-strain curve. Aluminium crystals show therefore typical stage III behaviour already after rather small deformations at room temperature.

3.3. *Fragmentation of Slip Bands*

Blewitt *et al.* (1955) have demonstrated that the slip markings visible on copper crystals in dark field illumination in an optical microscope extensively deformed at room temperature show 'fragmentation' (see e.g. figs. 5 (*d*) and 5 (*e*)). By a detailed investigation of this phenomenon we found that extensive fragmentation occurred only if the deformation was carried right into stage III. In stage II no fragmentation was observed. The beginning of the fragmentation appears to be connected with the rise of the $1/l$ versus ϵ graph (compare fig. 6).

Since the beginning of fragmentation seems to be related to the beginning of stage III ‡ it was thought worth while to investigate fragmented slip bands by the electron microscope. The electron microscope employed in the experimental part of this paper was an Elmiskop I (manufactured by Siemens Berlin, maximum voltage 100 kv). Three typical photographs are shown in figs. 13, 14, and 15. They were obtained from a copper crystal that was polished after a prestrain of $\epsilon \sim 0{\cdot}6$ at room temperature, strained in addition by an increment in shear strain of $\Delta\epsilon \sim 0{\cdot}05$, and treated with the same replica technique as used by Diehl *et al.* (1955). The replicas were shadowed with palladium in such a way that the projection of the shadowing direction on the surface of the replica formed a rather acute angle with the traces of the primary glide system.

---

† The stress–strain curve for Al at −185°C in fig. 2 of (Diehl *et al.* 1955) has been misdrawn; in reality stage III begins at $\tau_3 = 1{\cdot}4$ kg/mm^2.

‡ This is in line with the observation of Blewitt *et al.* (1955) that copper crystals deformed at 4·2°K show neither stage III nor fragmentation.

Figure 13 shows that fragmentation patterns may indeed contain traces of one of the secondary slip-planes. In this case as well as in all similar ones these traces coincided with the trace of the cross slip $\{111\}$—plane as predicted from the crystallographic orientation of the crystal. Figure 14 shows that between the adjacent ends of two fragments traces of both the primary and the cross-slip plane may occur in a kind of ' staircase pattern '. Figure 15 was included to demonstrate that sometimes only the primary slip-plane can be observed. Comparing this set of photographs there can be little doubt that these traces are also connected by cross slip, the cross slip lines however being so weak that they could not be made visible by our technique. A general idea of the strength of the cross slip lines between two fragments may be obtained by observing that the method of shadowing was such as to favour the cross slip traces. We conclude from this that the individual cross slip lines are rather weak as compared with the slip lines of the primary slip-system contained in the slip bands. Sometimes one gets the impression that the cross slip is distributed over a certain region rather than concentrated into individual lines (see e.g. fig. 16).

Comparing the fragmentation of the type shown in fig. 15 with the clustering of slip-lines into bands, one gets the impression that there is an intimate relation between them. The mechanism by which they are formed could well be the same. The electron microscope techniques at present available give little hope that cross slip between the slip lines of a slip band can be made visible. Since however slip bands and fragments are of closely related appearance and since both of them begin to occur at the beginning of stage III we feel justified in concluding that the formation of slip bands is due to cross slip. This conclusion had been reached earlier on the basis of somewhat more indirect arguments (Diehl *et al.* 1955, Seeger 1955 b).

The general impression from both ordinary microscope and electron microscope photographs is that in stage III the dislocations overcome the obstacles in the primary glide-plane not by breaking through them as supposed by Friedel (1955) and Cottrell and Stokes (1955) (see the discussion in § 3.1) but by surmounting and circumventing them. This argument can be made quantitative on the basis of the results presented in fig. 6. As already mentioned the active length of slip lines l in stage III was taken equal to the length of those portions of slip bands that follow a unique trace of a slip plane, counting the fragments separately. On the basis of the breakdown mechanism l should start to increase at the beginning of stage III. The experimental results show that contrary to this the onset of stage III is marked by an *accelerated decrease* of l. Even if it is admitted that the possibility of some of the weaker slip-lines invisible in stage II becoming visible through their sideways growth into slip bands might contribute to this acceleration it may be said that this observation contradicts flatly the breakdown hypothesis.

3.4. *Work-Softening*

It was already recognized by Cahn (1951) on the basis of investigations with the optical microscope that cross slip may be a prominent process in the deformation of aluminium single crystals at elevated temperatures. The surface patterns called cross slip by Cahn can be made very pronounced even at normal temperatures by work-softening of aluminium crystals (Cottrell and Stokes 1955, Kelly 1956). The work-softening procedure consists in prestraining a crystal at a lower temperature, until a flow-stress τ is reached which at a higher temperature would correspond to stage III. If the crystal is unloaded, warmed up to this higher temperature and strained again a stress–strain curve of the type shown in fig. 17 is observed. The explanation is that the work-hardened state reached at the lower temperature is unstable under the combined action of the higher temperature and the applied stress τ. We have already mentioned in § 3.1 that the mechanism by which the unstable part of τ_G is reduced in work-softening is thought to be the same as that responsible for the decrease of the rate of hardening in stage III.

Fig. 17

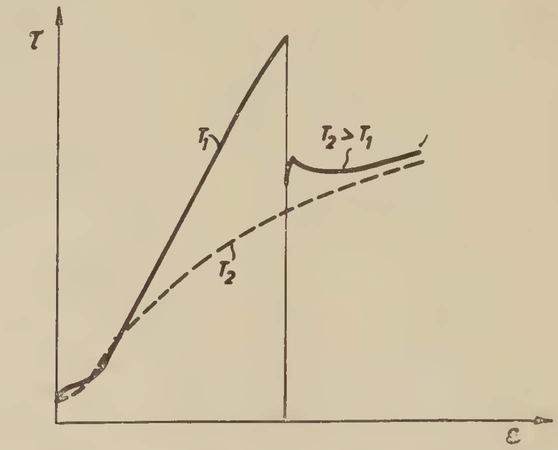

Stress-strain curves of a face-centred cubic metal crystal showing the phenomenon of work-softening when changing the temperature of the tensile test from T_1 to a higher temperature T_2. The dotted line gives the stress-strain curve at T_2. (Schematic.)

Figures 18 and 19, which were obtained on aluminium crystals prestrained at the temperature $T_1 = 90°\text{K}$ as shown schematically in fig. 17, polished, and further strained at room temperature (T_2), give the typical surface appearance of a work-softened crystal. At small magnifications the slip-bands appear wavy in the ordinary microscope (fig. 18). Larger magnification (fig. 19) shows that the slip-bands consist of straight pieces connected with what has been termed ‘ prominent cross slip ’ by Cahn (1951)†.

It must be stressed that this type of cross slip visible under the optical microscope only rarely follows the trace of the cross slip plane. Sometimes it does not appear to follow at all the trace of a crystallographic plane but to be of a non-crystallographic nature. In some cases Cahn was able to resolve such non-crystallographic cross slip into a zig-zag pattern by using high magnification of the ordinary microscope.

Definite results on these problems which can be used to discriminate between various theories of work-softening can be obtained by the electron-microscope. Figure 20 shows an electron micrograph of ‘ non-crystallographic ’ cross slip. It will be seen that it is resolved into a ‘ stair-case ’ of slip on the primary slip plane and on one of the secondary planes. The trace of the secondary slip plane was identified in this (and in all other cases investigated) as that of the cross slip plane. This is strikingly demonstrated in fig. 21, which is an electron micrograph of an aluminium crystal that showed double slip during work-softening. Slip bands were formed both by the primary slip system (dark traces) and by the conjugate slip system (white traces). The primary slip system and the conjugate slip system have their cross slip planes in common. The glide directions of the cross slip systems are different however. This is borne out in fig. 21. The cross slip traces of both types of slip lines are parallel. Since the glide directions in these traces and therefore also the nature of the surface steps are different they appear in different colours due to the shadowing technique. In the cross slip pattern of aluminium crystals work-softened at room temperature and not suitably oriented for double slip we never observed more than two different slip-planes, corresponding to the primary slip plane and the cross slip plane.

Cross slip can be made visible in the optical microscope also on copper crystals, as shown in figs. 22 (*a*), (*b*). They were obtained by prestraining $\epsilon = 0{\cdot}6$ at the temperature of liquid oxygen, polishing, and work-softening at 300°c with an additional average strain of $\Delta\epsilon = 0{\cdot}05$. As was to be expected the cross slip is less marked than on aluminium crystals work-softened at room temperature. This is confirmed by the electron micrograph fig. 23, which shows an appearance intermediate between the fragmentation of copper crystals deformed at room temperature (compare fig. 13 to 15) and aluminium crystals work-softened at room temperature (compare figs. 20 and 21).

---

† We think that the so-called ‘ intimate cross slip ’ observed by Cahn (1951) on aluminium is essentially the same phenomenon as the fragmentation discussed in § 3.3. It was resolved by Wilsdorf and Kuhlmann-Wilsdorf (1952 b) with the electron microscope into individual lines of cross slip, which were also rather weak compared with the slip lines clustered into bands.

We were unable to find on work-softened face-centred cubic metal crystals those very long slip bands (or slip-lines) that can be observed by the optical microscope on plastically deformed single crystals of zinc and that would be expected if work-softening were due to a break down of barriers in the primary glide plane. The surface pattern was always determined by a wavy or fragmented appearance of slip bands which with the aid of the electron microscope could be resolved into a sequence of slip in the primary slip system and in the cross slip system. This shows that under the conditions of work-softening (i.e. high temperature and high stresses) it is rather easy for the dislocations to change over from their primary slip plane to their cross slip plane and back again to the primary plane. The observations on work-softened crystals therefore fit very well into the picture which we have drawn for the processes responsible for the dynamical recovery in stage III.

Fig. 24

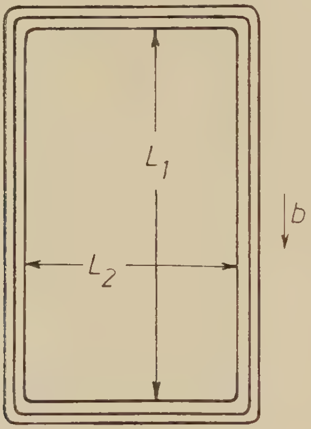

Rectangular dislocation loops. L_1 and L_2 are slip distances of edge and screw dislocations.

§ 4. THEORETICAL DISCUSSION

4.1. *General Discussion of Work-Hardening*

The discussion of our experimental findings as given in § 2 and § 3 was of a somewhat phaenomenological nature. For example, we have been talking of the effect of glide in secondary glide-systems on the propagation of slip in the primary glide system etc. Our present task is to translate these results into the language of dislocation theory and to fit them into a unified picture of the dislocation processes during the plastic deformation of face-centred cubic metal crystals.

We have seen that the flow-stress $\tau(\epsilon)$ of a metal crystal can be divided into two contributions τ_G and τ_S according to eqn. (1). In general τ_S is inversely proportional to the mean distance between dislocation lines penetrating the primary slip plane and therefore proportional to the square-root of the density of these dislocations (Seeger 1954 a, 1955 a). τ_G is somewhat more difficult to interpret quantitatively. It may be said however that it is the larger the smaller the mean distance between dislocations in the primary glide system is. The coefficient of work-hardening due to τ_G, which will be denoted by $\theta_G \equiv d\tau_G/d\epsilon$, is related to the mean slip distance L of dislocations in the primary glide system. The strain increment is proportional to the product of the density of gliding dislocations and the slip-distance. The increase in flow-stress however is independent of the distance L slipped by the dislocations before they get stuck in the crystal. θ_G is therefore small for large L and *vice versa*.

In § 1 we have briefly mentioned the characteristic features of stage I. Both the very long and rather weak slip-lines and the small coefficient of work-hardening (in typical cases of pure metals θ/G being of the order 2×10^{-4} to 10^{-3}) are readily explained by assuming that the mean slip-distance of the dislocations in stage I is rather large (of the order of 0·01 cm to 0·1 cm).

To simplify the following discussion of slip-distances and work-hardening we consider the dislocation rings in the glide plane to have the shape of rectangular loops. The slip-distances of edges and screws in such a loop are denoted by L_1 and L_2. The total number of such loops per unit volume is called N.

The observations reported in figs. 6 and 8 give the active length of slip lines l on the top surface of the crystal. We put them equal to twice the mean-slip distance L_2 of screw dislocations. Accordingly the active length of slip lines on the side surface will be identified with twice the slip-distance L_1 of the edge dislocations. The procedure of correlating the length of slip lines as observed on the surface of the crystal with the slip-distances of the dislocations in the bulk of the material is justified by the consistency of the results we shall obtain on the basis of this assumption presently.

Our observations of l gave $l=0{\cdot}20$ cm at the beginning of stage II (fig. 6). This is in good agreement with the discussion of stage I given above. During stage II $l/2$ (for which we now write L_2) decreases with increasing strain according to the law

$$L_2=\Lambda_2/(\epsilon-\epsilon^*) . \quad . \quad . \quad . \quad . \quad . \quad . \quad . \quad . \quad (2)$$

ϵ^* is slightly smaller than ϵ_2 and shows a similar dependence on crystal orientation as this quantity. A typical numerical value for a crystal in the central part of the orientation triangle is $\Lambda_2=4\times10^{-4}$ cm.

The available observations on the length of slip lines on the side surface are less detailed than those on the top surface, since the first mentioned type of slip-lines is more difficult to observe. It can however be said that they were always about twice as long as those on the top surface. We can therefore write

$$L_1 = \Lambda_1/(\epsilon - \epsilon^*) \quad . \quad . \quad . \quad . \quad . \quad . \quad . \quad . \quad (3)$$

with $\Lambda_1 \sim 2\Lambda_2$.

In copper crystals deformed at room temperature, stage II of the work-hardening curve can be well represented by a straight line (Blewitt *et al.* 1955, Diehl 1956 a). According to the discussion in § 2.3, θ is not very different from θ_G in this case. It seems to be a reasonable extrapolation from experiment to consider θ_G to be constant in stage II. The constancy of θ_G and the validity of the empirical law eqns. (2) and (3) can be related and understood with the following model of work-hardening (Seeger 1956 a).

θ_G is considered to be due to stress fields around statistically distributed groups of a small number of dislocations. The amplitude of the stress field generated by the edges of the dislocation loops can be written as

$$\tau_G = \alpha_1 bG(NL_2)^{1/2}. \quad . \quad . \quad . \quad . \quad . \quad . \quad . \quad . \quad (4)$$

NL_2 is the number of edge-dislocations of one sign per unit area and is therefore inversely proportional to the square of the mean distance between these edge dislocations. α_1 takes care of the numerical factors involved. It depends on the details of the geometrical arrangement of the dislocations, in particular on the effective number n of dislocations in the dislocation groups. This quantity is characterized by saying that the far reaching stress field around such a group is that of a single dislocation of strength nb. If τ_G is due to a distribution of individual dislocation lines ($n=1$) which is probably a good approximation to the situation in undeformed crystal (see Seeger 1954 a, c), α_1 should be of the order 1/5. In the present case we expect $\alpha_1 = 1/5\, n^{1/2}$. The infinitesimal increase $d\epsilon$ of the shear-strain due to dN dislocation loops per unit volume moving through the slip-distances L_1 and L_2 is given by

$$d\epsilon = bL_1 L_2\, dN. \quad . \quad . \quad . \quad . \quad . \quad . \quad . \quad . \quad . \quad (5)$$

When these loops get stuck in the crystal they will contribute to the stress field in the crystal and therefore cause a change in τ_G. The work-hardening coefficient of this change is

$$\frac{d\tau_G}{d\epsilon} = \frac{\alpha_1 Gb}{2}\left\{\frac{dN}{d\epsilon}(L_2/N)^{1/2} + \frac{dL_2}{d\epsilon}(N/L_2)^{1/2}\right\}. \quad . \quad . \quad (6)$$

If we eliminate L_2 and N from eqn. (6) with the aid of eqns. (2), (4), and (5), we obtain the differential equation

$$\frac{d\tau_G}{d\epsilon} = \frac{\alpha_1^2 Gb}{2\Lambda_1} \cdot \frac{\epsilon - \epsilon^*}{\tau_G} - \frac{1}{2}\,\frac{\tau_G}{\epsilon - \epsilon^*}. \quad . \quad . \quad . \quad . \quad . \quad . \quad (7)$$

The general solution of this equation is

$$\tau_G^2 = \frac{C}{\epsilon - \epsilon^*} + \alpha_1^2 G^2 \frac{b}{3\Lambda_1}(\epsilon - \epsilon^*)^2. \quad . \quad . \quad . \quad . \quad . \quad . \quad (8)$$

Since the stress at the beginning of stage II must be finite we have to put the constant of integration C equal to zero. The physically admissable solution of eqn. (8) is a linear stress–strain curve with the coefficient of work-hardening

$$\theta_G \equiv \alpha_1 \, . \, G \, . \left(\frac{b}{3\Lambda_1}\right)^{1/2}. \qquad \qquad (9)$$

The same type of treatment holds for screw-dislocations with suffixes 1 and 2 interchanged.

The observed coefficient of work-hardening of face-centred cubic metals is in stage II of the order $\theta_G=4\times10^{-3}\,G$. Inserting the Λ_1-value given above we find from eqn. (9)

$$\theta_G/G=\alpha_1 \, . \, 3\times10^{-3}. \qquad \qquad (10)$$

We conclude that α_1 is of the order 1 and n therefore of the order 20 to 25[†]. The implication that n does not vary very much with strain in stage II is in line with the result of Blewitt *et al.* (1955) on the electrical resistivity due to dislocations as a function of flow-stress. The electrical resistivity is under very general assumptions proportional to the number of dislocations per unit area[‡]. The experimental result is that it is proportional to the square of the flow-stress both in stage II and in stage III. This shows directly that eqn. (4) with α_1 fixed is applicable not only in stage II but also in stage III. A more complicated expression than eqn. (5) will have to be used for the strain-increment in stage III in order to allow for the contribution of the glide in the cross slip system.

4.2. *Formation of Obstacles to Slip in the Primary Glide-Plane : Lomer–Cottrell Dislocations*

From studies of the change of orientation with strain it is known that slip on secondary systems contributes very little to the glide in face-centred cubic crystals the orientation of which is in the interior of the stereographic triangle. In stage II the number of dislocations in secondary glide-systems is therefore in general small compared with the total number. The large effect that those dislocations have on θ_G must therefore be due to a 'catalytic' action. We have already (§ 2.3) pictured this as the formation of obstacles in the primary glide-plane which cannot be overcome with the help of thermal energy under the stress conditions of stage II. Such obstacles would decrease the slip-distances L_1 and L_2 and thereby increase the coefficient of work-hardening. The only type of obstacle in face-centred cubic metals known at present which fulfils these requirements is a special kind of sessile dislocation, the so called Lomer–Cottrell dislocation (Lomer 1951, Cottrell 1952). Lomer–Cottrell dislocations were used in the discussion of work-hardening by Mott as early as 1952 (Mott 1952) and later by Leibfried and Haasen (1954). They play also an essential rôle in the views on work-hardening and work-softening held by Cottrell and Stokes (1955) and Friedel (1955).

[†] This numerical estimate is not too reliable since the ratio between the active length of slip lines and the mean slip-distance may be somewhat different from two.

[‡] For recent discussions of the effect of dislocations on the electrical resistivity of monovalent metals see Seeger and Stehle (1956) and Seeger (1956 b).

Lomer–Cottrell dislocations are formed along the intersection of two $\{111\}$-planes and lie therefore along $\langle 110\rangle$-directions. The detailed arrangement of partial dislocations and stacking-faults is as shown in fig. 25. (This is the most important type with which we shall solely be concerned. Further types which are less ' stable ' are discussed by Haasen (1953) and Friedel (1955).) The essential feature is that the stacking-fault ribbon ' bends over ' from one octahedral plane to another. The combination of partial dislocations is confined to both of these planes and can therefore neither glide nor climb away from the line of intersection of these planes. Since these sessile dislocations can be removed only with a considerable expenditure of energy they form effective obstacles to the glide motion of dislocations meeting them.

Fig. 25

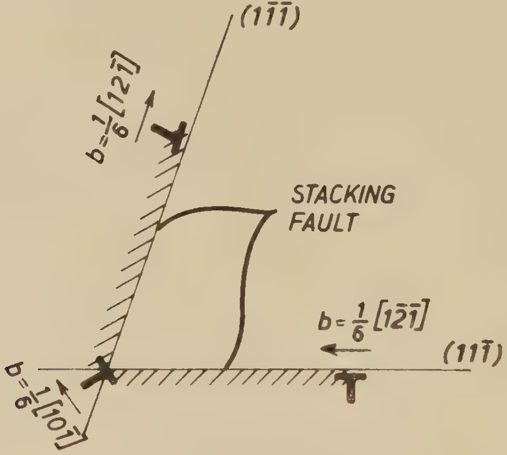
$(1\bar{1}\bar{1})$
$b=\frac{1}{6}[12\bar{1}]$
STACKING FAULT
$b=\frac{1}{6}[1\bar{2}\bar{1}]$
$(11\bar{1})$
$b=\frac{1}{6}[10\bar{1}]$

Lomer–Cottrell sessile dislocation, consisting of three partial edge dislocations connected by stacking fault ribbons.

The Lomer–Cottrell dislocation shown in fig. 25 can be formed in two ways, namely either by the reaction of a dislocation of type† 1/2 $[0\bar{1}\bar{1}]$, $(11\bar{1})$ with one of type 1/2 $[110]$, $(1\bar{1}\bar{1})$, or by a reaction between 1/2 $[1\bar{1}0]$, $(11\bar{1})$ and 1/2 $[01\bar{1}]$, $(1\bar{1}\bar{1})$. The dislocations of such a pair attract each other through their long-range stress fields. The Lomer–Cottrell dislocation formed as the result of the dislocation reaction between the dislocations of each of these pairs is 'stable' because energy is required to decompose it into the original dislocations and to separate these from each other.

---

† We denote here dislocations by giving their Burgers vectors and their glide planes. They are understood to run parallel to the Lomer–Cottrell dislocation.

The following discussion will be based on the convention that the primary glide system is 1/2 [101], (111). This is the octahedral system of maximum shear stress if the tensile direction lies in the interior of the triangle cross hatched with two perpendicular sets of lines (fig. 26).

Fig. 26

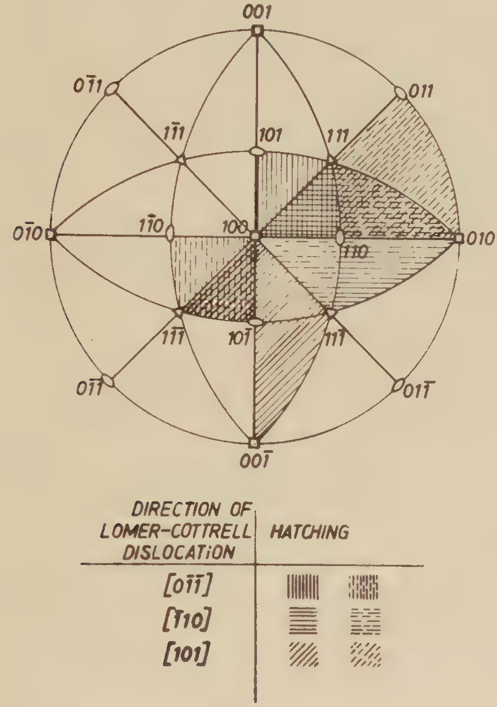

Combinations of glide-systems capable of yielding Lomer–Cottrell sessile dislocations. The direction of the Lomer–Cottrell dislocation is indicated by the direction of hatching.

The range of orientations in which the shear stress is a maximum in the other glide-systems with glide plane (111) are also cross hatched. The dislocations of the glide-systems with glide-plane $(11\bar{1})$ can form Lomer–Cottrell dislocations with those glide-systems whose triangles of maximum shear stress are hatched by the same set of lines†. The direction of the Lomer–Cottrell dislocation is uniquely related to the direction of hatching and is the same for full and for dotted lines as indicated in fig. 26.

---

† There are 12 octahedral glide systems and 24 triangles in the graph of fig. 26. Therefore two triangles of maximum shear stress belong two each of these glide-systems. We have hatched both triangles of such a pair only in the case where both are neighbours to the triangle belonging to the primary glide system.

Figure 26 is useful for a qualitative discussion of the relative resolved shear stress in different glide-systems. The smaller the distance between the point representing the tensile axis and one of the triangles belonging to a certain glide system, the larger is the resolved shear stress in this glide-system. For quantitative graphical representations see Diehl *et al.* (1954).

For the generation of an appreciable number of Lomer–Cottrell dislocations of a certain crystallographic direction it is prerequisite to have enough mobile dislocations of the types cooperating in their formation. This will be the case if the ‘ effective ’ resolved shear stress (applied shear stress minus the latent hardening in the slip system concerned) acting on these dislocations is larger than the critical shear stress. Since not very much is known about the latent hardening in stage I the following discussion is qualitative only and does not allow for the differences in the latent hardenings of different glide-systems.

Extending the idea first proposed by Röhm and Diehl (1952) we think that the transition from stage I to stage II begins when the applied stress becomes large enough to generate for the first time a considerable number of dislocations in secondary glide-systems which are able to form Lomer–Cottrell dislocations lying in the main glide-plane. This stress will in general, e.g. in copper, depend on temperature, since at least part of these dislocations have to cut the forest of dislocations in the primary glide-systems which has been built up during stage I. The resolved shear stress in the secondary systems corresponding to an appreciable production of dislocations increases with decreasing temperature. Since the slope of the easy glide region of the stress–strain curve is roughly independent of temperature this means that at a given orientation of the tensile axis the easy glide region should extend to larger strains ϵ_2 at lower temperatures than at higher ones (Seeger 1954 a). This is exactly what is observed experimentally (see fig. 1).

With the present picture it is possible to understand the variation of ϵ_2 with the crystallographic orientation of the tensile axis, too. The orientation dependence of ϵ_2 in the case of copper single crystals deformed at room temperature is given in fig. 27 taken from Diehl (1956 a). Its characteristic feature is that the largest values ϵ_2 occur for orientations in the [110]-corner of the orientation triangle but excluding the [110]-direction and its immediate neighbourhood. This is contrary to the orientation dependence of the critical shear stress which takes its minimum values in the *middle* of the stereographic triangle (see fig. 27). Our explanation of the variation with crystal orientation is as follows : In the whole region adjacent to the plane $(01\bar{1})$ (which contains the [100]-direction and the [111]-direction) there is a tendency to form those Lomer–Cottrell dislocations characterized in fig. 26 by the hatching with vertical full lines. They require dislocations in only one of the secondary systems, namely the so-called conjugate system. In the immediate neighbourhood of the [110]-direction of the tensile axis there is a tendency to form those Lomer-Cottrell dislocations characterized by horizontal hatching either with full or with dotted lines by the combination of dislocation pairs in secondary glide-systems. In whatever direction the orientation of the tensile axis moves away from the [110]-pole into the interior of the stereographic triangle the tendency for the formation of this sort of Lomer–Cottrell dislocations will rapidly diminish since the resolved shear stress in at least one of the two glide-systems of each of the pairs will decrease. This accounts for the principal features of the experimental situation.

Fig. 27

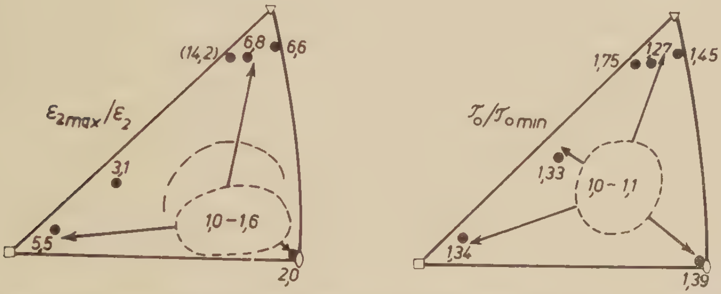

Dependence of $\epsilon_{2\max}/\epsilon_2$ and $\tau_0/\tau_{0\min}$ on the orientation of the tensile axis of copper crystals deformed at room temperature.

The end of the transition between stage I and stage II will presumably be reached when a sufficient number of Lomer–Cottrell dislocations in all of the three possible directions are formed. From there on the slope of the stress–strain curve is mainly determined by the rate of production of Lomer–Cottrell dislocations which must be such as to bring about the empirical law eqn. (2) for the variation of slip-distance with strain. These processes should be rather insensitive to the degree of perfection of the undeformed crystal, to its impurity content and to the diameter of the specimen. This agrees with the observations that for a given crystal orientation the work-hardening coefficient is very well reproducible in stage II. Its variation with crystal orientation is small compared with that of the length of stage I (Diehl 1956 a). This is understandable since so many secondary glide-systems cooperate in determining θ in stage II that a small dependence on the orientation of the tensile axis should result.

We have so far discussed the rôle of Lomer–Cottrell dislocations in holding up the dislocations moving in the primary glide plane and in determining the slip-distance and thereby also the coefficient of work-hardening in stage II. As was pointed out by Mott (1952), Lomer–Cottrell dislocations may significantly contribute to the stabilization of the deformed state against backward glide after unloading by forming obstacles in the rear of groups of dislocations piled up under the action of the applied stress. In our present picture this implies that the stability of the deformed state is less in the easy glide region where no Lomer–Cottrell dislocations are available than in stage II. We have found a striking confirmation of this view in a recent paper by Buckley and Entwistle (1956). These authors show in their fig. 8 that the rate of increase of the Bauschinger effect (measured in terms of the ' Bauschinger glide strain ' which is a measure for the instability of the deformed state under unloading or reversed loading) with increasing hardening is much larger in the easy glide region than in stage II and III of aluminium single crystals strained at room temperature.

4.3. *The Mechanism of Slip-Band Formation and Fragmentation*

The principal result of the discussion of experiments in § 3 was that the cross slip of screw dislocations is the governing process for the temperature dependence of the work-hardening in stage III, for the phenomenon of work-softening, for the formation of slip-bands, and for the fragmentation of slip-bands. The object of the present section is to consider some of the theoretical problems connected with these phenomena.

As pointed out earlier screw dislocations undergo cross slip in order to circumvent and surpass obstacles which they are unable to break through. The discussion in § 4.2 suggests that these obstacles are Lomer–Cottrell dislocations. The Lomer–Cottrell dislocations holding up screw dislocations are those which cannot be formed by dislocations of the primary glide system but require the cooperation of dislocations in the other glide-systems with the primary glide plane. It is therefore essential (Seeger 1956 a) not to restrict the discussion of Lomer–Cottrell dislocations to those formed by the dislocations in the primary system glide as was done by other authors.

Next we will take up the related problems of the detailed mechanism of cross slip and of the stability of Lomer–Cottrell dislocations against ' collapsing ' under the combined action of stress and temperature. Dislocations generated during plastic deformation in face-centred cubic metals are extended ones. They can undergo cross slip only if the two partial dislocations of an extended screw dislocations are brought together over a certain length. The resulting complete screw-dislocation may then separate into partials in the cross slip plane.

Lomer–Cottrell dislocations can give way to the pressure of a group of dislocations piled up against them in several ways which have been discussed by Stroh (1956). For our present purpose it suffices to consider that way with the lowest energy barrier. Its first step is to reunite over a certain length the partial dislocations which make up the Lomer–Cottrell dislocation. The calculations of the energy barrier (activation energy) involved is very similar to the calculation of the energy barrier of cross slip and will have to follow the lines indicated in a simple case by Schoeck and Seeger (1955), Seeger (1954 d). Since more detailed calculations of this type are still under way we will confine ourselves to a qualitative discussion of the relative magnitudes of the activation energies in both cases. The same stress component is involved in bringing together the partial dislocations of the screw dislocations and of the Lomer–Cottrell dislocations against which they are piled up. The lengths over which the recombination to complete dislocations has to be achieved depend on different components of the stress tensor but will not vary very much under typical conditions as shown by the calculations of Schoeck and Seeger (1954). The parameter which does determine the activation energies is the width of the stacking-fault ribbon between the partial dislocations involved. These widths are very much smaller in aluminium than they are in copper (or other low stacking fault energy metals) (Seeger and Schöck 1953). This implies that the activation energies for aluminium are much lower than those for copper under equivalent stress conditions. In a given material the width of the stacking-fault varies with the character of the complete dislocations. It is a minimum for screws and a maximum for edges. For Lomer-Cottrell dislocations it is somewhat smaller than for edges but still considerably larger than for screw dislocations. This has the consequence that the activation energy for cross slip is smaller than that for the collapse of Lomer–Cottrell dislocations, and that piled up groups of screw-dislocations will 'leak' by cross slip before they are able to break down the Lomer–Cottrell dislocations holding them up in the primary glide plane. The theoretical situation is therefore in agreement with the facts deduced from experiment.

The preliminary calculations so far available show that the temperature variation of τ_3 (being the resolved shear stress at which a noticeable rate of cross slip is reached) can be accounted for by the theory. The theory also explains fully the quantitative difference in the behaviour of aluminium and copper which is particularly obvious from the experimental results presented by Diehl *et al.* (1955). The empirical correlation with the magnitude of the stacking fault energy, though at that time based on much less complete experimental evidence than available now, was in fact the starting point for the work on slip bands presented here (Seeger 1955 a).

In §§ 3.2 and 3.3 we have presented the empirical evidence that the transfer of slip from one slip-line in a slip band to an adjacent one is due to cross slip. We shall now discuss possible mechanisms in some detail.

It follows from the preceding discussion that in stage III screw dislocations are pushed out by cross slip from the head of dislocation groups piled up against Lomer–Cottrell dislocations. The stress components at the head of such a pile up are proportional to the number of dislocations in the pile up (Eshelby *et al.* 1951). The strongest and longest slip-lines will therefore leak first. (In quantitative considerations one must take into account, however, that the number of dislocations effective in a pile-up will in general be considerably smaller than the number of dislocation rings in the slip-line due to the 'screening' effect of dislocations in the environment of the slip-line.) The dislocations in the cross slip plane will at first be pushed away from the group with a repulsive force varying roughly inversely proportional to the distance from the group. Later they will either get stuck in the work-hardened material, or they will meet another piled-up group of screw dislocations of the opposite sign. They will then annihilate with some of these, thereby giving the way free for more dislocations following the same way. Since the annihilated dislocations in the group just mentioned will in some cases be replaced from their source a weak slip line (say of the elementary structure type) may develop into a strong one. This mechanism is presumably stopped by the edges of the dislocation rings spreading in the cross slip plane. There are no dislocations groups with which they can annihilate ; they will therefore get stuck in the work-hardened material after a certain slip distance and create a pile-up the back stresses of which will eventually prevent further cross slipping. This accounts for the fact that the cross slip lines are rather weak as discussed in § 3.3. Since the stress magnification acting on dislocations which are not quite at the head of a pile-up is still large, these dislocations may undergo cross slip, too, thereby giving rise to more of these weak cross slip lines. This explains why one has frequently the impression that cross slip is spread out over an area rather than concentrated in strong lines.

The screw-dislocations which have not annihilated after having moved out of the primary glide plane by cross slip may under the action of shear stresses and temperature undergo once more cross slip back to the primary glide plane. Since by the argument given above the edges remaining in the cross slip plane will be held up somewhere the whole configuration forms a Frank–Read source in the primary glide plane and may by the Frank–Read mechanism generate a new slip line. This is (with modifications) the mechanism of " double cross slip " first envisaged by Koehler (1952 a, b). It should be mentioned that also a mixture might occur of the two mechanisms which we have discussed : the dislocations may annihilate after cross slipping back to the primary glide plane.

Depending on the scale on which these processes happen they may either lead to slip band formation or to fragmentation. If the new slip lines are formed within a few hundred Ångströms distance from the original one we observe clustering of slip lines into bands. If the dislocations slip farther away in the cross slip plane before creating a new line or making an existing one grow one obtains fragmentation. Both the ' double cross slip '—and the ' annihilation ' mechanism allow glide to proceed with a smaller increase in work-hardening than would correspond to stage II. They are therefore both able to account for the decrease of the work-hardening coefficient in stage III. The relative importance of the two mechanisms will depend on the conditions of stress and prestrain. If the material is very little work-hardened as is aluminium at the beginning of stage III at high enough temperatures double cross slip may well be important. In a highly work-hardened material however the annihilation mechanism should be predominant. It accounts in particular for the drop in flow-stress occurring during work-softening which in some way must be connected with the annihilation of dislocations which had contributed to the work-hardening.

We conclude with a few remarks on the conditions at large strains. As can be seen from fig. 24 of Diehl *et al.* (1955) at high enough strains there is no slip in the material between slip bands Slip proceeds by adding more lamellae to slip bands (and possibly also by growth of slip lines within the bands). The question may arise whether a slip-line at the edge of a band may be so weak and contain so few dislocations that none of these can be expelled by cross slip, thereby stopping the sideways growth of the band. The general impression is that bands continue to grow sideways with increasing strain. This is presumably due to the fact that the screw-dislocations in the interior of a band help to push out by cross slip the dislocations in the outer slip lines.

§ 5. Concluding Remarks

We shall not summarize here the conclusions concerning the various dislocation mechanisms in the work-hardening and work-softening phenomena of face-centred cubic metals reached in this paper. We should rather like to stress the unifying rôle played in these considerations by the *stacking-fault energy*. Dislocations generated during cold-work in face-centred cubic metals are extended ones, and their behaviour under the action of stress and temperature depends to a large measure on the width of the stacking-fault ribbons between the half dislocations. Until it was realized that aluminium, being a high stacking-fault energy metal, differs in this respect from other face-centred cubic metals such as copper, silver, gold and nickel it was impossible to integrate the seemingly conflicting evidence on the temperature-dependence of flow-stress, on the temperature-dependence and the shape of the work-hardening curve, on surface markings and slip-band formation into a unified picture valid for all face-centred cubic metals. We hope to have been able to develop such a picture, which of course still requires refinement by future investigations.

Acknowledgments

It is a great pleasure for the authors to thank Professor U. Dehlinger for his encouragement and for his kind interest in this work. They also acknowledge gratefully the financial support of the Deutsche Forschungsgemeinschaft.

References

Adams, M. A., and Cottrell, A. H., 1955, *Phil. Mag.*, **46,** 1187.

Andrade, E. N. da C., and Henderson, C. (1951), *Phil. Trans. Roy. Soc.*, A, **244,** 177.

Blewitt, T. H., Coltman, R. R., and Redman, J. K., 1955, *Rep. Conf. Defects in Solids* (London: Physical Society), p. 369.

Brown, A. F., 1952, *Advanc. Phys.*, **1,** 427.

Buckley, S. N., and Entwistle, K. M., 1956, *Acta Met.*, **4,** 352.

CAHN, R. W., 1951, *J. Inst. Met.*, **79,** 129.

COTTRELL, A. H., 1952, *Phil. Mag.*, **43,** 645.

COTTRELL, A. H., and STOKES, R. J., 1955, *Proc. Roy. Soc.* A, **233,** 17.

CRUSSARD, Ch., 1945, *Rev. Mét.*, **42,** 286.

DIEHL, J., 1956 a, *Z. Metallkde.*, **47,** 331 ; 1956 b, *Ibid.*, **47,** 411.

DIEHL, J., KRAUSE, M., OFFENHÄUSER, W., and STAUBWASSER, W., 1954, *Z. Metallkde.*, **45,** 490.

DIEHL, J., MADER, S., and SEEGER, A., 1955, *Z. Metallkde.*, **46,** 650.

DIEHL, J., and REBSTOCK, H., 1956, *Z. Naturforschung*, **11a,** 169.

ESHELBY, J. D., FRANK, F. C., and NABARRO, F. R. N., 1951, *Phil. Mag.*, **42,** 351.

FRIEDEL, J., 1955, *Phil. Mag.*, **46,** 1169.

v. GÖLER, K.-F., and SACHS, G., 1929, *Z. Phys.*, **54,** 666.

HAASEN, P., 1953, *Z. Phys.*, **136,** 26.

HAASEN, P., and LEIBFRIED, G., 1952, *Z. Physik.*, **131,** 538.

HEIDENREICH, R. D., and SHOCKLEY, W., 1948, *Rep. Conf. Strength of Solids* (London : Physical Society), p. 57.

KELLY, A., 1956, *Phil. Mag.*, **1,** 835.

KOEHLER, J. S., 1952 a, *Imperfections in nearly perfect crystals* (New York : Wiley & Sons), p. 146 ; 1952 b, *Phys. Rev.*, **86,** 52.

KUHLMANN-WILSDORF, D., and WILSDORF, H., 1953, *Acta Met.*, **1,** 394.

LEIBFRIED, G., and HAASEN, P., 1954, *Z. Phys.*, **137,** 67.

LOMER, W. M., 1951, *Phil. Mag.*, **42,** 1327.

LÜCKE, K., and LANGE, H., 1952, *Z. Metallkde.*, **43,** 55.

MASING, G., and RAFFELSIEPER, J., 1950, *Z. Metallkde.*, **41,** 65.

MOTT, N. F., 1952, *Phil. Mag.*, **43,** 1151.

MÜLLER, H., and LEIBFRIED, G., 1955, *Z. Phys.*, **142,** 87.

OVERTON, W. C., and GAFFNEY, J., 1955, *Phys. Rev.*, **98,** 969.

PATERSON, M. S., 1955, *Acta Met.*, **3,** 491.

PAXTON, H. W., and COTTRELL, A. H., 1954, *Acta Met.*, **2,** 3.

REBSTOCK, H., 1956, *Thesis*, T. H. Stuttgart, to be published in *Z. Metallkde.*

RÖHM, F., and DIEHL, J., 1952, *Z. Metallkde.*, **43,** 126.

SACHS, G., and WEERTS, J., 1930, *Z. Phys.*, **62,** 473.

SCHMID, E., and BOAS, W., 1935, *Kristallplastizität* (Berlin : Springer).

SCHÖCK, G., and SEEGER, A., 1955, *Rep. Conf. Defects in Solids* (London : Physical Society), p. 340.

SEEGER, A., 1954 a, *Z. Naturforschung*, **9*a*,** 870 ; 1954 b, *Phil. Mag.*, **45,** 771 ; 1954 c, *Z. Naturforschung*, **9*a*,** 758 ; 1954 d, *Ibid.*, **9*a*,** 856 ; 1955 a, *Phil. Mag.*, **46,** 1194 ; 1955 b, *Rep. Conf. Defects in Solids* (London : Physical Society), p. 328 ; 1955 c, *Encyclopedia of Physics*, Vol. 7/1 (Berlin-Göttingen-Heidelberg : Springer) ; 1956 a, *Colloquium on Deformation and Flow of Solids*, ed. R. Grammel (Berlin-Göttingen-Heidelberg : Springer), p. 90 ; 1956 b, *Can. J. Phys.*, **34,** 1219 ; 1956 c, *Z. Naturforschung*, **11*a*,** 958.

SEEGER, A., and SCHÖCK, G., 1953, *Acta Met.*, **1,** 519.

SEEGER, A., and STEHLE, H., 1956, *Z. Phys.*, **146,** 242.

STROH, A. N., 1956, *Phil. Mag.*, **1,** 489.

SUZUKI, H., IKEDA, S., and TAKEUCHI, S., 1956, *J. Phys. Soc. Jap.*, **11,** 382.

TAYLOR, G. I., and ELAM, C. F., 1925, *Proc. Roy. Soc.*, **108,** 28.

WILSDORF, H., and KUHLMANN-WILSDORF, D., 1952 a, *Z. angew. Phys.*, **4,** 361, 418 ; 1952 b, *Ibid.*, **4,** 409.

Intensity Fluctuations in Stationary Optical Fields†

By E. Wolf
The Physical Laboratories, University of Manchester‡

[Received October 11, 1956]

Introduction and Summary

It is the purpose of this note to show that the fluctuations in the instantaneous intensities at two arbitrary points in a stationary optical field are in general correlated and that this correlation is proportional to the square of the coherence function introduced into the theory of partially coherent fields by Blanc-Lapierre and Dumontet (1955) and independently by Wolf (1955). The result has a bearing on recent experiments by Hanbury Brown and Twiss (1956) in which fluctuations in the current output from two photoelectric cells situated close to each other and illuminated by an almost coherent beam of light were found to be correlated.

§ 1. A Theorem Concerning the Gaussian Random Process

The main result of the paper is an immediate consequence of a theorem on the two-dimensional stationary Gaussian random process, which we shall now establish.

Consider two random functions $X(t)$ and $Y(t)$ of time t and assume that the probability of finding X in the interval X, $X+\delta X$ and Y in the interval Y, $Y+\delta Y$ at any given instant is $P(X,\ Y)\delta X\delta Y$, where P is the two-dimensional Gaussian distribution

$$P(X,\ Y)=\frac{1}{2\pi\sqrt{(\mu_{11}\mu_{22}-\mu_{12}{}^2)}}\exp\left\{-\frac{\mu_{22}X^2+\mu_{11}Y^2-2\mu_{12}XY}{2(\mu_{11}\mu_{22}-\mu_{12})^2}\right\}. \quad (1.1)$$

Here $\mu_{ij}(i,j=1,\ 2)$ are the second moments defined by

$$\mu_{11}=\langle X^2\rangle,\quad \mu_{22}=\langle Y^2\rangle,\quad \mu_{12}=\langle XY\rangle, \quad . \quad . \quad . \quad (1.2)$$

sharp brackets denoting average value. We need not distinguish between a time average and an ensemble average as we are dealing with an ergodic ensemble.

It follows that the average value of the product X^2Y^2 is

$$\begin{aligned}\langle X^2Y^2\rangle&=\int_{-\infty}^{+\infty}\int_{-\infty}^{+\infty}X^2Y^2P(X,\ Y)\,dX\,dY\\&=\frac{1}{2\pi\sigma}\int_{-\infty}^{+\infty}\int_{-\infty}^{+\infty}X^2Y^2\exp\left\{-\frac{\mu_{22}X^2+\mu_{11}Y^2-2\mu_{12}XY}{2\sigma^2}\right\}dX\,dY,\end{aligned} \quad . \quad . \quad . \quad (1.3)$$

where

$$\sigma^2=\mu_{11}\mu_{22}-\mu_{12}{}^2. \quad . \quad . \quad . \quad . \quad . \quad . \quad . \quad . \quad . \quad . \quad . \quad . \quad . \quad . \quad (1.4)$$

---

† Communicated by Professor L. Rosenfeld.

‡ Now on leave of absence at the Institute of Mathematical Sciences, New York University.

To evaluate (1.3) we set

$$X=\sigma\sqrt{\left(\frac{2}{\mu_{22}}\right)}\xi, \quad Y=\sigma\sqrt{\left(\frac{2}{\mu_{11}}\right)}\eta. \quad . \quad . \quad . \quad (1.5)$$

We also set

$$\mu_{12}=-\sqrt{(\mu_{11}\mu_{22})}\cos\phi\,; \quad . \quad . \quad . \quad . \quad . \quad . \quad (1.6)$$

then

$$\sigma=\sqrt{(\mu_{11}\mu_{22})}\sin\phi. \quad . \quad . \quad . \quad . \quad . \quad . \quad . \quad . \quad (1.7)$$

Substitution from (1.5)–(1.7) into (1.3) gives

$$\langle X^2Y^2\rangle=-\frac{4\sigma^5}{\pi\mu_{11}{}^{3/2}\mu_{22}{}^{3/2}} \times\int_{-\infty}^{+\infty}\int_{-\infty}^{+\infty}\xi^2\eta^2\exp\left[-(\xi^2+\eta^2+2\xi\eta\cos\phi)\right]d\xi\,d\eta. \quad (1.8)$$

The integral on the right-hand side of (1.8) is well known ; its value is†

$$\int_{-\infty}^{+\infty}\int_{-\infty}^{+\infty}\xi^2\eta^2\exp\left[-(\xi^2+\eta^2+2\xi\eta\cos\phi)\right]d\xi\,d\eta=\frac{\pi[1+2\cos^2\phi]}{4\sin^5\phi}$$
$$=\frac{\pi[\mu_{11}\mu_{22}+2\mu_{12}{}^2]\mu_{11}{}^{3/2}\mu_{22}{}^{3/2}}{4\sigma^5} \quad . \quad . \quad . \quad (1.9)$$

Hence (1.8) becomes, if we also substitute from (1.2) :

$$\langle X^2Y^2\rangle=\langle X^2\rangle\langle Y^2\rangle+2\langle XY\rangle^2. \quad . \quad . \quad . \quad . \quad (1.10)$$

We also have the identity

$$\langle X^2Y^2\rangle-\langle X^2\rangle\langle Y^2\rangle=\langle \Delta X^2\Delta Y^2\rangle, \quad . \quad . \quad . \quad . \quad (1.11)$$

where

$$\Delta X^2=X^2-\langle X^2\rangle, \quad \Delta Y^2=Y^2-\langle Y^2\rangle. \quad . \quad . \quad . \quad (1.12)$$

From (1.10) and (1.11) we finally obtain

$$\langle \Delta X^2\Delta Y^2\rangle=2\langle XY\rangle^2. \quad . \quad . \quad . \quad . \quad . \quad . \quad . \quad (1.13)$$

The relation (1.13) implies that the fluctuations ΔX^2 and ΔY^2 are in general correlated and that this correlation is equal to twice the square of the correlation between X and Y.

§ 2. CORRELATION IN INTENSITY FLUCTUATIONS AT TWO ARBITRARY POINTS IN A STATIONARY OPTICAL FIELD

We now consider a stationary optical field and fix our attention on the disturbance at two points P_1 and P_2. For the sake of simplicity we shall regard the disturbance to be a real scalar, e.g. a rectangular component of the electric field vector.

Let $V_1(t)$ represent the disturbance at P_1 at time t and $V_2(t+\tau)$ the disturbance at P_2 at time $t+\tau$. Keeping τ fixed for the moment, we may regard V_1 and V_2 as the components of a two-dimensional vector which is the sum of a large number of independent random vectors (contributions from the randomly emitting atomic radiators that form the sources of the field). Under these circumstances the conditions of the central limit theorem† of the calculus of probability are effectively satisfied and consequently the joint probability distribution $P(V_1, V_2)$ may be assumed to be Gaussian. Hence we may apply the theorem (1.13), with $X(t)=V_1(t)$, $Y(t)=V_2(t+\tau)$. If we also set

---

† See, for example, Rice (1945), p. 69.

$$\left.\begin{array}{ll} I_1(t)=V_1^2(t), & I_2(t)=V_2^2(t), \\ \Delta I_1(t)=I_1(t)-\langle I_1(t)\rangle, & \Delta I_2(t)=I_2(t)-\langle I_2(t)\rangle, \end{array}\right\} \quad . \quad . \quad . \qquad (2.1)$$

we obtain

$$\langle \Delta I_1(t)\Delta I_2(t+\tau)\rangle = 2\langle V_1(t)V_2(t+\tau)\rangle^2. \quad . \quad . \quad . \qquad (2.2)$$

In the limiting case when the points P_1 and P_2 coincide and at the same time $\tau=0$, the discriminant $\mu_{11}\mu_{22}-\mu_{12}^2$ in (1.1) is zero; nevertheless the formula (2.2) retains its validity also in this case, as can be seen by considering the probability distribution for $X=V_1$ alone. One then obtains (dropping the common suffix)

$$\langle (\Delta I)^2\rangle = 2\langle I\rangle^2. \quad . \quad . \quad . \quad . \quad . \quad . \quad . \quad . \qquad (2.3)$$

The cross-correlation function

$$J_{12}(\tau)=\langle V_1(t)V_2(t+\tau)\rangle \quad . \quad . \quad . \quad . \quad . \quad . \quad . \qquad (2.4)$$

which occurs on the right-hand side of (2.2) and which is a generalization of the mutual intensity function of Zernike (1938) was introduced into the theory of partially coherent fields by Blanc–Lapierre and Dumontet (1955) and independently by the present writer (Wolf 1955). Morover, it was shown in the latter paper that *in vacuo*, the correlation function obeys rigorously the two wave equations

$$\nabla_s^2 J_{12}(\tau) = \frac{1}{c^2}\frac{\partial^2 J_{12}(\tau)}{\partial \tau^2} \quad (s=1, 2), \quad . \quad . \quad . \quad . \quad (2.5)$$

where ∇_s^2 is the Laplacian operator with respect to the coordinates of the point P_s. Thus although J is a quadratic function of the basic field variable (V), it behaves as the *amplitude* of a wave. By analogy with other wave theories one might have therefore suspected that J^2 should also possess a physical significance. Our formula (2.2) shows that J^2 is, in fact, *proportional to the correlation between the intensity fluctuations at the points P_1 and P_2, the intensity at P_2 being considered at time τ later than at P_1.*

To measure $J_{12}(\tau)$ one may isolate the vibrations at P_1 and P_2, for example by placing an opaque screen across the field, with two small openings at these points. From observations on the (time averaged) intensity some distance behind this screen, the values of $J_{12}(\tau)$ may be determined (Wolf 1955, pp. 252–253). In an important recent publication, Hanbury Brown and Twiss (1956) proposed a radically new method for the measuring of correlations between light beams. Here photoelectric cells are placed at P_1 and P_2 and the correlation between the fluctuations in the current output from the two cells is determined. Hanbury Brown and Twiss (1956, 1957) found (see also Kahn 1957) that in certain cases this correlation is closely related to the correlation that exists between the amplitudes V_1 and V_2. The principle of this method may at once be understood from the formula (2.2):

---

† See, for example, Rice (1944), p. 331.

A photocell measures effectively the square of the electric vector, so that under ideal experimental conditions the left-hand side of (2.2) and hence the amplitude correlation $J_{12}(\tau)$ may be determined by such an arrangement. In practice, one has not, of course, ideal square law detectors and ideal correlators, but instruments with finite resolving time (high-frequency cut-off). In consequence one cannot measure the correlation between the instantaneous values ΔI_1 and ΔI_2 but rather the correlation between certain weighted short-time averages $\overline{\Delta I_1}$ and $\overline{\Delta I_2}$. Moreover, at very low intensities, the quantum nature of the absorption process may play an important part. Nevertheless, the basic principle of the method proposed by Hanbury Brown and Twiss is clearly brought out by the relation (2.2), which also suggests that this method is of very general validity.

ACKNOWLEDGMENTS

It is a pleasure to thank Professor L. Rosenfeld for stimulating discussions. I am also indebted to Mr. R. Hanbury Brown, Dr. R. Q. Twiss and Dr. F. Kahn for allowing me to see manuscripts of their papers prior to publication.

This work was carried out during the tenure of an Imperial Chemical Industries Research Fellowship, the award of which, by the University of Manchester, is gratefully acknowledged.

REFERENCES

Blanc-Lapierre, A., and Dumontet, P., 1955, *Rev. Opt.* (*théor. instrum.*), **34**, 1.

Hanbury Brown, R., and Twiss, R. Q., 1956, *Nature, Lond.*, **177**, 27 ; 1957, in press.

Kahn, F., 1957, in press.

Rice, S. O., 1944, *Bell Syst., tech. J.*, **23**, 282 ; 1945, *Ibid.*, **24**, 46 (reprinted in *Selected Papers on Noise and Stochastic Processes*, ed. N. Wax, New York: Dover Publications, 1954).

Wolf, E., 1955, *Proc. Roy. Soc.* A, **230**, 246 ; see also *Il Nuovo Cimento*, 1954, **12**, 884.

Zernike, F., 1938, *Physica*, **5**, 785.

On the Formation and Properties of Helical Dislocations†

By S. Amelinckx, W. Bontinck, W. Dekeyser and F. Seitz
Laboratorium voor Kristalkunde der Rijksuniversiteit, Rozier, 6, Gent, Belgium

[Received August 20, 1956]

Summary

The factors influencing the development of helical dislocations found in CaF_2 by Bontinck and Amelinckx are discussed. At temperatures near and below 700° c the principal electrolytic current in CaF_2 appears to be carried by the negative ions. Thus climb of dislocations is difficult to produce as a result of processes inducing electrolytic flow. It is proposed that the positive ions carry a larger component of the current near 1200° c and that maintenance of the electrolytic currents induced during additive coloration produce what might be termed mild climb. Under this climb dislocations having a strong screw component are induced to assume a helical or spiral prismatic form as proposed earlier by Seitz. The model of F-centres in CaF_2 and their equilibrium characteristics are discussed. It is pointed out that helical dislocations should be generated in many materials under a wide variety of circumstances in which climb occurs and that such dislocations are, in principle at least, capable of generating whiskers when they occur sufficiently near the surface. Such whiskers would grow from the base and should possess many of the attributes found in the whiskers of this type which are observed in practice. It is proposed that controlled climb of any material may be produced with the use of an appropriate temperature gradient if the production or annihilation of lattice defects at the dislocations engenders climb and if the production lies in an attainable temperature range.

§ 1. Introduction

Bontinck and Dekeyser (1956) have demonstrated that dislocation lines in calcium fluoride can be decorated by the colloids formed during the precipitation of excess metal in additively coloured crystals. A fraction of the dislocations decorated after additive coloration at higher temperatures, near 1200° c, possess helical character and merit particular discussion. The axes of the helical dislocations appear to be preferentially oriented in the $\langle 110 \rangle$ directions, which presumably are also the directions of the Burgers vectors of the dislocations. As pointed out by Bontinck and Amelinckx (1957), they seem to be one species of the spiral prismatic dislocations proposed by Seitz (1950 a, b, 1952) in 1950 which can be formed by the addition or subtraction of molecules (climb) from a dislocation which is primarily, or at least strongly, of screw character. The spacing between successive turns of the helix is large compared to the Burgers vector in the cases observed in this laboratory. The purpose of this note is to discuss some of the circumstances surrounding the formation of helical dislocations in CaF_2 and to point out possible attributes of such dislocations, particularly their ability to form whiskers under appropriate conditions. It should be emphasized that although whisker growth has actually been observed on calcium fluoride in this laboratory, the conditions under which whiskers appear have not yet been clearly associated with spiral dislocations.

---

† Communicated by the Authors.

§ 2. ADDITIVE COLORATION OF CALCIUM FLUORIDE

Mollwo (1934) has found that CaF_2 may be additively coloured by the addition of excess calcium under conditions which resemble very closely those under which the alkali halides may be coloured. Both electrolysis and addition from the vapour or bulk metal are effective. Actually CaF_2 appears to accept excess calcium far more readily than the alkali halides accept alkali metals. Mollwo has presented a figure (Mollwo, 1934, fig. 6) which indicates that the concentration of excess calcium varies in the manner $A \exp(-E/kT)$ with temperature. Here as usual, A and E are constants, k is Boltzmann's constant and T is the absolute temperature. The experimental values of the concentration of excess metal were determined by various investigators in four different ways over four ranges of temperature extending from 300°c to the melting point at 1360°c. The constant E was found to be nearly the same as the heat of sublimation of elemental calcium (about 48 kg cal per mol), however the constant A was about 10^4 times larger than the corresponding constant in the expression for the density of atoms in the equilibrium vapour of the metal.

In any event, the experiments show that deviations from stoichiometry of the order of 1% or more can be obtained by additive means at appropriate temperatures near 1000°c. The decrease in mass density of the crystals during such addition suggests that, when atomically dispersed, the stoichiometric excess is present in the form of fluorine-ion vacancies to which electrons are attached. In fact Mollwo used this assumption to determine the concentration of excess metal in the corresponding range of temperature. Unfortunately, the lattice parameter measurements which should be made in conjunction with density measurements to test this model have not yet been carried out. As an alternative, it is possible that the excess metal is present interstitially. It is evident that the order of the reaction governing solution of the metal in the salt would be different in the two cases because of the divalent character of calcium and the monovalent character of fluorine. We shall discuss the nature of the colour centres further below after considering other evidence.

When appropriately quenched from high temperatures, the additively coloured crystals exhibit two prominent absorption bands, provided the concentration of added metal exceeds that of the miscellaneous impurities present, which seem to be of the order of 10 or more parts per million in the typically good crystals available at present. One of the bands, designated the α band by Mollwo, occurs near 3·3 ev (3850Å) and appears to be the analogue of the F band. The other, termed the β band, is near 2·3 ev (5200Å) and seems to be the analogue of the R or M band as in the alkali halides, although the information available concerning its properties are meagre. Lüty (1953) has shown that many of the bands observed by Smakula in x-rayed specimens are the result of combination of the α and β centres with the foreign agents present in the best crystals available at present.

Additive coloration has been produced in the crystals studied in this laboratory by heating with calcium and by heating either in the presence of hydrogen or sodium. Sodium has been used in the manner developed by Rexer (1932) and employed by Amelinckx (1956) in the case of sodium chloride. Presumably the treatment with hydrogen or with the alkali metal produces partial reduction and a relatively moderate density of excess metal. The extinction coefficient at the peak of the α band attains values of the order of several mm^{-1} in quenched specimens, corresponding to concentrations of centres between 10^{17} and 10^{18} per cm^3. More intense darkening can be obtained with the use of calcium. The decoration of dislocations can be observed in specimens darkened at 700°c, however the helical dislocations have been observed only in specimens darkened at higher temperatures, in the vicinity of 1200°c.

Other observations on x-ray darkened crystals appear in publications of Barile (1952), Smakula (1953, 1954), Schulman *et al.* (1952), Urbanck (1951) has studied photoconductivity, whereas Deïgen (1951) has given a theoretical treatment of double centres at high concentrations. Feofilov (1953) considered the F-centres to be anisotropic, situated in the crystals with a definite orientation.

CaF_2 is a moderately good ionic conductor. For example, Smakula (1950) has found conductivities of the order of 10^{-13} $(\text{ohm cm})^{-1}$ at 100°c which are comparable to the conductivities of alkali halides of normal purity. The question of the sign of the carrier in the halides of the divalent metals has been a topic of general discussion for an extended period and it now appears that Ure (1956)† has demonstrated that the negative ions carry the bulk of the current in the range from room temperature to 900°c, the disorder corresponding to Frenkel defects (i.e. vacancies and interstitial ions) in the fluorine lattice. This has been established by studying the electrical properties of crystals doped with NaF and with YF_3. The first addition presumably enhances the density of F-ion vacancies and the second the density of interstitial F ions. Ure has found that the activation energy for migration of the vacancies is $20 \pm 1{\cdot}5$ kg cal per mol at 200°c and decreases to about 12 ± 1 kg cal per mol at 600°c. The activation energy for migration of interstitials is 38 ± 8 kg cal per mol in the range between 640° and 920°c. He has found that the energy of formation of the defects is about 32·6 kg cal per mol in the same range of temperature, this being twice the activation energy for formation of the defects, presumably by a bimolecular process.

---

† We are indebted to Professor Smakula for providing us with an account of this work.

It may be worth noting at this point that the positions occupied by the interstitial fluorine ions in the simple cubic lattice of the normal fluorine ions found in CaF_2 presumably are body-centred ones. Half of such positions are occupied by calcium ions. Thus the ideal free volume available is equivalent to that of a calcium ion. The radius of a fluorine ion is about 30% larger than that of a calcium atom (about 1·33 *A*, compared to 1·06). Hence the fit is tight, but not unreasonably so.

Actually, Ure's results seem to be in excellent accord with the results of older work (Hauffe 1955) which may be summarized as follows. First the transport numbers of the negative constituents of the halides of divalent metals are usually close to unity (Tubandt 1932). PbI_2 seems to provide an exceptional case among the salts studied. Second, the conductivity of the salts can be enhanced (Gyulai 1931, Seith 1929) by the addition of the alkali halides. This is the case for example when NaCl is added to $PbCl_2$. Presumably the alkali ion enters substitutionally and is matched by a halogen ion vacancy. This procedure has been used by Ure in the work quoted above. Third and probably closer to the problem at hand, Zintl and Udgard (1939) have found that when appreciable quantities (33·5%) of YF_3 are added to CaF_2, the Y ions enter substitutionally in the CaF_2 lattice and the extra F ions are located in interstitial positions which are probably the normally unoccupied body centred positions in the simple cubic lattice of fluorine ions. Zintl and Udgard have drawn the same conclusion for the system SrF_2–LaF_3 and the system CaF_2–ThF_4. Ure has used the properties of YF_3 additions in his work.

In view of the existing evidence, it seems safe to conclude that the most common defects affect only the halogen lattice and are of the Frenkel type. It may be noted in passing that the activation energy for migration of the carriers in Smakula's specimens is about 0·9 ev which is close to the value Ure obtained for the halogen ion vacancies. It is not possible to state whether the carriers are vacancies or interstitial fluorine ions.

It follows that the transport and structural work supports the view that the colour centres formed by adding excess calcium are halogen vacancies in which electrons are bound. In the range where the electrolytic conductivity is essentially exclusively the result of the migration of halogen ions, the process of colouring additively by diffusion from the surface would appear to involve the simultaneous migration of electrons and halogen ion vacancies from the surface into the volume and of interstitial ions to the surface. The flow of halogen ion vacancies should be the most important of the two modes of migration of the fluorine ion if Ure's activation energies are valid. The additional calcium ions and the halogen ions brought to the surface by the creation of halogen ion vacancies there or by the migration of interstitial ions to the surface form new layers of the salt. It seems natural to suggest that this mechanism of additive colouring operates exclusively in the lower range of temperature near 700°c. Unless some of the calcium atoms diffuse into the crystal along dislocations, which emerge at the surface, and form F-centres within the crystal by giving up the valence electrons and capturing interstitial fluorine ions, so as to induce climb of the dislocation, there is no good reason for expecting a change in the dislocation pattern during the colouring process. Ultimately, when the crystal is cooled and the F-centres form colloids the existing edge dislocations will be decorated. The condensation of F-centres may then cause climb of the dislocations, but we shall assume this effect is small.

The specimens which are darkened at higher temperatures, near 1200°c, display helical dislocations and hence give evidence that climbing does occur at the higher temperature. It is possible that such climb is the result of the diffusion of calcium atoms along dislocations in the manner described above. However it seems much more likely that the lattice of the metal ion begins to become disordered at the higher temperature. A pair of interstitial fluorine ions may be converted into a calcium ion vacancy at a dislocation. Although this process is endothermic, it is evident that entropy will be gained because of the disordering of the Ca-ion lattice once interstitial halogen ions become abundant. Thus it seems entirely reasonable to suppose that a fraction of the lattice defects present near 1200°c are positive ion vacancies.

Once positive ion vacancies become available as carriers, a part of the electron current from the surface may be neutralized by a flow of positive ion vacancies to the surface. This component of compensating current is particularly important because the electrons will have a tendency to become bound at the halogen ion vacancies and immobilize them in part. New positive and negative ion vacancies will be generated at dislocations (and other sources such as voids, if present) to replace those which are consumed by diffusion to the surface or by conversion to F-centres. Thus the dislocations are induced to climb as a result of the presence of a subnormal concentration of vacancies of both types. Some climb presumable would occur merely as a consequence of heating and the production of the normal equilibrium density of positive ion defects at the higher temperatures, but the climb will be enhanced by additive coloration. During slow cooling, the positive ion vacancies which do not migrate to the surface or become involved in F-centres should return to the sources, which then act as sinks. In an uncoloured crystal, one might expect the climb of dislocations when they act as sources during heating to be balanced by the climb in the opposite direction when they act as sinks, although a redistribution of material from one part of the lattice to another could be associated with irreversible changes in the dislocation pattern. On the other hand, one should always expect an irreversible climb during the process of additive coloration at higher temperatures if the mechanism postulated here in which a part of the electrolytic current countering that of the electrons is carried by positive ion vacancies is valid. The magnitude of the irreversible climb should depend upon the intensity of coloration.

Let us now return to the problem of the origin of the high density of colour centres which can be obtained in CaF_2. We shall assume that they consist of halogen ion vacancies which are neutralized by single electrons and that two such centres are formed for each excess calcium added to the crystal. We shall also assume that the cohesive energy of the electron to the F-centre is of the order of 1·5 ev, so that the fraction which are ionized under equilibrium conditions at 1200°c is not sufficient to affect the order of the reaction

$$\text{Ca (atom)} \rightleftharpoons 2\ \text{F-centres.} \qquad . \quad . \quad . \quad . \quad . \quad . \quad . \qquad (1)$$

We shall adopt a reference state in which the free energy of a calcium atom in the metal is zero at absolute zero of temperature and is r_m, a positive quantity, at the energy of formation of F-centres. The chemical potential of an atom in the vapour will be taken in the form

$$r_v=\epsilon_v+kT\log(c_v/C) \qquad . \quad . \quad . \quad . \quad . \quad . \quad . \quad . \qquad (2)$$

in which c_v is the number of atoms per unit volume of the vapour and C is equal to $(2\pi MkT/h^2)^{3/2}$ in which M is the mass of the calcium atom, k is Boltzmann's constant, T is the absolute temperature and h is Planck's constant. The corresponding chemical potential for a Ca atom dissolved in the crystal to form two F-centres will be taken in the form

$$r_c=\epsilon_c+2kT\log(2c_c/\kappa N_0) \qquad . \quad . \quad . \quad . \quad . \quad . \quad . \qquad (3)$$

in which c_c is the concentration of excess calcium atoms in the crystal of CaF_2 and κ is a parameter, presumably of the order of 100 which takes account of the additional entropy gained by the crystal over and above the mixing entropy N_0 is the density of fluorine sites in the crystal. The quantities ϵ_v and ϵ_c are the heats of formation associated with the calcium atoms in the vapour and CaF_2, respectively.

We may determine the density of atoms in the vapour from the relation $r_v=r_m$ and the partition of calcium atoms between vapour and crystal from the condition $r_v=r_c$. If we use these equations to determine the ratio c_c/c_v, we obtain

$$c_c/c_v=(N_0/2C)\exp\{(2\epsilon_v-\epsilon_c-r_m)/2kT\}. \qquad . \quad . \quad . \quad . \quad . \qquad (4)$$

If we accept Mollwo's relation, according to which this ratio is approximately 10^4 over a wide range of energy, we may conclude that

$$\epsilon_c\simeq 2\epsilon_v=96\ \text{kg cal per mol} \qquad . \quad . \quad . \quad . \quad . \quad . \quad . \quad . \qquad (5)$$

and

$$(N_0\kappa/2C)\exp(-r_m/2kT)\simeq 10^4. \qquad . \quad . \quad . \quad . \quad . \quad . \quad . \quad . \qquad (6)$$

The first relation implies that the energy required to dissolve a calcium atom in CaF_2 from the vapour is about 48 kg cal per mol or about 2·1 ev per atom. We shall consider this further below. The relation (6) seems to imply that κ is considerably larger than 100. The quantity N_0 is $8{\cdot}0 \times 10^{22}$ per cm^3, whereas C is $2{\cdot}8 \times 10^{22}$ at 1500°K. Since the exponential coefficient is less than unity, it follows that κ should be of the order of 7×10^8 or more.

The very large value of κ found in this way presents somewhat of a mystery since it seems doubtful if the contribution to the internal entropy of the crystal, exclusive of the mixing term, can be associated with a factor so large. In this respect the situation would not be improved, but rather made worse, if we were to assume that the electrons which are normally bound to the F-centres become free during the process of additive coloration. The partition factor corresponding to C above arising from free electrons is smaller by a factor $(m^*/M)^{3/2}$, in which m^* is the effective electron mass and M is the mass of a calcium atom, so that the contribution to crystal entropy from the electrons would be small at best. The principal change induced is that the relation (5) would be altered to $\epsilon_c = 4\epsilon_c$.

Actually, the formal situation would be improved if we were to assume that the units formed during additive coloration are combinations containing two halogen ion vacancies and two electrons, that is diatomic units analogous to those which Seitz has ascribed to R-centres in the alkali halides. In this case the reaction replacing (1) would be a monomolecular one ; Mollwo's observed relation would imply that the heat of solution of a free calcium atom in CaF_2 is very small and that the parameter analogous to κ is about 10^4. This value still seems large, but is not preposterously so. In lieu of more definitive experimental work, it seems wisest to regard the issue as an unsolved problem.

It is interesting to discuss the energy of solution of a calcium atom in CaF_2 obtained in the foregoing way in more detail. Let us first regard the F-centres in the alkali halides as if formed from free atoms of alkali metal by a sequence in which the metal atoms are ionized, the positive ions are incorporated in the lattice in normal positive-ion sites and the electrons are substituted for halogen ions. For comparative purposes we shall assume that the electron behaves like a halogen ion. Under these circumstances the energy of formation of an F-centre from the neutral free metal, regarding endothermic energies as positive, would be $E_I - H_I$ in which E_I is the ionization energy of the atom and H_I is the energy of dissociation of the lattice into free ions. The appropriate values for NaCl, KCl and LiF are given in the table, along with the observed values for the first three cases. The value for CaF_2 is also presented, E_I being the ionization energy for removal of two electrons from Ca, and H_I being again the energy of dissociation of the crystal into free ions. The 'observed' value for CaF_2 is that calculated from Mollwo's observations, quoted above by the method leading to eqn. (5). We note that the estimated values are too low by an amount between about 2·5 and 3·0 ev in the first three cases, for which observed values are available. The discrepancies presumably originate in the fact that the electron is broadly distributed and does not use the cavity associated with the F-centre as effectively as halogen ion would. The discrepancy seems to be about 7 ev per F-centre in the case of CaF_2 if we assume the bimolecular relation (1). Unfortunately a comparable value for LiF is not available. The discrepancy would not be altered much if we assume the centres are diatomic. On the whole, it appears that the electron associated with the F-centre in CaF_2 may be distributed even less favourably than in the alkali halides. This may originate in the fact that the positive ions are arranged tetrahedrally about the F-centre and that, relative to the positive ions, the neighbouring negative ions are proportionally much closer to the vacancy in CaF_2 than in the alkali halides. The ratio of distances is $2/\sqrt{3}=1{\cdot}16$ in the first case and $\sqrt{2}=1{\cdot}41$ in the second. Thus the wave functions of the F-centre electrons may vary much more rapidly with angle in CaF_2 than in the alkali halides.

Estimated and observed values of the energy of solution of metallic atoms in salts to form F-centres. Endothermic values are regarded as positive (expressed in ev). (Rögener 1937, Mollwo 1933, 1934)

	E_I	H_I	E_I–H_I	Observed
NaCl	5·2	7·9	−2·7	0·0
KCl	4·0	7·1	−3·1	−0·1
KBr	4·0	6·9	−2·9	−0·25
LiF	5·4	10·4	−5·0	—
CaF_2	17·9	30	−12·1	(+2·10)

Mollwo quotes work of Wöhler and Rodewald (1909) showing that essentially half the fluorine ions can be replaced by electrons. Presumably the resulting lattice should possess the zinc blende structure and the electrons should be distributed somewhat in the nature of a gas through the interstitial regions of the lattice.

§ 3. CLIMB OF A GENERAL DISLOCATION WITH A BURGERS VECTOR EQUAL TO AN ALLOWED TRANSLATION

We may summarize the discussion of §§ 2 and 3 by stating that the specimens of CaF_2 which have been additively coloured near 1200°c behave as if the dislocations present in them have undergone climb. In particular some of the dislocations have developed helical character. It is not certain, but highly probable, that the climb is associated with the generation of an appreciable density of vacancies in the calcium ion lattice as well as in the fluorine lattice. It also seems highly probable that the process of additive coloration has enhanced the climb, although some of it may be connected with the generation of lattice defects.

It is evident that many types of reactions in solids which involve the lattice defects can produce climb. We shall restrict attention to the case of a dislocation whose Burgers vector is an allowed translational vector so that the climb does not generate a surface of misfit. This case seems to be of particular interest in CaF_2. We shall also focus attention on dislocations which have a strong component of screw character, for these appear to be the natural sources of the helical dislocations observed in CaF_2.

Consider a straight dislocation line, running between two node points A and B, which possesses a strong screw component, that is which does not lie entirely in a plane PN normal to the Burgers vector. For the moment we shall not be concerned with the nature of the node points, but shall only assume that they are fixed. The line possesses a projection A′B in the plane normal to the Burgers vector passing through the node B (see fig. 1). Motion of the dislocation in the plane containing AA′B is possible without climb, being essentially a form of slip or glide. Actually such glide may require an activation energy unless the plane AA′B is a special one.

Fig. 1

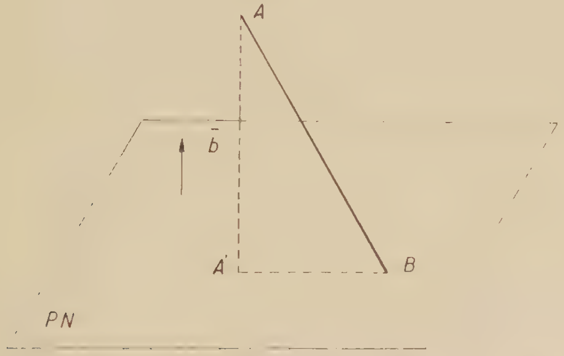

A straight-line dislocation and its projection in the plane PN normal to the Burgers vector **b**. A and B are the node points whereas A′ and B are their projections in the plane PN, which has been chosen to pass through B for convenience.

Motion of the dislocation out of the plane AA′B corresponds to climb and requires addition or subtraction of ions from the dislocation, the direction of displacement being opposite in the two cases. A direct measure of the amount of material added or subtracted is determined by the area F in the plane PN lying between A′B and the projection of the dislocation line on this plane (fig. 2), the volume of the added material being Fb, where b is the magnitude of the Burgers vector **b**. In cases in which the projected curve between A′B in plane NP winds into a spiral, the total area under the multiple-valued curve must be employed in determining the amount of material involved in the climb. We shall have particular interest in the cylindrical sheet generated by the lines parallel to **b** passing through the dislocation line. In the initial case in which the dislocation line is straight, this sheet is simply the plane AA′B, however the cylinder becomes curved once the dislocation climbs if the node points remain essentially fixed. Motion of the dislocation along the cylinder. parallel to **b**, can occur by glide without the addition of material to the dislocation. Again, such prismatic glide or slip may require an activation energy.

The energy per unit length of a dislocation depends upon its orientation relative to the Burgers vector, even in the isotropic case, and on its orientation relative to the general crystallographic axis as well in the anisotropic case. The second case has been discussed in detail for NaCl by Huntington *et al.* (1955) for NaCl, in which the anisotropic results do not appear to be radically different from those for the isotropic case.

Fig. 2

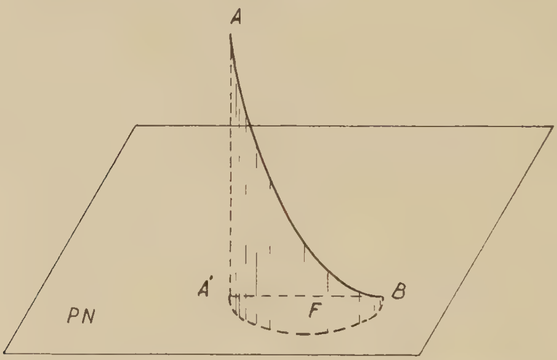

The change induced in the dislocation shown in fig. 1 by climb. The node points have remained fixed. The dislocation line is curved in space; its projection in the plane PN is also curved. The area F is proportional to the amount of material added or lost in climb. The dislocation can move along the cylinder generated by lines parallel to **b**, and passing through it. without the addition of material, provided the nodes remain fixed. This corresponds to prismatic slip.

Consider a segment of a dislocation which possesses a radius of curvature of magnitude R directed normal to the Burgers vector, so that the curvature is maintained by a supersaturation of the agent (eg. Schottky defects) which cause the climb. It is readily found that the superconcentration required to maintain the local curvature is given by the relation (Bardeen and Herring 1951).

$$\frac{1}{R} = \frac{kT \log (N/N_0}{\epsilon} \frac{b}{\omega} \quad \ldots\ldots\ldots \quad (7)$$

in which N is the concentration of the agent inducing climb, N_0 is the equilibrium concentration for the given temperature, ϵ is the energy per unit length of the segment, which is assumed to be short compared to R, ω is the increment of volume per deposited unit inducing climb and b is the magnitude of the Burgers vector. We shall focus attention, for simplicity, on a type of 'zero-order' approximation in which ϵ can be regarded as essentially constant. We then note that there is no restriction on the climb of the dislocation if the ratio N/N_0 is sufficiently large that $R_c<\mathrm{AB}$. It is interesting to observe that the dislocation having a strong screw character possesses a great advantage for the process of climb in the case in which

$$\mathrm{AB}>R_c>\mathrm{A'B}$$

where R_c is the critical radius for climb, equal to the reciprocal of the right-hand side of (7), if N is the actual concentration. In this case a pure edge dislocation of length A′B could not climb beyond a limiting point, whereas the mixed dislocation could climb indefinitely.

Fig. 3

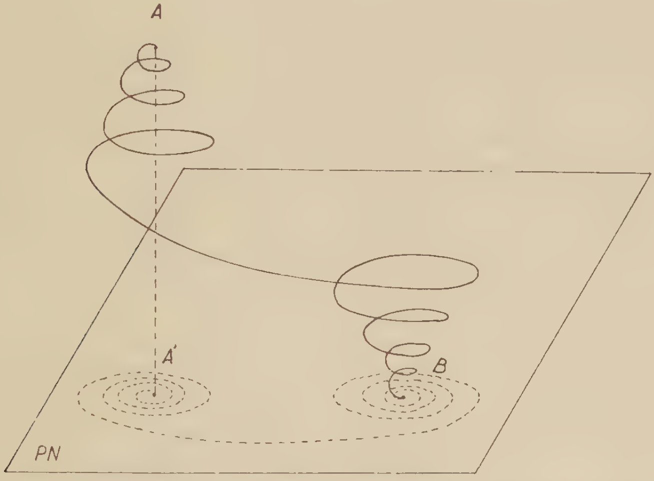

A climb, more general than that shown in fig. 2, in which the dislocation has become helical in form. Its projection on the plane PN is a double spiral centred about the points A′ and B. The amount of material added is determined by the area under the multiple-valued double spiral in the plane PN. The dislocation can still undergo prismatic slip along the cylinder parallel to **b**.

The ultimate shape of a climbing dislocation which has a strong screw component initially seems to be governed by the following factors:

(1) Magnitude of the supersaturation.

(2) Rate of arrival to the dislocation of the agent which determined climb.

(3) Rate of redistribution of such material along the dislocation line.

(4) Ease with which prismatic glide may occur along the cylinder determined by lines parallel to **b**.

(5) The variation of ϵ with direction relative both to **b** and to the crystallographic axes.

(6) The interaction of the various elements of the dislocation with one another through the elastic field.

It seems clear that if the material is redistributed along the dislocation at a rate that is rapid relative to that of arrival, either because the diffusion coefficient along the dislocation is very rapid compared to that within the bulk material or because the supersaturation is very small, the dislocation will tend to assume the shape of lowest energy concomitant with the bound points and projected area. If ϵ is a constant we might expect this to be

Fig. 4

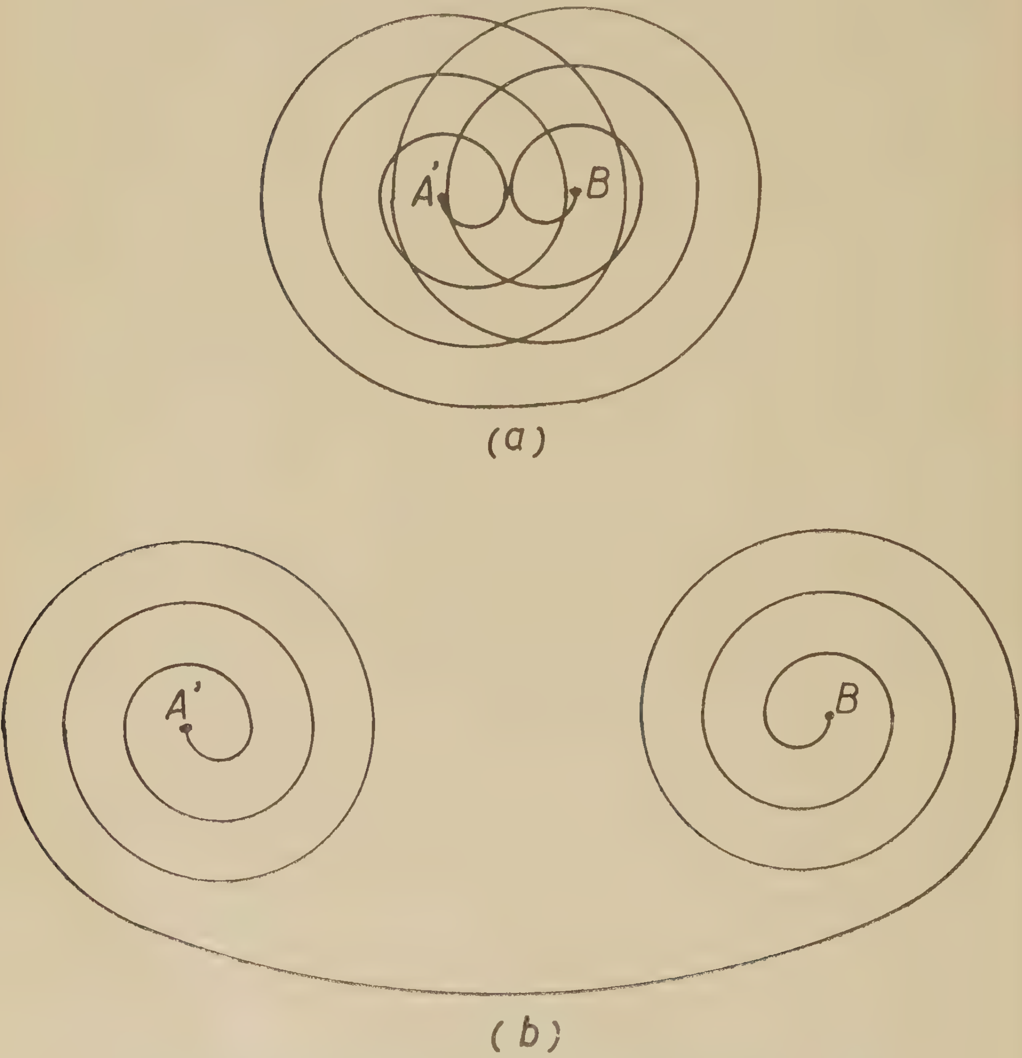

The projections in PN corresponding to two interesting forms of helical dislocations. In fig. 4 (*a*) the points A′ and B are inside most of the loops of the double spiral, whereas in fig. 4 (*b*) only one arm rotates about the projection of each node point, the two arms being connected by a single loop. The dislocation shown in fig. 3 corresponds to a case such as that illustrated in fig. 4 (*b*).

the arc of a circle. If N/N_0 is sufficiently small the limiting radius would be determined by (7) but the radius could be arbitrarily large if $R_c < AB$. A form other than circular will occur in this case if ϵ depends strongly on orientation.

On the other hand, if the material arrives at the dislocation at a substantially greater rate than it is redistributed along the dislocation, as can occur if there is a relatively high superconcentration and if the rate of diffusion along the dislocation is not exceedingly high relative to the diffusion of the agent inducing climb in the bulk material, the amount of climb will tend to be the same over the entire length. The projection of the dislocation on the plane PN will ultimately become a double spiral with the points A′ and B serving as centres of each half of the double spiral (fig. 3). In three dimensions, the dislocation will become a form of helix in which the radius and pitch varies along the length in the general case. The winding of the helix about an axis parallel to the Burgers vector occurs preferentially near the nodes, that is near the centres of the double spiral, for one obtains the greatest angle of rotation there for a given increment of material, much as in spiral growth of crystals from the vapour or solution.

It is readily seen that if prismatic slip is difficult, the helical dislocation will eventually develop lower pitch near the nodes than in intermediate regions, as additional turns are added. On the other hand, if prismatic glide is relatively easy, the arms of the helix will tend to move toward the centre from both ends as they are generated so that the pitch will become relatively uniform over the entire length. There are two interesting cases to consider: In one the central points A′ of B of the double spiral in the plane PN are well within the arms of the double spiral (fig. 4 (*a*)). In this case the outer loops are free to glide parallel to the Burgers vector in such a way as to form a relatively simple helix which winds around the original dislocation, provided prismatic glide is possible. In the second case (fig. 4 (*b*)) most of the arms of the double spiral have a radius less than A′B relative to the appropriate centres of rotation. In such a case the loops, on undergoing prismatic glide, will form two helices which are interconnected by a loop. It is evident that the two cases become equivalent if the radius of curvature of the loops grow larger than A′B.

Presumably the interaction between the various elements of length of the entire dislocation will determine the amount of prismatic slip which occurs if glide is easy. In general it appears that neighbouring portions of successive turns will repel one another, much like edge dislocations of the same sign moving in the same slip plane. On the other hand, diametrically opposite sides of a given turn or successive turns should behave like dislocations of opposite sign and attract one another, at least as far as motion in the direction of the Burgers vector is concerned. The problem of the long range elastic interaction evidently is worthy of quantitative study.

It seems worthwhile noting that as the helical dislocation winds and expands it automatically sweeps through a volume of space. This process may aid the speed of growth by placing the dislocation into new regions where the supersaturation of the agent causing climb is large as the old regions become depleted.

The helical dislocations which have been observed thus far in this laboratory evidently were formed from dislocations which were almost of pure screw type running in one of the ⟨110⟩ directions. It appears that during an important part of the period of growth of the helix the conditions favoured deposition along the length rather than redistribution along the dislocation line. Thus the regions near the nodes were able to make a number of windings. It is also evident that prismatic slip was possible during at least part of the history, for successive turns of the helices tend to be evenly spaced, as if slip occurred with comparative ease during the process of climb (Plate (*a*)).

Fig. 5

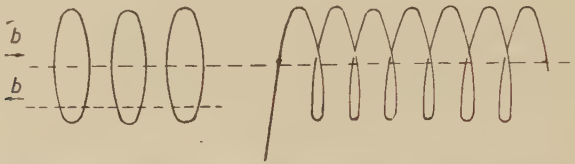

The conversion of a portion of a helical dislocation into single-valued prismatic loops. In the case shown, there were present originally two parallel dislocations primarily of screw character (horizontal dashed lines), the upper one being longer than the lower. It is assumed that the screws wind in opposite directions, so that they would have the same sign if connected by an edge at the left hand end. Both dislocations have developed helical character as a result of climb. The helices in the overlapping sections have combined to form single valued loops.

The step-height of the helices is usually of the same order of magnitude as the diameter of the loops. Moreover a major fraction of the turns appear to be uniform in diameter and spacing in many of the helices, although an abnormally large or abnormally small turn is not unusual. The general uniformity of many of the helices suggest that the prismatic glide occurred from the ends along with climb so that the turns formed earliest were gradually pushed toward the regions midway between the nodes where the superconcentration was fairly homogeneous and gradually dropped, perhaps because of the high density of sinks as represented by the helix itself. It is quite conceivable that winding up also takes place simultaneously at points of the screw dislocation other than the endpoints. A small local deviation from the pure screw orientation is all that is needed to give rise to winding up. This, with the help of prismatic glide, would ensure an equal spacing of loops more rapidly.

The relatively homogeneous helix frequently terminates rather abruptly, one or more relatively straight dislocations running off. There does not seem to be evidence for segments near the ends which have diminishing radius of curvature and which were the most rapidly turning portions during growth. It is possible that such regions existed during growth but 'unwound' and disappeared after the superconcentration subsided because the curvature there was too high.

Occasionally a helix terminates and is followed, along the same axis, which corresponds to the line of the original dislocation, by a sequence, of closed loops having about the diameter and spacing of the successive turns of the helix (fig. 5) (Plate (*b*)). It is not certain how such patterns are generated, however the result is what one would expect if the original dislocation had running parallel to it for a portion of its length a screw dislocation of opposite sign (fig. 5) which generated a helix winding in the opposite direction. Ultimately the two helices will meet as their diameters grow. The regions of contact will join with annihilation of the screw component and closed prismatic dislocations or loops will result. There seems to be no evident reason why the two screw dislocations of opposite sign should run so nearly parallel to one another.

In connection with the preceding discussion, it may be worth noting that one of the simplest ways of promoting the irreversible climb of dislocations would seem to be to establish a temperature gradient in the specimen at a temperature where the defects causing climb are readily generated at the dislocations. As a result of the thermal gradient, the defects should diffuse from one region of the specimen to another causing the dislocations in different parts to climb in opposite directions. This procedure might prove particularly fruitful in materials such as silicon and germanium in which the lattice defects have a high activation energy for formation. In such cases one might expect to observe relatively open helices such as those found in CaF_2. The techniques developed by Dash (1956) of the General Electric Research Laboratories regarding decorating dislocations in silicon with copper might prove useful in displaying the effect in that material.

§ 4. THE GENERATION OF WHISKERS FROM HELICES

As noted in § 3, the helical dislocations found in CaF_2 probably were formed under circumstances in which the factors inducing climb were not as great as they might be because of the intervention of electrolytical currents associated with Frenkel disorder in the halogen lattice. Apparently only a small fraction of the defects which play a rôle in the additive coloration originate in a process requiring climb. This probably explains why the helices found have a step height that is large compared to the length of the Burgers vector.

It is clear that the situation would be very different if a vigorous reaction that occurred at the surface of a crystal consumed lattice defects which could be generated only by climb in the interior of the specimen. In this event all sources would operate more intensely. In particular the helical dislocations of the type observed in this laboratory could become much more tightly wound. Under the proper circumstances such spiral prismatic dislocations could generate a type of whisker on the surface. We shall discuss some of the properties of such whiskers which may be anticipated. It will become clear that they are of a type which would grow from a base within the solid and seem on the whole to be like the whiskers which have been grown on tin and other coatings of metals under specialized conditions, such as when in an appropriate reactive atmosphere or when squeezed in a vice.

It should be emphasized that two general types of whiskers have been prepared and studied. The first type, which grows from the base was first made the object of careful physical study by Herring and Galt (1952) after observations of technological interest by Cobb (1946) and by Compton *et al.* (1951). They have been produced by mechanical strain by Fisher *et al.* (1954). The mode of growth has been the object of

Fig. 6

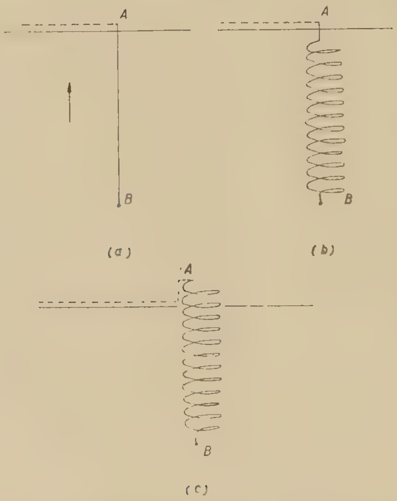

Schematic picture showing the development of a whisker from a spiral or helical prismatic dislocation. In fig. 6 (*a*) the upper horizontal full line represents the surface of the specimen. The vertical line *AB* corresponds to the screw dislocations whose Burgers vector **b** is shown. The horizontal dashed line above the full line representing the surface and running to the left from *A* represents the ridge on the surface associated with the screw dislocation. In fig. 6 (*b*), the screw has climbed into a helical form as a result of the addition of material. In 6 (*c*), some of the loops of the helix have been attracted to the surface, moving by prismatic slip, and have formed a cylindrical protrusion or whisker. The whisker can continue to grow by addition of loops from beneath the surface. In the case shown it is assumed that the prismatic slip of the helix to the surface has taken place in such a way that the ridge on the surface (horizontal dashed line) is cut and part is raised to the top of the whisker. In this event, the whisker would possess a screw along its axis (see fig. 7). Actually one would expect the screw to be unstable at the upper end of the whisker in this idealized case and to slip out of the cylinder, at least at sufficiently high temperature.

systematic study by Baker (unpublished)† and by Levy and Kammerer (1955). The second type of whisker is grown by deposition of material from the vapour phase or from solution and has been the object of study by many investigators in recent years (Sears 1953, Sears *et al.* 1954, Johnson and Amick 1954, Piper and Roth 1953, Gyulai 1954, Brenner and Morelock 1956, Brenner and Sears 1956). The mechanism of formation of the second type of whisker appear to be closely related to that of crystal growth from the vapour or from solution. Such whiskers will not be of primary interest to us here. Mechanisms for the growth of the first type of whisker have been proposed by Peach (1952), Eshelby (1953), Frank (1953) and Seitz (comment by Eshelby 1953). The mechanism of Peach does not provide an explanation of the fact they grow from the base, whereas the other three mechanisms do. Eshelby postulated an internal source of simple prismatic dislocations, such as that proposed by Bardeen and Herring (1951), and suggested that the prismatic dislocations slip to the surface, being guided by a stress field. Frank's

Fig. 7

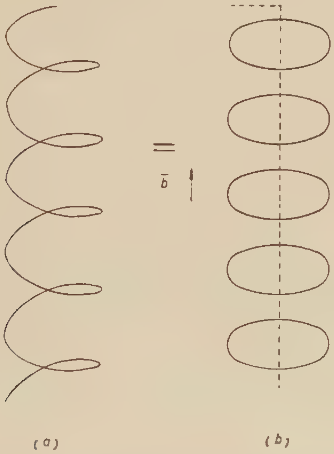

A tightly wound helical or spiral prismatic dislocation for which the step height is equal to the Burgers vector (fig. 7 (*a*)) is equivalent to a stack of discs, or simple prismatic loops, through which a screw dislocation runs (fig. 7 (*b*)) when the helix protrudes from the surface. The screw is represented by the vertical dashed line running from B to A.

---

† Unpublished work undertaken in cooperation with J. S. Koehler. Baker carried out an extensive study of whiskers formed on coatings of tin and Pb–Sn alloy upon iron, on solid Pb–Sn alloy, on layers of cadmium electroplated upon copper and iron, on layers of Cd–Hg electroplated upon copper covered with mercury, on electroplated zinc, and on a thin layer of $AgNO_3$ upon glass. Whiskers grew best on electroplated layers on the whole and not as well on the thicker hot-dipped layers. A few of Baker's numerous valuable conclusions are summarized in the text of the present paper.

mechanism proposes that the whiskers are formed by the repeated circular motion of the terminal end of a screw dislocation that cuts the surface. This mechanism is somewhat related to the processes described in this paper. Seitz proposed formation by the action of a helical, or spiral, prismatic dislocation along the lines discussed in more detail here. The authors are much indebted to Drs. Baker and Levy for the opportunity of reading unpublished work.

We shall assume that the thermodynamic driving force inducing climb is very great so that climb is not halted merely by forces between dislocations which act over the normal distances involved in networks, of the order of 10^{-4} cm. We shall consider the case in which the climb adds material to the dislocation, that is, interstitial atoms condense or vacancies evaporate.

Fig. 8

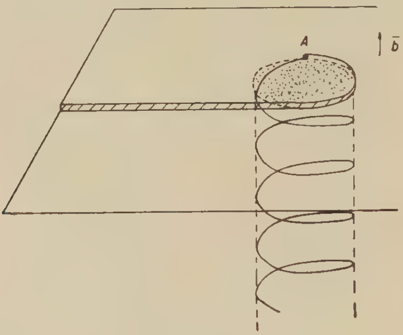

An alternative direct method for forming a whisker without a screw on its axis from a helical dislocation. The surface of the specimens is shown along with the internal spiral prismatic dislocation and the ridge associated with the termination of a dislocation having the associated screw character on the surface. The ridge is straight on the left-hand side of the diagram but curves along the line corresponding to the projection of the helix on the surface and dwindles to zero at the point where the helix reaches the surface. As the helix moves to the surface by prismatic slip, the ridge extends around the loop on the surface corresponding to the projection of the helix. Once each turn a complete disc of crystal, one Burgers unit high, will be formed on the surface. These discs will form a whisker which does not have a screw dislocation. This process probably does not occur when whiskers are formed rapidly.

The simplest case to consider in a geometrical way is that shown in fig. 6 (*a*). Here a screw dislocation terminates at a ridge on the surface and at a node point inside the solid. The two terminal points may be regarded as equivalent to A and B in fig. 1. More exactly, the terminal end conjugate to B could be regarded as a point outside the lattice which is the image of B in the surface. If this dislocation is induced to climb into a helix by the development of loops at the bottom point, inside the solid, and by prismatic glide, the form could, at least in an idealized case, achieve the state indicated schematically in fig. 6 (*b*). The neighbouring loops of the helix repel one another, but should be attracted to the surface as a result of the image forces. As a result, the system could achieve the state shown in fig. 6 (*c*). In this schematic case it has been assumed that in breaking through the surface the loops have cut the ridge and raised the segment running to the centre of the cylinder. Elementary reasoning shows that the protruding helix in which neighbouring turns are now separated by the Burgers vector, is equivalent to a stack of discs, or a rod, having a screw dislocation running down its centre (fig. 7). Thus in the idealized case shown, the whisker would possess a screw dislocation along its axis. Actually the screw could probably be very unstable in the case shown, for the 'bend-point' A in figs. 6 (*c*) and 7 (*b*) should be attracted to the side of the cylinder and should pull the upper part of the screw dislocation with it. This may be expected to occur in the case illustrated when the cylinder has protruded by a distance of the order of or larger than its diameter. Thus the whisker would probably lose its screw dislocation in the course of growth.

Fig. 9

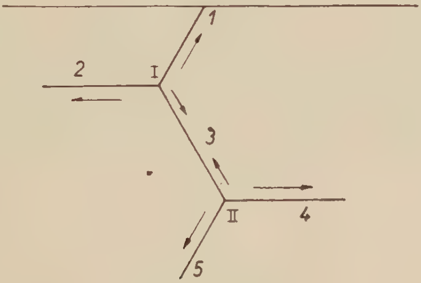

A part of a dislocation network which terminates at a surface. In the case illustrated, all the dislocations in the network are assumed to have screw character and hence may be converted into helical dislocations as a result of climb. Dislocation 1 is in an ideal position to form a whisker. The spiral prismatic dislocations formed from 2 and 4 are poorly oriented to break through the surface, however those generated from 3 and 5 could eventually force their way outward by compelling the node points I and II to move. In this case the initial whisker could develop two kinks as the two nodes emerge, assuming the growth remains continuous (see figs. 10 and 11).

In a somewhat more idealized case, shown in fig. 8, the whisker would grow from start without a screw dislocation along its axis. In this case the terminal point of the helix at the surface rotates around the circle marking the intersection of the whisker with the original surface of the solid, making one revolution for each loop which protrudes. In effect, a complete disc of solid one Burgers unit high is formed at the base of the protruding cylinder for each revolution of the point where the helical dislocation emerges at the surface.

The experimental investigations of whiskers grown from the base indicate that few conform to the ideal situation shown in these figures. Most appear to have an irregular initial, or 'head' portion which is not tightly attached. Frequently a large fraction are kinked, the kink angle being more or less well defined. Levy has observed cases, relatively rare, in which successive kinks have the same sign so that the whiskers have a spiral form. All investigators appear to agree that the kinks formed during the growth process and not after the whisker has emerged.

Fig. 10

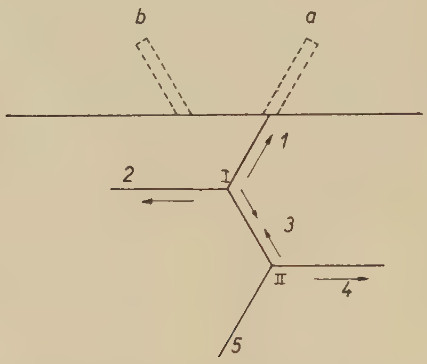

The case in which dislocation 3 shown in fig. 9 has formed its own whisker (schematic). The bars projecting from the surface represent the whiskers, directed more or less along the Burgers vectors in the two case.

Fig. 11

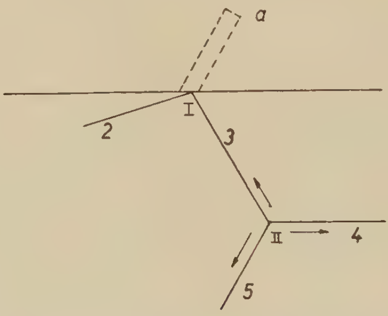

In this case node I shown in fig. 9 has moved to the surface as a result of climb and the pressure exerted by the underlying prismatic dislocations. The whisker produced by dislocation 1 continues growth, but with a kink each time a node emerges.

Actually, the mechanism of whisker growth based on the assumption that they originate in helical dislocations formed by the climb of those having Burgers character seems to have ample room for describing the observed phenomena if we take into account the fact that most of the dislocations near the surface are involved in network structures and do not have the simple form shown in fig. 6 (*a*). Consider the more realistic situation shown in fig. 9 in which a part of a dislocation network which terminates at the surface is shown. For illustrative purposes five dislocations having mainly screw character are shown, number 1 terminating at the surface. Dislocations 2, 4 and 5 link with other parts of the network not shown. All should be transformed to helices if the environment favours climb. The helix formed by dislocation 1 could produce a relatively simple whisker of the type described above, but growing diagonally from the surface in the direction of the Burgers vector. The direction of glide for dislocations 2 and 4 is poorly situated for formation of whiskers on the surface shown. On the other hand, the Burgers vectors for dislocations 3 and 5 are disposed in such a way that the helices formed from them could produce whiskers if the helices could reach the surface. Because of the repulsive forces between successive turns of the helix, the helices will exert forces upon the node points I and II in the directions one might expect from compressed springs. If the forces between turns of the helix formed from dislocation 3 become strong enough they could glide to the surface in the direction of the Burgers vector and form a new whisker (fig. 10). On the other hand, it is also possible that the node I would be induced to climb to the surface as a result of the forces upon it (fig. 11), and the opportunity for climb inherent in the situation, so that the whisker formed from dislocation 1 would eventually stop growing and be joined to a whisker, oriented in a different direction formed from dislocation 3. The angle of kink should be closely related to the angle between the Burgers vectors of dislocations 1 and 3, although it need not be exactly the same if the whisker has not grown parallel to the Burgers vector on the surface.

Fig. 12

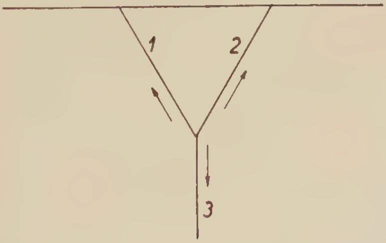

A dislocation pattern which may produce a Y whisker, with its base on the surface, of the type observed by Baker. The two whiskers produced by the upper dislocations join into one as the node point is forced to the surface as a result of climb and the action of the lower one.

Similarly, the helix formed from dislocation 5 could eventually force node II to the surface and produce a second kink. Thus the ultimate kinked structure of the whisker would reflect, in a somewhat crude way, a part of the internal structure of the network.

It is not clear to what extent the dislocations formed in this way would have a screw dislocation running down the centre of each segment between kinks. In the case illustrated, we might expect the part of the whisker originating in dislocation 1 to be relatively perfect since it conforms somewhat to the situation shown in fig. 6 (*a*). On the other hand the screw dislocations may or may not remain entrapped in the segments originating in dislocations 3 and 5, depending upon somewhat accidental circumstances.

If dislocation 1 in fig. 9 does not terminate on the surface, but is tied back into the network the helix formed from dislocation 3 would still attempt to break through to the surface. This could occur by a type of prismatic punching process in which a more or less cylindrical block of material between the node I and the surface would be forced out as a result of prismatic slip of the helix derived from dislocation 3 in the direction of its Burgers vector. Once the helix has reached the surface, the node point I would effectively be there also and further whisker growth would occur in what may be regarded as a normal way. It is possible that the head portions found on many whiskers correspond to the segments which are punched through prior to the establishment of conditions for development of a normal whisker.

More complex situations than that described evidently are possible. Baker has found that pairs of whiskers can move together during growth and join to form a Y whose base is attached to the surface. A case of this kind could originate from the simple dislocation structure shown in fig. 12. In the case quoted by Baker the two upper arms of the Y were curved downward toward the surface. Bending of this type, and in fact bending of whiskers in general, is not difficult to understand if the nodes are induced to move so that the points at which the helices break through the surface shift during the course of formation of whiskers.

Levy's spirally kinked whiskers seem to require a more complex sequence of events. One must assume that a sequence of node points distributed in a more or less spiral manner inside the solid are forced to the surface in turn and that successive kink angles are in the same direction. Such cases are relatively uncommon and may be determined in the main by a somewhat chance sequence of events.

It is clear that the basis for the explanation of the occurrence of kinks, i.e. the climbing of a node, does not depend strictly on the validity of the particular growth mechanism described here, but can be applied to any dislocation mechanism where the axis of the whisker is determined by the Burgers vector of the underlying dislocation

Eshelby (1953) has proposed that the driving force for whiskers of the type found on tin plate is the result of internal tensions related to the desire of a convex portion of the metal surface to increase in area in order to form more oxide. This explanation of the source of climb seems to be in good accordance with the fact that whisker growth can also be stimulated by the action of mechanical stresses, as at the edge of a specimen mounted in a vice, for in the second case it is evident that the dislocations in the region just outside the vice desires to accept material from the regions under pressure and should climb in the way needed to form whiskers. In general, the principal condition required for the formation of whiskers, apart from the presence of appropriate dislocations, is an unstable energetic situation which can be brought nearer equilibrium by the migration of imperfections and the appropriate climb of dislocations.

It is found that the whiskers require an incubation time before appearing. This presumably is the time needed for the helix to grow to a size at which the internal and image forces are sufficiently great to induce it to move to the surface. In general, we might expect the diameter at which this is achieved to be comparable to the depth of the source below the surface, that is to the linear spacing in the network. Baker has observed that the whiskers, although normally quite strong under bending or tensile stress, would flatten relatively easily if compressed normal to the axis of the whisker. This observation would bear further investigation since it seems to imply the presence of sources of dislocations possessing a Burgers vector normal to the whisker axis. The discussion given above would not appear to offer a simple explanation of the origin of such sources.

ACKNOWLEDGMENT

This work is part of a research scheme supported by I.R.S.I.A. (Institut pour l'encouragement de la Recherche Scientifique dans l'Industrie et l'Agriculture ; Comité pour l'étude de l'Etat Solide) Brussels.

REFERENCES

AMELINCKX, S., 1956, *Phil. Mag.*, **1**, 269.
BARDEEN, J., and HERRING, C., 1951, *Imperfections in Nearly Perfect Crystals* (New York : Wiley and Sons), p. 279.
BARILE, S., 1952, *J. Chem. Phys.*, **20**, 297.
BONTINCK, W., and AMELINCKX, S., 1957, *Phil. Mag.*, **2**, 94.
BONTINCK, W., and DEKEYSER, W., 1956, *Physica*, **22**, 595.
BRENNER, S. S., 1956, *Acta Met.*, **4**, 62.
BRENNER, S. S., and MORELOCK, C. R., 1956, *Acta Met.*, **4**, 89.
BRENNER, S. S., and SEARS, G. W., 1956, *Acta Met.*, **4**, 269.
COBB, H. L., 1946, *Amer. Electroplaters Soc.*, **33**, 28.
COMPTON, K. G., MINDIZZA, A., and ARNOLD, S. M., 1951, *Corrosion*, **7**, 372.
DASH, W. C., 1956, *Phys. Rev.* (in the press).
DEĬGEN, M. F., 1951, *Zhur Ehspth Teoret. Fiz.*, **21**, 992.
ESHELBY, J. D., 1953, *Phys. Rev.*, **91**, 775.
FEOFILOV, P. P., 1953, *Doklady Akad. Nauk. S.S.R.*, **92**, 545 ; 1954, *U.S. Atomic Energy Comm. N.S.F.* tr. 203.
FISHER, R. M., DARKEN, L. S., and CARROL, K. G., 1954, *Acta Met.*, **2**, 368.
FRANK, F. C., 1953, *Phil. Mag.*, **44**, 854.
GYULAI, Z., 1931, *Z. Phys.*, **67**, 812 ; 1954, *Ibid.*, **138**, 317.
HAUFFE, K., 1955, *Reaktionen in und an Festen Stoffen* (Berlin : Springer), Chap. 3.
HERRING, C., and GALT, J. K., 1952, *Phys. Rev.*, **85**, 1060.
HUNTINGTON, H. B., DICKEY, J. C., and THOMSON, R., 1955, *Phys. Rev.*, **100**, 1117.
JOHNSON, E. R., and AMICK, J. A., 1954, *J. Appl. Phys.*, **25**, 1204.
LEVY, P. W., and KAMMERER, O. F., 1955, *J. Appl. Phys.*, **26**, 1182.
LÜTY, F., 1953, *Z. Phys.*, **134**, 596.

Mollwo, E., 1933, *Z. Phys.*, **85,** 56 ; 1934, *Nachr. Wiss. Göttingen*, **1,** 79.

Peach, M. O., 1952, *J. Appl. Phys.*, **23,** 1401.

Piper, W. W., and Roth, W. L., 1953, *Phys. Rev.*, **92,** 503.

Rexer, E., 1932, *Z. Physik*, **78,** 538.

Rögener, H., 1937, *Ann. Physik*, **29,** 386.

Sears, G. W., 1953, *Acta Met.*, **1,** 457.

Sears, G. W., Gatti, A., and Fullman, R. L., 1954, *Acta Met.*, **2,** 727.

Seith, W., 1929 a, *Z. Physik*, **56,** 802 ; 1929 b, *Ibid.*, **57,** 869.

Seitz, F., 1950 a, *Phys. Rev.*, **79,** 529 ; 1950 b, *Ibid.*, **80,** 239 ; 1952, *Advanc. Physics*, **1,** 43.

Schulman, J. H., Ginther, R. J., and Kirk, R. O., 1952, *J. Chem. Phys.*, **20,** 1966.

Smakula, A., 1953, *Phys. Rev.*, **77,** 408 ; 1953, *Ibid.*, **91,** 1570 ; 1954, *Z. Physik*, **138,** 276.

Tubandt, C., 1932, *Hand. d. Exp. Physik* (Leipzig : Akad. Press), **12.**

Urbanck, J., 1951, *Acta Phys. Austriaca*, **5,** 69.

Ure, R. W., 1956, *J. Chem. Phys.* (in the press).

Wöhler, L., and Rodewald, T., 1909, *Z. anorg. Chemie*, **61,** 54.

Zintl, E., and Udgard, A., 1939, *Z. anorg. Chemie*, **240,** 150.

Quenching Vacancies in Gold †

By F. J. Bradshaw and S. Pearson
Royal Aircraft Establishment, Farnborough, Hants.

[Received October 24, 1956, and in revised form November 7, 1956]

Abstract

Increases in the electrical resistivity of gold wires due to quenching have been measured and interpreted in terms of vacancies. The energy for vacancy formation was deduced to be 0·95 ev and the concentration of vacancies at the melting point 6×10^{-4}. Annealing measurements between 70° and 130°c indicated that the movement energy of a vacancy was 0·68 ev and that it had on average a life of 10^8–10^9 jumps.

§ 1. Introduction

We have recently given the results of experiments on the changes in electrical resistivity of platinum wires after quenching from high temperatures and after annealing (Bradshaw and Pearson 1956). The increases in resistivity caused by quenching were interpreted as being due to vacancies. Since the published results of similar experiments on gold were somewhat conflicting (see table) we have also made measurements on gold wires using the same methods as before.

The wires were from Johnson Matthey ‘Specpure’ material and were 0·2 and 0·14 mm dia. They were heated by electric current to temperatures between 560° and 960°c and quenched into water at ~ 4°c. Their annealing characteristics were studied by immersing them in liquid baths at temperatures between 70° and 130°c; to ensure complete removal of vacancies at the end of an anneal they were heated briefly to ~ 400°c. The changes of resistance following quenching and at appropriate stages during annealing were found by measurements in liquid nitrogen. Potential leads 0·02 mm dia. were welded on for this purpose. The temperatures of the wires just before quenching were obtained by measuring the hot resistance and using resistance/temperature data provided by the N.P.L. (Powell, private communication). The gold wires were welded on to platinum leads whose diameters were chosen so as to make the temperature gradient between the potential leads on the gold negligible at the quenching temperature.

---

† Communicated by the Authors.

§ 2. Quenching

The values of $\Delta\rho_0$, the increase in resistivity resulting from quenching from different temperatures, were plotted on the assumption that the usual relation would hold,

$$v=A \exp(-\Delta H_1/kT)$$

where v is the vacancy concentration, ΔH_1 is the energy required to form a vacancy and A is the entropy factor. Figure 1 shows a plot of $\Delta\rho_0$ against $1/T$ for the two wire sizes. Each point is the mean of about six observations. Using Abelès' (1955) estimate for the resistivity of vacancies (1 atm % corresponds to 1·45 μ ohm cm) the values of A from the lower temperature linear portions of the graph are found, for the 0·2 and 0·14 mm wires, to be 1·9 and 3·1. The values of ΔH_1 were 0·92 and 0·98 ev.

Fig. 1

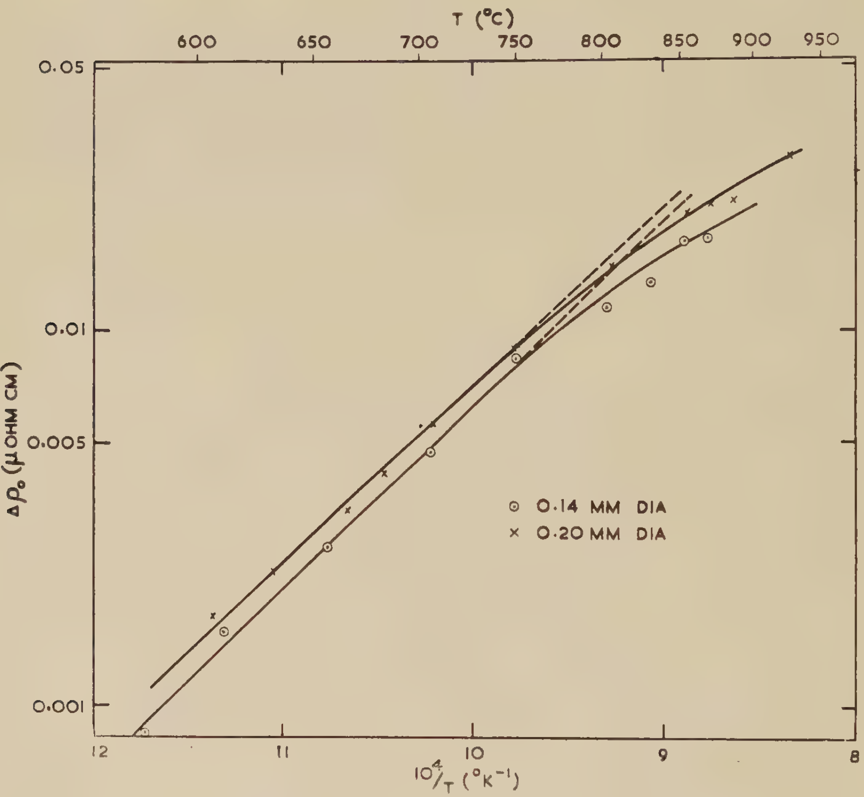

Increase of resistivity by quenching.

Assuming that the same annealing process for vacancies operated at the higher temperatures during quenching as during the annealing experiments (see below) we have calculated, as in the paper on platinum, the transition temperature above which one might expect to lose vacancies on quenching owing to their high mobility. The initial quenching rates were estimated from the previous work on platinum to be 30°/msec (0·2 mm) and 60°/msec (0·14 mm). The transition temperatures were calculated to be $1/(10{\cdot}2\times10^{-4})$ and $1/(9{\cdot}9\times10^{-4})$°K. It is interesting that both lines appear to be straight to temperatures higher than the calculated transition temperatures, although one would expect them to start curving some way below this. (A similar result may be deduced from the figures given by Bauerle *et al.* 1956.) The calculated transition temperatures would have been compatible with what was observed if ΔH_2 had been ~ 0·57 ev ; this is outside our experimental scatter. The best evidence for adequately rapid quenching and hence correct values of ΔH_1 is the straightness of the lines in the figure at lower temperatures and the agreement between the results for different wire sizes. The shift between the lines is thought to be due to slight errors in estimating the temperature. The mean figures for formation energy and entropy factor are given in the table. We suggest that the total error in ΔH_1 is probably ± 0·1 ev. Also given with the results previously published for gold are values of A calculated from the data provided. We agree reasonably with the figures of Bauerle *et al.* and would predict a concentration of 6×10^{-4} vacancies at the melting point.

	ΔH_1 ev	A	ΔH_2 ev	nB
Kauffmann and Koehler (1952)	1–2	—	0·4 ±0·14	—
Kauffmann and Koehler (1955)	1·28±0·03	12	0·68±0·03	$1{\cdot}0\times10^{-8}$
Bauerle *et al.* (1956)	1·02±0·06	5·1	0·66±0·06	$0{\cdot}3\times10^{-8}$
Lazarev and Ovcharenko (1955)	0·79	0·2	0·52	$4{\cdot}0\times10^{-11}$
Present work	0·95±0·1	2·4	0·68±0·05	$1{\cdot}0\times10^{-8}$

§ 3. ANNEALING

Most anneals were carried out on wires quenched from temperatures in the region of 850°C and, as with platinum, the decay of $\Delta\rho$, the increase in resistivity, with time happened in a single stage. There were measurable differences in the annealing rates even for the same wire with the same $\Delta\rho_0$ and annealing temperature and, for different wires, characteristic differences in the shape of the decay curves were also observed (see fig. 2). However, the general curve shape usually approximated to that of a second order reaction (down to ~ 15% $\Delta\rho_0$ remaining). To see whether varying $\Delta\rho_0$ had any effect, a few anneals were done at the same temperature on the same wires quenched from ~ 710°C and ~ 960°C. For a wire quenched from ~ 960°C the annealing curve shape was about the same as that for wires quenched from ~ 850°C but for wires quenched from ~ 710°C the initial slope was only about half that for wires quenched from the higher temperatures and the curve shape approached that of a third order reaction (fig. 3).

Fig. 2

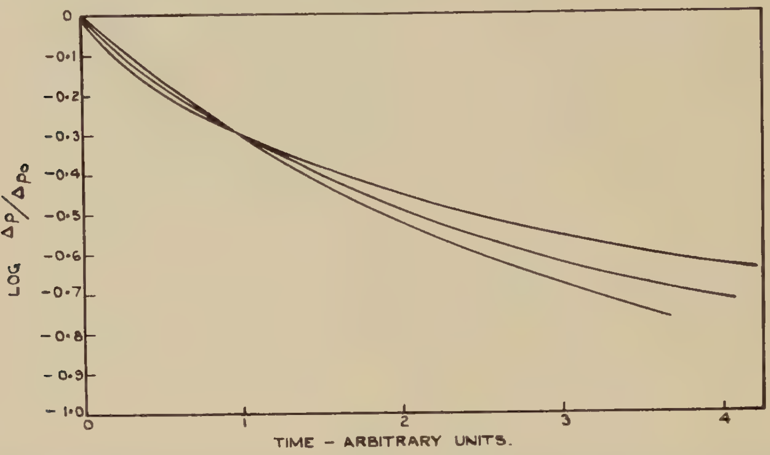

Annealing curves showing differences in curve shape for different specimens quenched from the same temperature (the annealing times are expressed in terms of the time to reach $\Delta\rho_0/2$).

Fig. 3

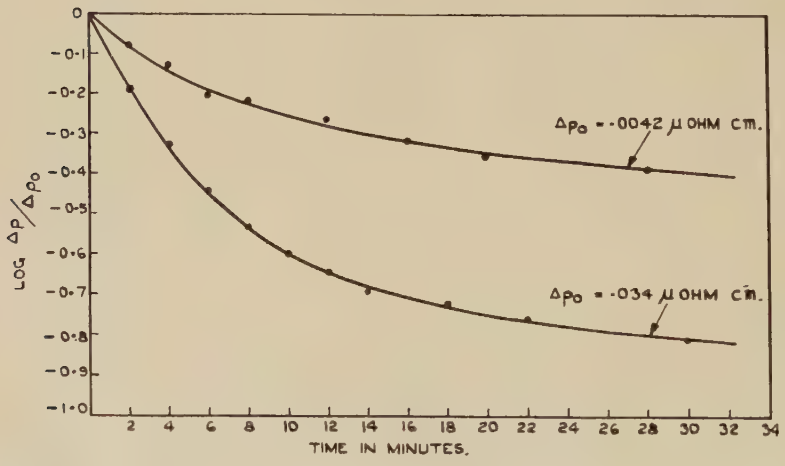

Annealing curves for one specimen showing effect of $\Delta\rho_0$ on annealing behaviour.

If n is the probability per jump that a vacancy is lost, and if despite the shape of the annealing curve we interpret annealing in terms of

$$-\frac{d \ln v}{dt} = 12\, n\nu_{\mathrm{D}} B \exp\left(-\Delta H_2/kT\right)$$

where ν_{D} is the atomic frequency (assumed here to be 10^{13} per sec), B is the entropy factor for vacancy movement (probably in the region between

1 and 10) and ΔH_2 is the activation energy for movement, then the differences in annealing can be regarded as being due to differences in n at any instant†.

ΔH_2 was obtained by altering the annealing temperature to a new value when $\Delta\rho$ had decayed to $\sim \frac{1}{2}\Delta\rho_0$ and noting the change of annealing rate. Values of ΔH_2 obtained by straightforward complete anneals at different temperatures in the cases where n appeared to be stabilized did not differ significantly. The mean value of ΔH_2 for both wire sizes was 0·68 ev ; it had an S.D. of 0·02 ev. The total error limits were perhaps $\pm 0{\cdot}05$ ev. The mean value of nB was $1{\cdot}0\times 10^{-8}$ (for quenches from ~ 850°c and when $\Delta\rho \simeq \frac{1}{2}\Delta\rho_0$), though this figure should only be taken as giving an order of magnitude. These figures are compared in the table with those of other workers (nB calculated from their figures). The grain sizes varied from those equal to the full wire diameter down to $\sim 0{\cdot}03$ mm diameter. Sizes of this order imply that the grain boundaries and surfaces were not important as sinks for vacancies since assuming B is between 1 and 10 they would lead to values of n considerably smaller than the mean value of n obtained experimentally.

Despite the shapes of the annealing curves approximating to second or third order a value of n lying between 10^{-8} and 10^{-9} when v was 10^{-4} would appear to preclude the idea of annealing by vacancies pairing or clustering. As with platinum the picture of dislocations providing the sinks seems to be more plausible, though the observed annealing behaviour indicates that the process is not a simple one.

The predicted value of 1·63 ev for self-diffusion activation energy agrees reasonably with the most recent experimental value of 1·70 ev (Okkerse 1956).

REFERENCES

ABELÈS, F., 1955, *J. Phys. Radium*, **16,** 34S.
BAUERLE, J. E., KLABUNDE, C. E., and KOEHLER, J. S., 1956, *Phys. Rev.*, **102,** 1182.
BRADSHAW, F. J., and PEARSON, S., 1956, *Phil. Mag.*, **1,** 812.
KAUFFMAN, J. W., and KOEHLER, J. S., 1952, *Phys. Rev.*, **88,** 149 ; 1955, *Ibid.*, **97,** 555.
LAZAREV, B. G., and OVCHARENKO, O. N., 1955, *Dokl. Akad. Nauk. S.S.S.R.*, **100,** 875.
OKKERSE, B., 1956, *Bull. Amer. Phys. Soc.*, **1,** 149.

---

† The factor 12 arises since there are 12 atoms round the vacancy which can jump into it. We are grateful to Dr. B. S. Berry for pointing out that the factor was omitted in a previous paper on Pt. This however does not affect the conclusions therein except that n for Pt should have been $\sim 10^{-10}$, not $\sim 10^{-9}$.

The Existence of a Metastable Phase Isomorphous with the Stable Phase of a Pure Metal†

By J. H. O. Varley
Metallurgy Division
Atomic Energy Research Establishment, Harwell, Berks.

[Received July 21, 1956 ; and in revised form October 10, 1956]

Abstract

A study of the factors controlling the coefficient of volume expansion of a pure metal, in a previous paper, has led to the conclusion that there are two isomorphous states, differing only in volume, of any given crystal structure. In this paper the relative stabilities of these phases is discussed and the possibility of isomorphic transformations is examined. A satisfactory description of a paradoxical phase change observed by Bridgman in the case of caesium under high pressures is achieved. An isomorphic transition observed in cerium appears to be another example of this type of phase change which, under suitable conditions imposed by the external variables, pressure and temperature, and possibly composition in the case of alloys, is possible in all metals.

§ 1. Introduction

Recently an analysis of the factors which control the thermal expansion of a pure substance has been carried out (Varley 1956) in an earlier paper hereinafter referred to as loc. cit. It has been found that the equation relating the volume coefficients of expansion α, to the electronic and vibrational characteristics of a metal (analogous to Grüneisen's relation) is quadratic in α ; $a\alpha^2+b\alpha+c=0$. Of the two possible roots for α one is positive and the other negative and the root with the larger modulus corresponds to the state of lower free energy. The argument for this is based on the fact that (C_p-C_v) is proportional to α^2 where C_p, C_v are the total specific heats at constant pressure and volume respectively. There is no restriction upon the sign of α so that the stable state can have a positive or negative coefficient of volume expansion, dependent upon the details of the electronic and lattice vibrations of the solid.

If, then, one considers a plot of *all* possible values of the Gibbs free energy, G and not only those values obeying the equation of state, as a function of volume at constant temperature and pressure, the curve will show two minima separated by a maximum. At 0°K the minima and maximum will coalesce into a single minimum. The maximum will always occur at a volume $V_0(P)$ which is the volume of the substance at 0°K for a given pressure P. The free energy at the maximum is then the free energy of the substance at constant volume $V_0(P)$ and temperature T. That this point must be a maximum can be seen from the argument that heating a crystal at constant pressure from absolute zero will result in a change of volume and an associated increase in entropy ; and since $C_p - C_v$ is proportional to α^2 and is greater than zero, G must have a lower value than if the substance were held at constant volume, $V_0(P)$, whatever the sign of the change in volume.

---

† Communicated by the Author.

There will be a family of curves of G as a function of V at constant T and P, one for each value of the pressure. The loci of the minima give the equilibrium relation between G and P at constant T. Again, a plot of G as a function of T at constant P will give a trace of the values of G for the two minima which occur in the equilibrium relation between G and V. In other words, the loci of the minima define the equation of state of the substance.

As the pressure upon the substance is increased at constant temperature one will expect, by Le Chatelier's principle, that the state with the smaller volume will tend to become more stable. Thus, for a substance with a positive coefficient of volume expansion, the state (minimum) with the lower volume will have a higher free energy than that with the larger volume, at low pressures. As the pressure on the substance is increased the family of curves of G as a function of V will be sheared in such a way that ultimately the state (minimum) with the smaller volume will have the lower free energy.

For a substance with a negative coefficient of volume expansion similar arguments apply with the sign of the pressure reversed, e.g. for a crystal in a polycrystalline solid under internal stresses giving rise to negative pressures.

The two states (minima) will have equal free energies when the coefficients of volume expansion are of equal and opposite sign, that is when the coefficient of the linear term in the quadratic expression for α is zero. If this condition can be achieved by a suitable variation of pressure and/or temperature an isomorphic phase change will occur.

§ 2. PHASE CHANGES UNDER PRESSURE IN CAESIUM

It can be shown, loc. cit., that for a solid in which the valence electrons may be considered as distributed in a free electron spectrum (Fermi gas), the coefficient b, of the linear term is

$$b = C_L \gamma_L/(1+\beta) + 2C_e/3 \qquad \text{. . . . . (1)}$$

where C_L and C_e are the lattice and electronic specific heats at constant volume, respectively, $\gamma_L = -(\partial \ln \theta/\partial \ln V)_T$, $\beta = -(\partial \ln \theta/\partial \ln T)_V$ and θ is the characteristic temperature defining the thermal entropy of the lattice (approximating to the Debye-θ).

Consider now the metal Caesium. For an alkali metal such as this $C_e \ll C_L$ at normal temperatures so that the condition for equal free energies reduces to $\gamma_L \simeq 0$. Now θ, the characteristic temperature is proportional to $V^{1/6}\ K^{1/2}$ for a Debye solid with, in addition, Poisson's ratio independent of volume (Slater 1939). To take into account the variation of Poisson's ratio with volume it will be assumed that this quantity varies through K and that

$$\theta \propto V^{1/6} K^n \quad . \ . \ . \ . \ . \ . \ . \ . \ . \ . \ . \quad (2)$$

where n is a constant.

Then $$\gamma_L = -(\partial \ln \theta / \partial \ln V)_T = -\tfrac{1}{6} - n(\partial \ln K / \partial \ln V)_T . \quad . \ . \quad (3)$$

For caesium $\gamma_L = 1{\cdot}29$ at normal pressure and temperature. Also, from Bridgman's measurements (1949, p. 180) it is found that K for Cs is proportional to V, approximately

$$K = K_1 + m(V_1 - V)/V_1 \quad . \ . \ . \ . \ . \ . \ . \quad (4)$$

where K_1 and V_1 are the bulk modulus and volume at normal pressure and m is the rate of change of K with V/V_1. Using these results for Cs it is found that $m \simeq 10 K_1$, $K_1 = 16{\cdot}3$ kg cm^{-2}. Substitution of this data into (3) and using the relation $dK/dV = -m/V_1$ gives the value 0·146 for n.

The volume at which the two phases have the same free energy can now be obtained by substituting the condition $\gamma_L = 0$ into (3). This gives

$$V/V_0 \simeq 0{\cdot}59.$$

Experimentally Bridgman (1949, p. 181) finds two transformations under pressure in caesium, one occurring at a pressure of 23 000 kg cm^{-2} at a relative volume $V/V_0 = 0{\cdot}6284$ and a second one at 45 000 kg cm^{-2} at a relative volume $V/V_0 = 0{\cdot}498$. One of these transformations (at the lower pressure) is attributed to a polymorphic transformation from the body-centred cubic structure to the face-centred cubic form. The other is a paradox. The above arguments remove this paradox and lead one to expect an *isomorphous* phase change from a structure with a relatively large atomic volume to one with a smaller atomic volume. Two phases with the same crystal structure but with different atomic volumes are always possible, and with a suitable adjustment of external variables (P and T) a transformation from one to the other of these can be brought about in suitable cases. The above calculations suggest that the transformation at the lower pressure in caesium is associated with this isomorphic transition while the high pressure transformation is due to a polymorphic transition to a more closely packed structure.

Referring back to the quadratic expression for α it will be seen that at the transition point the coefficients of expansion α_t have the values $\pm(c/a)^{1/2}$. There will be a discontinuous volume change, therefore, of $2V_t \int_0^T |\alpha_t|\, dT$ where V_t is the volume of the substance at the transition pressure and 0°K.

Assuming, once again, that the valence electrons behave as a Fermi gas, it can be shown, loc. cit. that the coefficient C in the equation for α is given by

$$c=C_e\left(\frac{\partial n(\epsilon_F)}{\partial\epsilon_F}\right)_V\sqrt{\left[\frac{1}{Vn(\epsilon_F)^3}\right]}$$

where $n(\epsilon_F)$ is the density of states per unit volume at the Fermi surface.

Also $a=KV$, loc. cit., and hence ΔV_t, the volume change at the transition point, is

$$\Delta V_t=2V_t\int_0^T|\alpha_t|\,dT=\frac{\pi^2k^2T^2V}{6\epsilon_F}\sqrt{\left[\frac{n(\epsilon_F)}{K}\right]}.$$

Evaluation for $T=300^\circ$K with $V=0{\cdot}59V_1$, $V_1=71$ cm³ and again using the experimental data of Bridgman (1949, p. 180) for K, gives $\Delta V_t/V_1=1{\cdot}9_5\times10^{-3}$ which is to be compared with the corresponding experimental quantity 6×10^{-3}. The theoretical calculation is thus of the right order of magnitude and supports the suggestion that it is the low pressure transformation which is the isomorphic transition since the experimental relative volume change at the higher pressure transformation is $5{\cdot}6\times10^{-2}$. However, more detailed calculations may indicate the converse to be true.

§ 3. ISOMORPHIC PHASE CHANGES IN CERIUM

An isomorphic transformation will always be expected if the external variables, P and T, can be varied in such a manner as to make the linear coefficient b, in the quadratic expression for α pass through zero. The transition in caesium has already been discussed. There is another example in cerium†.

It has been observed (cf. Lawson and Tang 1949) that under high pressure and at low temperatures cerium undergoes a transition from one face-centred cubic structure to another with a smaller lattice parameter. At the transition volume the coefficient b in the quadratic expression for α must be zero.

Now b is given by, loc. cit.,

$$b=\frac{C_L\gamma_L}{(1+\beta)}+C_e\left\{1+\left(\frac{\partial\ln n(\epsilon_F)}{\partial\ln V}\right)_{\epsilon_F,T}-\frac{N}{n(\epsilon_F)^2}\left(\frac{\partial n(\epsilon_F)}{\partial\epsilon_F}\right)_V\left(1+\frac{\partial\ln N}{\partial\ln V}\right)_{\epsilon_F,T}\right\}$$

where N is the number of electrons per unit volume in partially filled bands and $n(\epsilon_F)$ is the density of states at the Fermi energy, ϵ_F.

Experimentally, Bridgman (1949, p. 168) finds that for cerium the change of compressibility χ, with volume is negative, and since this term is a major factor in γ_L then $\gamma_L<0$. The coefficient of expansion of cerium at normal pressure is positive so that $b>0$ at large volume and low pressure.

If, as a result of the compressibility decreasing with increasing volume, γ_L becomes more negative on compression then, since the coefficient of $C_e>0$ at normal pressures, b will for some value of V pass through zero. An isomorphic transition will then occur to a phase with a smaller atomic volume.

---

† The writer is indebted to Dr. L. Gutman for drawing his attention to this.

Again, if the pressure is held constant and the temperature reduced the coefficient b may again pass from positive to negative values. This is possible if the coefficient of C_e is large enough. At very low temperatures, where the electronic term in b predominates the structure should transform back again to a continuation of its room temperature form.

§4. CONCLUDING REMARKS

Isomorphic transitions are first order phase changes and will be accompanied by a latent heat of transformation. This is evident since there is a discontinuous change in volume and hence in internal energy.

Thus whenever the coefficient of volume expansion changes sign, as it must do when the coefficient b, of the linear term in the quadratic expression for α changes sign, an isomorphic transformation will occur with a discontinuous change in crystal volume.

In practice there may be a gradual transition from one structure to the other, a complete transformation at any given temperature being hindered by the generation of internal strains.

ACKNOWLEDGMENTS

The author wishes to acknowledge stimulating and helpful discussions with Dr. H. M. Finniston, Dr. J. Adam, Dr. L. Gutman and Dr. P. C. L. Pfeil.

REFERENCES

BRIDGMAN, P. W., 1949, *The Physics of High Pressures* (Bell and Sons).
LAWSON, A. W., and TANG, T-Y., 1949, *Phys. Rev.*, **76**, 2, 301.
SLATER, J. C., 1939, *Introduction to Chemical Physics* (New York: McGraw-Hill).
VARLEY, J. H. O. 1956 *Proc. Roy. Soc.* A, **237**, 413.

The Magnetic Susceptibility of α and β Brass†

By B. G. Childs and J. Penfold
Atomic Energy Research Establishment, Harwell

[Received September 21, 1956]

Summary

The magnetic susceptibility has been measured at 77° and 300°K of a series of copper–zinc alloys, ranging in composition from 0–47·6 atm% zinc, and of one silver–cadmium alloy containing 30·5 atm % cadmium. For the copper–zinc system the absolute susceptibility ranges from $-0{\cdot}085\times10^{-6}$ e.m.u./g for pure copper to $-0{\cdot}191\times10^{-6}$ e.m.u./g for 47·6% zinc. No significant difference was found between the values for a given alloy at the two temperatures of measurement.

The significance of the results is discussed in relation to a theory recently proposed by Henry and Rogers.

§ 1. Introduction

This paper deals with the measurement and interpretation of the magnetic susceptibility of brass as a function of zinc content over the face-centred cubic, α, range and at a single composition in the more restricted, body-centred cubic, β, range. A single measurement on the analogous silver–cadmium solid solution is also reported. Two temperatures of measurement were used, 77° and 300°K.

The copper-zinc system was chosen because of the relatively large amount of experimental information on various properties already available. Such a concentration of effort on one system should make easier the task of interpreting the behaviour of any one property and of formulating a general theory to account for the effects of alloying in a solid solution of this type.

When the work was started the variation of susceptibility, χ, through the α and β ranges was known approximately through measurements by Weber (1920) and by Endo (1925). These showed that χ in these ranges decreases with zinc concentration though the actual values obtained are probably not reliable. Endo also reported values for the γ range which are larger than those found (Smith 1935, Marcus 1949) by several later observers (e.g. $-1{\cdot}02$ instead of $-0{\cdot}78\times10^{-6}$ e.m.u./g at 67 atm % zinc). Neither worker made any check on the possible errors arising from ferromagnetic impurities.

Since the present investigation was completed the results have been published of an extensive series of measurements by Henry and Rogers

---

† Communicated by the Authors.

(1956) of the room temperature susceptibility of four copper based solutions including copper–zinc. They put forward an interpretation of the decrease in χ with concentration based on a suggestion by Friedel (1952). This is that in calculating the contribution to the diamagnetism the solute atoms can be considered as being singly ionized and free from interaction with other ions. Henry and Rogers require further that the slope of the electronic density of states curve for copper should be negative, the decrease in density of states at the Fermi level and hence in the Pauli paramagnetism as the electron to atom ratio is increased being the chief reason for the decrease in χ. The discussion in the present paper centres on showing that this latter assumption is probably not valid and that some other explanation must be found for the decrease in the magnetic susceptibility.

§ 2. METHOD OF MEASUREMENT

The method of measuring susceptibility was that due to Faraday. A specimen placed in a region of non-uniform magnetic field experiences a force in, say, the X-direction proportional to the susceptibility and to the average, over the specimen, of the quantity $H(dH/dX)$, where H is the magnetic field at X. In the present case it was arranged that the force acted principally in the vertical direction, the horizontal Y and Z components being very small.

The apparatus (see fig. 1) thus consisted essentially of two sections, an electromagnet for producing fields of the required intensity and intensity distribution, and a sensitive balance for measuring the force exerted on the specimen. This force was of the order of one dyne in the present tests.

2.1. *Magnet and Field Calibration*

The magnet was designed to give a maximum field of 15 000 oersted under continuous operation, the power consumption being 50 amp at 100 volt. Cooling was provided by a forced air draught in the case of the coils and by water for the magnet core. The pole pieces were machined to a cylindrical profile $r^{3/2} \cos 3\theta/2 = \text{constant}$ (r being the radius vector and θ the angle to the vertical), calculated by Davy (1942) to give an extended region of constant force. The size of this region was limited in practice by errors in machining and by the necessarily finite cross sectional area of the magnet core. The minimum gap of the polepieces was set at 1 in. and their width and maximum vertical height at 4 in.

The magnet was mounted on a trolley running on rails which allowed it to be removed from the rest of the apparatus when assembling the specimen.

The power supply was from a mercury arc rectifier, the current being adjusted manually with a bank of resistances in series with the magnet. The order of precision required in measurement and control of the current to give an error of less than 0·1% in susceptibility was, for example, 0·01 amp at 20 amps.

The calibration of field strength H_i and $[H(dH/dX)]_i$—the 'force constant' F_i—as functions of current i, was carried out by two methods. The first of these was the conventional search coil and fluxmeter method, the usual precautions being taken to avoid the cutting of lines of flux by parts of the circuit other than the coil. The coil—the dimensions of which, 4 mm long by 5 mm diameter, were accurately measured—was mounted on a brass holder which allowed it to be rotated and its position adjusted and measured to 0·1 mm in three dimensions. The fluxmeter itself was calibrated by reversing a known current through a standard mutual inductance in series with it.

Fig. 1

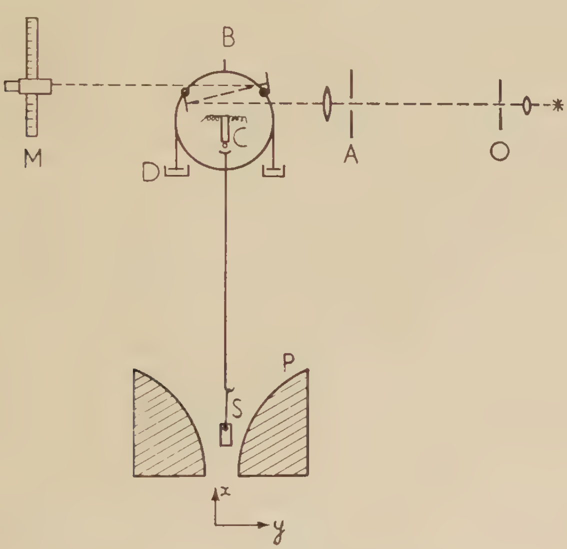

Schematic Arrangement of Apparatus.

M, Travelling microscope; A, Rectangular aperture; O, Slit source; B, Sucksmith balance; D, Damping member; S, Specimen; P, Pole pieces; C, Calibrating device.

This field calibration was carried out for five currents 13, 16, 20, 26 and 40 amp which were selected after a rough preliminary measurement to give approximately equal increments of $1/H$ (see § 3). It was made at intervals of about 5 mm over a volume 2 cm high by 2 cm deep by 1 cm in width over which the force constant was a maximum and approximately independent of position. The accuracy was limited to about 1% in H on account of the small size of search coil required.

In the second calibration method F_i was measured directly as a function of position and current in terms of the force on a small piece of tantalum, the susceptibility of which had previously been measured accurately by Hoare and Walling (1951) using the Gouy method. By integration of the F_i–X curves, values were found for the variation with x of $\varDelta H^2$, $\varDelta H^2$ being the difference between H^2 at the point x and at the centre of the calibrated region. These values were fitted to the directly measured curve of H^2 against X, thus allowing its accuracy to be improved. Mean force constants for specimens of any length lying within the limits of the calibrated region could then be calculated from this curve using the relation $F_i=\frac{1}{2}(H_1^2-H_2^2/X_1-X_2)$. A small further correction (up to about 2%) was applied to these values to allow for the effect on F_i of the differences in diameter between the specimens and the standard. This also was found experimentally.

2.2. *Balance*

A Sucksmith (1929) ring balance was constructed to measure the forces on the specimens. The ring was of beryllium copper strip 0·15 mm thick by 4 mm wide by 14 cm in diameter and had mirrors attached at positions of maximum sensitivity 50° above the horizontal diameter. From the bottom of the ring was suspended a silica rod 1 mm diameter by 40 cm long which ended, outside the constant force region, in a hook. The specimens were hung from this hook on a loop of fine gold wire.

Vibration of the ring as a whole was prevented by attaching oil damping members to points half way up the ring at the ends of the horizontal diameter. The upper quadrants of the ring which carried the mirrors were still free to vibrate in their normal modes, but vibrations of this frequency were prevented from reaching the ring by mounting the metal frame which carried the balance and optical train on suitably designed sponge rubber pads. The vibrational amplitude was thus reduced by a factor of 1000.

The deflection of the ring was measured with a travelling microscope in terms of the angular displacement of a beam of light reflected at the two mirrors. To get the required accuracy of force measurement the position of the beam had to be observed to an accuracy 0·002 mm or better. For this purpose a fine structure of about 0·01 mm in width was introduced into the image formed at the microscope. This was done by interposing a rectangular aperture in the path of the beam between a horizontal illuminated slit source and a focusing lens, both of which were on the opposite side of the balance from the microscope. The image of the slit, formed in the focal plane of the microscope, was thus superimposed with a diffraction pattern of fine black lines. It was found possible to set the cross wires on one of these lines to a precision of ±0·001 mm.

The balance was calibrated using a series of known wire weights. The calibration was found to be linear within 0·2% over a range of 40 dyne, the sensitivity being about 4 dyne/mm for a microscope to balance distance of 2 m. A further calibration could be made during an experiment by dropping a steel ball of known weight from a small electromagnet on to a pan attached to the balance. This electromagnet was normally switched off, the ball being held in contact with it, off the balance, by remanent magnetization.

2.3. *Ancillary Equipment*

The temperature of the specimen could be varied between 23° and 300°K by passing a stream of hydrogen or nitrogen gas from a reservoir of the boiling liquid through a heat exchanger coil wound around the tube which enclosed the specimen. Thermal insulation was provided by a Dewar flask which fitted between the poles of the magnet. In this particular investigation only two temperatures of measurement were employed, liquid nitrogen temperature 77°K and room temperature 298°K.

The specimen temperature was measured to an accuracy of 1°K using a calibrated copper–constantan thermocouple soldered to the outside of the heat exchanger tube level with the specimen. Preliminary calibration experiments determined the conditions under which the temperature recorded by this thermocouple was within 1°K of the temperature of a dummy specimen measured by a thermocouple in contact with it.

To prevent condensation on the specimen at the low temperatures and to reduce temperature fluctuations of the balance the specimen and balance enclosures were evacuated. It was necessary to keep the balance temperature as constant as possible because of the temperature sensitivity of the deflection which amounted to about 1 mm/°C. This was chiefly due to an additional elongation of the ring under its static load of about 10 g as a result of the variation with temperature of the elastic modulus. Accordingly the room temperature was controlled to ±0·1°C over the period of an experiment, using a multijunction thermocouple as a sensitive element. The thermal capacity of the balance enclosure and the insulation provided by the vacuum reduced still further the temperature fluctuation at the balance and, providing the balance was in equilibrium with the room before pumping down, the resulting zero drift was relatively small and could be allowed for.

§ 3. OPERATING PROCEDURE

The specimens used were for the most part of low susceptibility. They were made in the form of cylinders about 4 mm diameter and 1·5–1·8 cm in length. A hole was drilled along a diameter near one end of the cylinders to enable them to be hung from the balance.

In the case of the brass specimens appropriate amounts of 99·995% pure copper and zinc containing about 10 p.p.m. hydrogen and 50 p.p.m. of oxygen, were melted in a high frequency induction furnace. The ingots obtained were sectioned and examined metallographically for traces of segregation, samples also being taken from the top and bottom to check that the concentration was uniform. The individual specimens were machined from pieces cut from the centres of the ingots.

After manufacture the specimens were weighed, after a preliminary acid treatment to remove any traces of iron contamination from the surface. They were then suspended from the balance in a measured position, small weights being added or subtracted at the balance to keep the total load approximately constant and avoid grossly distorting the ring. The optical system was then adjusted to obtain the required sharp and achromatic diffraction image at the microscope. Care was taken to avoid the mirrors acting as additional stops and introducing a subsidiary diffraction pattern. The balance lid, heat exchanger tube and Dewar flask were next put on and the magnet moved into position. The apparatus was then evacuated, first to a pressure of 1 mm Hg and then, after the specimen had reached the required temperature for the experiment, to 10^{-3} mm Hg.

At the start of a run a number of readings of the zero position of the image were made as a function of time over about 2 min. The magnet current was then switched on and adjusted to 13 amp, particular care being taken to avoid overshooting the current and introducing field errors due to hysteresis. Readings of the deflected position were taken as a function of time over the next 2 min, after which the magnet current was switched off, a small current being passed momentarily in the opposite direction to demagnetize.

A further series of zero readings were taken for the next 2 min after which the magnet current was switched on at the next value (16 amp). In this way a series of readings of undeflected position of the zero were obtained as a function of time, interspersed by deflected readings corresponding to the five standard currents. At the end of the series the balance was recalibrated.

By plotting the zero readings against time, interpolated zero readings were obtained corresponding to each deflected reading, and hence the actual deflections for each magnet current. After correcting these for the deflections due to the suspension, corresponding values of the apparent mass susceptibility (χ_{app}) for each current were calculated using the force constants, balance sensitivity and mass of the specimen.

To correct χ_{app} for errors due to ferromagnetic impurities, which introduce a field dependent term, the method of Honda (1910) and Owen (1912) was used in which, providing the impurity is saturated,

$$\chi_{\text{true}} = \chi_{\text{app}} + \frac{\sigma}{H_i},$$

σ being the saturation magnetic moment of the impurities per g of specimen and H_i the average field.

χ_{true} is thus found by plotting χ_{app} against $1/H_i$ and extrapolating to $1/H = 0$.

§ 4. Results

As a check on the accuracy of the calibrations the susceptibility was first measured of 99·995% pure copper, silver, gold, aluminium and platinum. Table 1 gives the values found for these compared with apparently reliable values found by various other observers. Since our figures are relative to tantalum as $0{\cdot}849\times10^{-6}$ e.m.u./g the value found by Donoghue for tantalum is included. Agreement is generally satisfactory except in the case of platinum where Donoghue's value is appreciably higher than our own. This may be connected with the particular sample used by Donoghue since he found appreciably different values for two apparently identical specimens.

Table 1. The Susceptibility of Various Pure Metals

Metal	Specimen Number	Temp. °C	χ_m e.m.u./g $\times10^6$	χ_m found by other observers at room temperature e.m.u./g $\times10^6$			
Cu	1	22	−0·084±0·002	−0·086 (D)	−0·085 (HRe)	−0·085 (A)	−0·086 (HRo)
	2	22	−0·084±0·002				
	3	20	−0·084±0·002				
		−196	−0·085±0·002				
Ag	1	22	−0·177±0·002	−0·183 (D)	−0·185 (V)	−0·176 (A)	−0·182 (HRo)
	2	22	−0·179±0·002				
	3	22	−0·177±0·002				
Au		24	−0·140±0·002	−0·142 (D)	−0·145 (V)	−0·140 (A)	−0·142 (HRo)
Al		22	+0·615±0·005	+0·608 (D)	+0·62 (HRe)		
Pt		23	+0·967±0·005	+0·988 +1·011	+0·971 (HW)		
Ta				0·864 (D)	0·849 (HW)		

References (D) Donoghue, J. J., 1953, NAA-SR-117.
(HRe) Hutchinson, T. S., and Reekie, J., 1948, *Phys. Rev.*, **73**, 517.
(V) Vogt, E., 1932, *Ann. d. Physik*, **14**, 1.
(A) Auer, H., Riedl, E., and Seeman, H. J., 1934, *Zeits. Phys.*, **92**, 291.
(HW) Hoare, F. E., and Walling, J. C., (1951).
(HRo) Henry, W. G., and Rogers, J. L. (1956).

The silver results are interesting since they demonstrate what errors can be introduced by quite small amounts of impurities in ferromagnetic form and also the reliability of the Honda–Owen method of correction. Figure 2 shows the apparent susceptibility as a function of $1/H$ for the specimens Ag1, Ag2 and Ag3. These were prepared from a single rod of spectrographically pure silver supplied by Messrs. Johnson Matthey. Ag1 was machined directly from the rod and showed only a moderate degree of ferromagnetic impurity. Ag2 was Ag1 annealed *in vacuo* for 1 hr at 900°C. The slope of the curve, proportional to the saturation magnetic moment of the impurities, is greater for this specimen. Ag3 was remelted *in vacuo* and cooled slowly. Here the slope of the curve is greater still, the values of apparent susceptibility for the low fields being actually positive instead of negative as for pure Ag.

In each case any surface contamination of the specimen was removed by boiling it in concentrated HCl while in the case of Ag2 the specimen was removed once from the apparatus to be reboiled in HCl and a second time to have its surface removed by electropolishing. This treatment had no effect on the apparent susceptibility.

Despite the great range of slopes the values of χ_{true} taken from the intercepts of the curves at $1/H=0$ coincide within the experimental error. The fact that the lines are straight indicates that the impurities were saturated at the lowest field (5500 oersted). Analysis of the samples after measurement showed in each case the principal ferromagnetic impurity to be 15 p.p.m. of iron. The presence of nickel and cobalt could not be detected, the limits of sensitivity being 1 and 5 p.p.m. respectively. The difference in the ferromagnetic behaviour of the three samples is presumably to be attributed to the varying degrees of precipitation of the iron content on going from Ag1 where the metal was chill cast and heavily cold worked to Ag3 where the metal was cooled slowly from the melting point. Metallographic examination of Ag3 at magnification of 1300 showed no indisputable signs of a precipitate which could have been responsible for the ferromagnetism though this is not necessarily surprising since, as shown by Reincke (1954) in the case of thin iron films permanent magnetization can occur at a thickness of only 11 Å.

Fig. 2

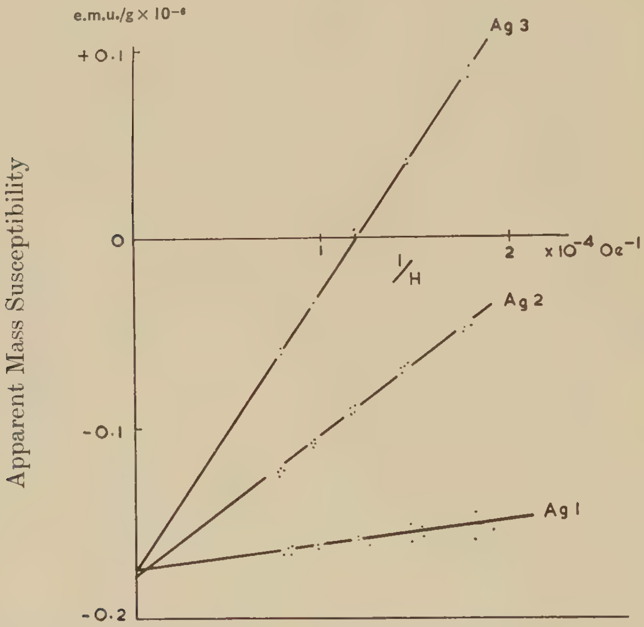

Apparent Susceptibility—1/H for Three Silver Specimens.

The exceptionally high ferromagnetic impurity content of Ag2 and Ag3 characterized by the large slopes of the $\chi_{\text{app}}-1/H$ curves did not occur for the other metal and alloy specimens. The slopes for these were roughly the same as for Ag1.

Table 2. The Mass and Atomic Susceptibilities of Brass

Concentration atomic % zinc	$-\chi_m \times 10^6$ e.m.u./g at		$-\chi_A \times 10^{-6}$ e.m.u./g atom at	
	77°K	298°K	77°K	298°K
0	0·085	0·084	5·41	5·34
4·9	0·089	0·090	5·67	5·74
8·2	0·0925	0·0925	5·89	5·89
11·4	0·095	0·097	6·06	6·18
18·8	0·108	0·109	6·90	6·97
25·0	0·122	0·121	7·81	7·75
30·4	0·136	0·135	8·71	8·65
31·0	0·1365	0·139	8·75	8·9
47·6	0·191	0·190	12·31	12·25

Estimated accuracy of χ_m is ± $0{\cdot}0015 \times 10^{-6}$.

Fig. 3

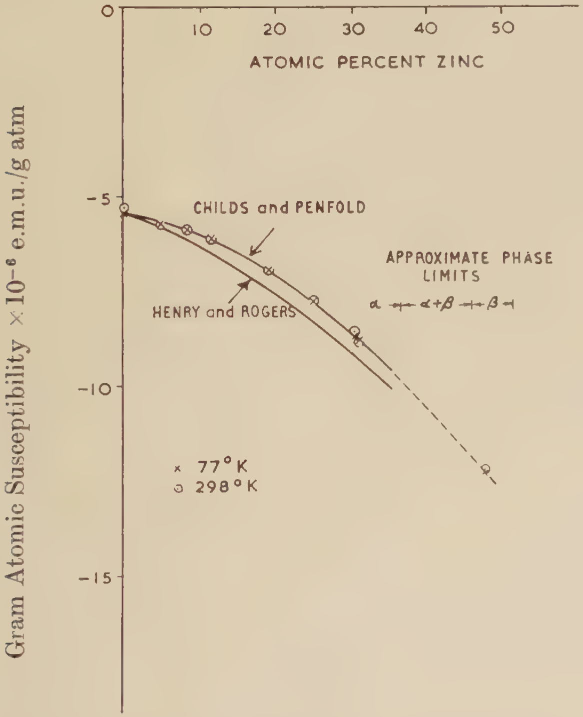

The Atomic Susceptibility of Brass as a Function of Zinc Concentration.

The variation of the mass χ_m and atomic χ_A susceptibilities of the copper–zinc solution at 77° and 298°K are shown in fig. 3 and table 2. Each point shown is the average of six separate measurements, each corrected for ferromagnetic impurity.

Over the range of α solid solution from 0–32% zinc the alloys become increasingly diamagnetic the values of χ_m ranging from $-0{\cdot}084\times10^{-6}$ for pure copper to $-0{\cdot}138\times10^{-6}$ e.m.u./g for 32 atm % zinc. The value for β brass, 47·6 atm % zinc, is lower again at $-0{\cdot}190\times10^{-6}$ e.m.u./g. Within the experimental error, estimated at about $\pm0{\cdot}015\times10^{-6}$, the values of the susceptibility at 77° and 298°K are the same. Also reproduced in fig. 3 are the values found by Henry and Rogers. Their values for the α range are systematically more diamagnetic than our own, the discrepancy at the higher concentrations being about 6% of our value. There seems no obvious explanation for this.

In connection with another investigation, a single measurement was also made on a specimen in the analogous silver–cadmium system at 30·5 atm % cadmium. The values found were $-0{\cdot}215$ and $-0{\cdot}217\pm0{\cdot}002\times10^{-6}$ e.m.u./g for χ_m at 77° and 295°K respectively, compared with $-0{\cdot}177$ at 295°K for pure silver. In atomic units this represents a decrease of $4{\cdot}6\times10^{-6}$ e.m.u./g atom between 0 and 30 atm % compared with a decrease of $3{\cdot}2\times10^{-6}$ e.m.u./g atom over the same concentration interval for copper–zinc.

§ 5. DISCUSSION

The total magnetic susceptibility of an alloy is usually discussed theoretically in terms of separate and distinct contributions made by various groups of electrons. Distinction may be made in the case, say, of the copper–zinc system between contributions from electrons

(*a*) up to and including the $(3d)^{10}$ shell of the Cu^+ ions ;

(*b*) up to and including the $(3d)^{10}$ shell of the Zn^{++} ions ;

(*c*) distributed around the Zn^{++} ions to screen their single excess charge.

These three groups give rise to an orbital diamagnetism of the type first treated classically by Langevin.

The 4s electrons from the copper and zinc atoms which enter the conduction band give

(*d*) a paramagnetic effect (Pauli paramagnetism) as a result of the partial nett alignment of their spins. This contribution, is at 0°K proportional to $n(\zeta)$ the density of states at the Fermi level. It may be further enhanced by exchange interaction effects which, if positive, tend to increase any existing inequality in the numbers of + and − spins.

(*e*) A diamagnetic effect due to the curvature, imposed by the field, on the paths of these electrons as they move through the lattice.

(In this treatment any orbital contribution to the diamagnetism from the copper 4s and second zinc 4s electrons has been ignored).

No one of these contributions can be calculated exactly (although some separation is possible in practice using information from other types of experiment) so that, in cases such as copper–zinc where the contributions are believed to be all of the same order of magnitude, no great accuracy can be expected in the final theoretical value for the absolute susceptibility at any particular concentration.

Variations in susceptibility with concentration can be expected to arise in varying degrees from the following :

(i) The replacement of Cu^+ ions by smaller Zn^{++} ions having a smaller diamagnetism.

(ii) The change in the individual contributions of Cu^+ ions and Zn^{++} ions as, with the expansion of the lattice on alloying, the ions move further apart and their 3d shells (responsible for about 85% of the diamagnetism) interact less.

(iii) The total diamagnetic contribution from the screening 4s electrons which will increase with zinc concentration.

(iv) Changes in the shape of the $n(E)$ curve and hence in the Fermi level and $n(\zeta)$ for a given conduction electron concentration due to (*a*) the overall expansion of the copper lattice and (*b*) by local perturbations of the periodic potential.

(v) Filling of the band as the concentration of conduction electrons increases with zinc concentration.

(vi) Variation with lattice parameter and wave function symmetry of exchange interaction effects.

(vii) Variation of the conduction electron diamagnetism as the first Brillouin zone is filled.

The problem of deciding which of these are the major effects and of estimating their size is no easy one.

In their treatment of this problem Henry and Rogers follow Friedel (1952) in assuming that one important term governing the slope of the susceptibility concentration curves for their copper base alloys is the resultant change in orbital diamagnetism of (i) and (iii). The distribution of screening charge is assumed to be the same as that of a (4s) electron on an isolated Zn^{++} ion. Stoner's (1929) formula for ionic diamagnetism is used with the charge distribution for Cu^+, Zn^{++} and Zn(4s) calculated by the self consistent field method. This orbital term accounts for about $\frac{1}{2}$—$\frac{1}{4}$ of the observed negative slope found by Henry and Rogers for copper–zinc, copper-gallium, copper–germanium and copper–arsenic, but provides a small positive contribution in the case of copper–aluminium where the nett slope is also negative.

The major contribution to the slope is assumed to come from a decrease in the Pauli paramagnetism (governed by (iv) and (v)), a change in the shape of $n(E)$ solely with lattice spacing being assumed which is the same as that for free electrons. For the $n(E)$ curve for copper, Henry and Rogers take the curve postulated by Jones (1937 b) to account for the α and β solubility ranges in copper–zinc and similar alloys : in this the Fermi level is close to a maximum beyond which $n(E)$ decreases roughly linearly with electron/atom ratio. Henry and Rogers assume that ζ is actually past the maximum so that addition of further electrons on adding zinc (or on Friedel's model the subtraction of states from the bottom of the band) produces a linear decrease in $n(\zeta)$ with concentration. This term is the one in their view primarily responsible for the decrease in susceptibility; other possible effects such as (ii), (iv *b*) and (vi) are ignored.

The agreement cited by Henry and Rogers between theory and experiment for the slopes of their five solid solutions is apparently excellent (cols. 2 and 3, table 3) and at first sight the assumptions made seem to be amply justified. On closer examination, however, there seems considerable doubt as to whether the basic assumption of a negative slope of $n(E)$ for copper is in fact correct. This point will now be examined in some detail.

Table 3. Calculated and Observed Slopes Derived from Henry and Rogers

(1)	(2)	(3)	(4)
Cu–Zn	−7·2	−8·1	−2·9
Cu–Ga	−19·3	−13·3	−2·9
Cu–Ge	−27·4	−23·6	−8·0
Cu–As	−38	−29·8	−9·0
Cu–Al	−6·8	−6·7	+3·7

(1) alloy system; (2) slopes observed by Henry and Rogers; (3) quoted 'calculated' slopes; (4) 'calculated' slopes for zero slope of $n(E)$ for Cu. The slopes of the curves of susceptibility against concentration are in units of 10^{-6} e.m.u./g atm.

In his calculation of $n(E)$ Jones proposed an expression for E as a function of k_x, k_y and k_z to hold in the *immediate* neighbourhood of the k_z-direction (taken as one of the 8 equivalent (111) directions). This was arrived at purely intuitively as being the simplest expression which satisfied certain necessary conditions at the zone boundary and centre. $n(E)$ was obtained from this by the further arbitrary approximations of assuming the $E(\bar{k})$ relation to hold over a circular cone of solid angle $\frac{1}{2}\pi$ in $\bar{k}$ space and of replacing the actual Fermi surface by the surfaces associated with 8 such cones, one for each octahedral face of the first Brillouin zone. Thus Jones' $n(E)$ curve cannot be regarded as sufficiently firmly based for a numerical calculation and the quantitative agreement which he finds for the α and β solubility limits may well be fortuitous.

What evidence there is for the actual $n(E)$ curve for copper suggests in fact that the Fermi level is well on the *low* energy side of a maximum so that $n(E)$ *increases* initially with E, or in other words that the Fermi surface has not touched the zone boundary.

Thus for example Cauchois (1953) in an analysis of the copper K and L x-ray absorption spectra finds an absorption maximum for the L III band at about 1·0 ev beyond the absorption edge. Since this corresponds to transitions to states of primarily s symmetry in the band and the s character decreases and p increases with increase of energy, this must imply that $n(E)$ itself is *increasing* with E up to this point.

A maximum in the K absorption band at 2·7 ev indicates that $n(E)$ probably has a maximum, with a fair admixture of p character, at about this energy. Beyond 2·7 ev $n(E)$ is believed to drop to a minimum before rising again, corresponding to overlap of the first and second zones. This experimentally deduced behaviour agrees well qualitatively with the theoretical $n(E)$ curve for copper derived by Rudberg and Slater (1936) from Krutter's (1935) quantum mechanical calculations of E as a function of $\bar{k}$. Rudberg and Slater predict that $n(E)$ rises to a maximum about 1·5 ev beyond ζ with a minimum at about 3·5 ev and a second maximum at 5 ev†.

If $n(\zeta)$ in the alloy depended, apart from a slight correction for changes in lattice parameter, simply on filling the copper conduction band, then it seems most likely that it should increase with concentration and not decrease as required by Henry and Rogers. The situation is not as straightforward as this however since as shown by Bearden and Friedman (1940) the edges of the copper and zinc K absorption bands for copper–zinc alloys do not shift appreciably relative to the fine structure of the bands as the composition is increased. This would seem to imply that in fact little movement in ζ occurs relative to the first maximum in $n(E)$ for copper the actual slope of $n(E)$ not being the factor principally determining $n(\zeta)$ in the alloys.

Fortunately direct information about $n(\zeta)$ is now available from measurements by Smith (unpublished work in progress) of the electronic specific heat, C_E, in the copper–zinc system. Smith finds $\gamma(=C_E/T)$ which is proportional to $n(\zeta)$ to show a significant increase with zinc content from a value of $1{\cdot}65 \pm 0{\cdot}05 \times 10^{-4}$ cal/g/atm/deg^2 for pure copper to a value of $2{\cdot}00 \pm 0{\cdot}05 \times 10^{-4}$ cal/g/atm/deg^2 for 32 atm % zinc, a behaviour quite at variance with that on which Henry and Rogers base their calculations. Thus it seems likely that $n(\zeta)$ and hence the paramagnetic term in the total susceptibility for copper-zinc should *increase* initially with zinc content. Even if it only remains constant however the agreement obtained on Henry and Roger's treatment is completely destroyed (see column 4, table 3).

We must accordingly anticipate a diamagnetic effect additional to those which Henry and Rogers have considered and one, moreover, probably related in some way to the valency of the solute so as to give the observed increase, with solute atom valency, in the negative slopes of the susceptibility/concentration curves. Such a contribution could come from the conduction electrons since, as Krutter shows, these cannot be considered as free, the energy surfaces being far from spherical.

---

† A similar calculation of $E(\bar{k})$ made by Howarth (1953) for the (111) and (200) directions in phase space also predicts that $n(E)$ should increase initially, the Fermi surface being 1·2 ev below the energy at which the surface first touches the zone boundary.

In the case of bismuth and the γ brasses Jones (1934, 1937 b) has shown that the relatively much larger diamagnetism can be accounted for by supposing that the energy surfaces of the electrons overlapping into the second zone are highly ellipsoidal.

Unfortunately it is difficult to make a reliable estimate of the conduction electron diamagnetism for the α solutions. Until this can be done however further speculation as to the reason for the drop in susceptibility would not appear profitable.

§ 6. Conclusion

The decrease in magnetic susceptibility with concentration found by Henry and Rogers for the copper–zinc, copper–arsenic, copper–gallium and copper–germanium solid solutions and by ourselves for copper–zinc does not appear to be attributable to a decrease in Pauli paramagnetism consequent on filling an electron band derived from the copper conduction band. Neither, allowing for the inaccuracies in the calculation, does it seem likely that the additional diamagnetism of the solute ions—assumed singly ionized—can be the major factor. No satisfactory explanation can be suggested at present for the decrease. It may, however, be due at least in part to an enhancement of the conduction electron diamagnetism.

Acknowledgments

We would like to express our thanks to Dr. W. M. Lomer and Mr. A. D. LeClaire for theoretical discussions, to Mr. C. Thomas for preparing the alloys and to Mr. C. Austing for the analyses. Thanks are also due to Dr. P. L. Smith for allowing us to make use of his results before publication.

References

Bearden, J. A., and Friedman, H., 1940, *Phys. Rev.*, **58,** 387.
Cauchois, Y., 1953, *Phil. Mag.*, **44,** 173.
Davy, N., 1942, *Phil. Mag.*, **33,** 575.
Endo, H., 1925, *Sci. Report Tohoku Univ.*, **14,** 479.
Friedel, J., 1952, *Phil. Mag.*, **43,** 159.
Henry, W. G., and Rogers, J. L., 1956, *Phil. Mag.*, **1,** 237.
Hoare, F. E., and Walling, J. C., 1951, *Proc. Phys. Soc.* B, **64,** 337.
Honda, K., 1910, *Ann. d. Phys.*, **32,** 1046.
Howarth, D. J., 1953, *Proc. Roy. Soc.* A, **220,** 513.
Jones, H., 1934, *Proc. Roy. Soc.*, **144,** 225 ; 1937, *Ibid.*, **147,** 396 ; 1937 b, *Proc. Phys. Soc.*, **49,** 250.
Krutter, H., 1935, *Phys. Rev.*, **48,** 664.
Marcus, J. A., 1949, *Phys. Rev.*, **76,** 621.

Owen, M., 1912, *Ann. d. Phys.*, **37**, 666.
Reincke, W., 1954, *Z. Phys.*, **137**, 169.
Rudberg, E., and Slater, J. C., 1936, *Phys. Rev.*, **50**, 150.
Smith, C. S., 1935, *Physics*, **6**, 47.
Stoner, E. C., 1929, *Proc. Leeds Phil. Lit. Soc.*, **1**, 484.
Sucksmith, W., 1929, *Phil. Mag.*, **8**, 158.
Weber, R. H., 1920, *Ann. d. Phys.*, **62**, 666.

Ferromagnetism of a Gas of Hard Sphere Fermions †

By JOACHIM B. EHRMAN
Nucleonics Division, U.S. Naval Research Laboratory, Washington, D.C.

[Received October 10, 1956]

SUMMARY

The energy of a gas of fermions of spin $\frac{1}{2}$, interacting with a hard sphere repulsion, is obtained by means of Brueckner's approach to the many-body problem. The single particle potential is computed in the effective mass approximation, and the value of the maximum density for which this approximation is valid, is derived. By means of a modification of the effective mass approximation, in which the effective mass becomes spin-dependent, it is shown that above a certain critical density, the gas becomes ferromagnetic.

§ 1. INTRODUCTION

THE method which has been developed by Brueckner and his co-workers (Brueckner and Levinson 1955) for the derivation of the properties of a nucleus in its ground state and in states of not too high an excitation is applicable to any many-body problem in which the particles interact by means of two-body forces only, even when these are very strong, and in which it is sufficient to treat two particle correlations precisely without a precise treatment of correlations of three or more particles. In particular, the method should be applicable to the theory of liquid ^{3}He. Since we are dealing with a system obeying Fermi–Dirac statistics, the arguments of Brueckner (1955 b) and of Bethe (1956) concerning the smallness of the cluster terms should hold, although the three particle cluster must, of course, be evaluated in order to estimate the error in the energy. In fact the theory is applicable to this problem in a much cleaner fashion than to the nuclear one, since in the former case, the only source of error arises from the cluster term, whereas the terms inversely proportional to the number of particles constitute no source of error whatever, and there is strict conservation of momentum throughout the problem. Furthermore, in the nuclear case, a precise treatment involves the guessing and making self consistent of a single particle potential matrix which is, in general, not diagonal in any simple representation like position or momentum, and the definition of matrix elements of various operators with respect to Slater determinants which are not built up from plane waves, but from functions whose form must be changed in the course of the guessing in the self consistent calculation. Although Brueckner (1955 a) and Skyrme (1956) have carried out calculations taking nuclear surface effects into account, no calculation which takes into account the full complication of the finite nucleus case has as yet been carried out.

---

† Communicated by the Author.

In this paper, only results for the idealized case of a gas of hard spheres with spin $\frac{1}{2}$ and Fermi-Dirac statistics are discussed. Those for liquid ^{3}He will be presented in a subsequent paper. In § 2, an expression for the single particle potential in the effective mass approximation (e.m.a.) is written down. In § 3, the value of the effective mass is derived in the low density limit, and an expansion of the energy as a function of density is given. In § 4, the effective mass and the energy are calculated at higher densities, and the limit of validity of the e.m.a. is clearly set forth. In § 5, the spin-dependent effective mass approximation (s.d.e.m.a.) is introduced and the single particle potentials are obtained. The effective masses and energy in the low density limit are given in § 6, while in § 7 is calculated the value of the density above which the antiferromagnetic configuration is no longer the least energetic. In § 8, the characteristics of the gas in the ferromagnetic region of densities at absolute zero are given, as well as a model which leads to an overestimate of the Curie temperature.

§ 2. SINGLE PARTICLE POTENTIAL IN THE EFFECTIVE MASS APPROXIMATION

Let the interaction between a pair of particles be denoted by v_{ij}, while the corresponding reaction matrix is denoted by G_{ij}. The (non-symmetrized) matrix elements of v will be denoted by

$$(n_i'n_j'|v_{ij}|n_in_j)=\int \psi^*(n_i';\mathbf{r}_i)\psi^*(n_j';\mathbf{r}_j)v_{ij}(r_{ij})\psi(n_i;\mathbf{r}_i)\psi(n_j;\mathbf{r}_j)\,d^3r_i\,d^3r_j \tag{1}$$

where $\psi(n_i;\mathbf{r}_i)$, etc. denote the solutions of the Schrödinger equation with the single particle potential. The $\psi(n_i;\mathbf{r}_i)$ are plane waves in our case, since the single particle potential V is diagonal in the momentum representation for an infinite medium. In writing the matrix element $(n_i'n_j'|v_{ij}|n_in_j)$, it is understood that all particles not explicitly written down are in the same state as in the chosen configuration (Bethe 1956). (When a definite particle is said to be in a definite one particle state, a convention like picking out the main diagonal of a Slater determinant is being used.) Of course, no single particle state is ever multiply occupied.

In general, let

$$v_{ij}=v_t \text{ or } v_s, \quad . \; . \; . \; . \; . \; . \; . \; . \tag{2}$$

for a triplet or singlet pair, so that

$$v_{ij}=\tfrac{1}{4}(3v_t+v_s)+\tfrac{1}{4}(v_t-v_s)(\boldsymbol{\sigma}_i\,.\,\boldsymbol{\sigma}_j). \quad . \; . \; . \; . \; . \tag{3}$$

Then the reaction matrix for two particles with spins pointing in the same direction is given by the integral equation : †

$$\begin{aligned}(\mathbf{k}_i'\mathbf{k}_j'|G_{ijI}|\mathbf{k}_i\mathbf{k}_j)&=(\mathbf{k}_i'\mathbf{k}_j'|\tfrac{1}{2}(1-P_M)v_t|\mathbf{k}_i\mathbf{k}_j)\\ &\quad-(2\pi)^{-3}\int d^3\mathbf{k}_i''(\mathbf{k}_i'\mathbf{k}_j'|\tfrac{1}{2}(1-P_M)v_t|\mathbf{k}_i''\mathbf{k}_j'')\\ &\quad\times\frac{P}{E(\mathbf{k}_i'')+E(\mathbf{k}_j'')-E(\mathbf{k}_i)-E(\mathbf{k}_j)}(\mathbf{k}_i''\mathbf{k}_j''|G_{ijI}|\mathbf{k}_i\mathbf{k}_j), \qquad . \quad . \quad (4)\end{aligned}$$

where P_M is the Majorana exchange operator. That for spins pointing in opposite directions is given by

$$\begin{aligned}(\mathbf{k}_i'\mathbf{k}_j'|G_{ijII}|\mathbf{k}_i\mathbf{k}_j)&=(\mathbf{k}_i'\mathbf{k}_j'|\tfrac{1}{2}(1-P_M)v_t|\mathbf{k}_i\mathbf{k}_j)+(\mathbf{k}_i'\mathbf{k}_j'|\tfrac{1}{2}(1+P_M)v_s|\mathbf{k}_i\mathbf{k}_j)\\ &\quad-(2\pi)^{-3}\int d^3\mathbf{k}_i''[(\mathbf{k}_i'\mathbf{k}_j'|\tfrac{1}{2}(1-P_M)v_t|\mathbf{k}_i''\mathbf{k}_j'')+(\mathbf{k}_i'\mathbf{k}_j'|\tfrac{1}{2}(1+P_M)v_s|\mathbf{k}_i''\mathbf{k}_j'')]\\ &\quad\times\frac{P}{E(\mathbf{k}_i'')+E(\mathbf{k}_j'')-E(\mathbf{k}_i)-E(\mathbf{k}_j)}(\mathbf{k}_i''\mathbf{k}_j''|G_{ijII}|\mathbf{k}_i\mathbf{k}_j). \qquad . \quad . \quad (5)\end{aligned}$$

In eqns. (4) and (5), $\mathbf{k}_i'+\mathbf{k}_j'=\mathbf{k}_i''+\mathbf{k}_j''=\mathbf{k}_i+\mathbf{k}_j$, the single particle states being denoted by the wave number $\mathbf{k}$ of their plane waves. The integral over $\mathbf{k}_i''$ is such that neither $\mathbf{k}_i''$ nor $\mathbf{k}_j''(=\mathbf{k}_i+\mathbf{k}_j-\mathbf{k}_i'')$ is occupied in the chosen configuration, while $\mathbf{k}_i$, $\mathbf{k}_j$ are assumed to be the wave numbers of particles i and j in the chosen configuration. $E(\mathbf{k})$ is the single particle energy for wave vector $\mathbf{k}$, and we have assumed that the excitation energy of $(\mathbf{k}_i''\mathbf{k}_j''\mathbf{k}_a^0\ldots)$ with respect to $(\mathbf{k}_i\mathbf{k}_j\mathbf{k}_a^0\ldots)$ can be expressed entirely in terms of one particle energies, as in eqns. (3)–(8) of Bethe 1956. Goldstone (see Bethe 1956) has pointed out that this is not in general true, but we shall make use of it as a simplifying assumption throughout this paper.

We take $v_s=v_t=v$, and we assume that v is an ordinary (Wigner) force. The single particle potential in the chosen configuration is given by the integral over the diagonal elements of the reaction matrix :

$$V(\mathbf{k}_i)=(2\pi)^{-3}\int d^3\mathbf{k}_j(\mathbf{k}_i\mathbf{k}_j|2G_{ijI}+G_{ijII}|\mathbf{k}_i\mathbf{k}_j) \quad . \quad . \quad . \quad . \quad (6)$$

where the integrals run over all $\mathbf{k}_j$ in the chosen configuration. The factor 2 in front of G_{ijI} in (6) arises from the possibility of having both spins up or both spins down.

In the e.m.a. one assumes that $V(\mathbf{k}_i)$ can be written down as

$$V(\mathbf{k}_i)=V(0)+bk_i^2 \quad . \quad . \quad . \quad . \quad . \quad . \quad . \quad . \quad (7)$$

where an effective mass M^* is defined by the equation

$$\frac{1}{M^*}=\frac{1}{M}+2b \quad . \quad . \quad . \quad . \quad . \quad . \quad . \quad . \quad (8)$$

since $E(\mathbf{k}_i)$ is then given by

$$E(\mathbf{k}_i)=V(0)+k_i^2/2M^*. \quad . \quad . \quad . \quad . \quad . \quad . \quad (9)$$

Let us now take for the chosen configuration that in which all states with wave numbers from 0 to a certain maximum (Fermi) wave number

---

† In this paper, only neutral fermions are considered. There are 4 instead of 2 different reaction matrices if two charges (isotopic spin orientations) are also allowed.

k_F are occupied by two particles of opposite spin, while all single particle states with wave numbers $k > k_F$ are empty. Then the integral in eqns. (4) and (5) runs only over those $\mathbf{k}_i''$ for which $k_i'' > k_F$ and $|\mathbf{k}_i'' - \mathbf{k}_i - \mathbf{k}_j| > k_F$. Let us simplify the problem by neglecting this restriction and integrating over all $\mathbf{k}_i''$ instead. The effects of this replacement will be discussed below.

The reaction matrix is now that for the interaction of two particles of mass M^* each. For a hard sphere interaction of radius a, i.e. $v_{ij} = +\infty$ for $r_{ij} < a$ and 0 for $r_{ij} > a$, the solution is well known to be

$$(\mathbf{k}_i'\mathbf{k}_j'|G_{ij}|\mathbf{k}_i\mathbf{k}_j) = \frac{4\pi}{M^*}\frac{1}{\sqrt{(k_{ij}'k_{ij})}}\sum_{l=0}^{\infty}(-1)^l(2l+1)\frac{J_{l+1/2}(k_{ij}'a)}{J_{-l-1/2}(k_{ij}a)}P_l(\cos\theta) \quad (10)$$

where $k_{ij} = \frac{1}{2}|\mathbf{k}_i - \mathbf{k}_j|$, $k_{ij}' = \frac{1}{2}|\mathbf{k}_i' - \mathbf{k}_j'|$, and θ is the angle between $\mathbf{k}_i - \mathbf{k}_j$ and $\mathbf{k}_i' - \mathbf{k}_j'$. For the diagonal matrix elements, we may write

$$(\mathbf{k}_i\mathbf{k}_j|G_{ij}|\mathbf{k}_i\mathbf{k}_j) = \frac{-4\pi}{M^*}\frac{1}{k_{ij}}\sum_{l=0}(2l+1)\tan\delta_l \quad . \quad . \quad . \quad . \quad (11)$$

where

$$\tan\delta_l = (-1)^{l+1}J_{l+1/2}(k_{ij}a)/J_{-l-1/2}(k_{ij}a) \quad . \quad . \quad . \quad . \quad (12)$$

δ_l is the phase shift for orbital angular momentum l for a hard sphere of radius a. (Eqn. (11) applies to any central potential.)

Hence, eqn. (6) becomes, for a central potential writing $V(k_i)$ for $V(\mathbf{k}_i)$:

$$V(k_i) = -\frac{1}{(2\pi)^3}\int_0^{k_F}\iint d^3\mathbf{k}_j\frac{4\pi}{M^*k_{ij}}\sum_l(2l+1)f_l\tan\delta_l(k_{ij}) \quad . \quad . \quad (13)$$

where

$$f_l = 2 + (-1)^{l+1} \quad . \quad . \quad . \quad . \quad . \quad . \quad . \quad . \quad (13a)$$

δ_l is the phase shift for orbital angular momentum l caused by v †. By means of a straightforward transformation of variables, (and writing x for k_{ij}) this may be written as :

$$V(k_i) = -\frac{8}{\pi M^*}\int_{x=0}^{1/2(k_i+k_F)}dx\cdot xP_{k_i}(x)\sum_l(2l+1)f_l\,\delta_l(x) \quad . \quad . \quad (14)$$

for $k_i < k_F$, while for $k_i > k_F$, we get

$$V(k_i) = -\frac{8}{\pi M^*}\int_{x=1/2(k_i-k_F}^{1/2(k_i+k_F)}dx\,.\,xQ_{k_i}(x)\sum_l(2l+1)f_l\,\delta_l(x). \quad . \quad (15)$$

$$\text{Here, } P_k(x) = \begin{cases} 2 \text{ for } 0 < x < \frac{1}{2}(k_F - k) \\ \dfrac{\frac{1}{4}k_F^2 - (\frac{1}{2}k - x)^2}{kx} \text{ for } \frac{1}{2}(k_F - k) < x < (\frac{1}{2}k_F + k) \end{cases} \quad . \quad . \quad . \quad . \quad (16)$$

---

† Riesenfeld and Watson have shown that the integral eqns. (4) and (5) should, in a more rigorous treatment, contain a matrix element of the reaction matrix as a term in the denominator of the propagator, and that therefore the factor $\tan\delta_l$ in (13) should be replaced by δ_l. This treatment corresponds to enclosing the entire system in a very large but finite box and imposing the suitable boundary condition of wave functions going to zero on the surface of the box. In what follows, $\tan\delta_l$ will be systematically replaced by δ_l. The author is very much indebted to Dr. W. Wada for bringing this point to his attention.

$$Q_k(x)=\frac{\frac{1}{4}k_F^2-(\frac{1}{2}k-x)^2}{kx} \text{ for } \tfrac{1}{2}(k-k_F)<x<\tfrac{1}{2}(k_F+k). \quad . \quad . \quad (17)$$

In the chosen configuration, we do not need eqn. (15), since $k_i<k_F$, but in § 5, this case will be required and it has therefore been derived here.

For the case of a hard sphere interaction, (14) becomes

$$V(k_i)=-\frac{8}{\pi M^*}\int_{x=0}^{1/2(k_i+k_F)} dx\,.\,xP_{k_i}(x)\sum_l(2l+1)f_l$$
$$\arctan\left[(-1)^{l+1}\frac{J_{l+1/2}(xa)}{J_{-l-1/2}(xa)}\right]. \quad . \quad . \quad . \quad . \quad . \quad (18)$$

After this paper had been written, the author read a preprint of a paper by Bethe and Goldstone, who criticize the computation of the effective mass by considering only the range $0<k<k_F$. The reasoning used in the present paper is based on the arguments at the end of § III of Bethe (1956). Since $V(k)$ is not a well defined quantity for $k>k_F$, no attempt has been made in this paper to make it self consistent for $k>k_F$. Bethe and Goldstone find that their criteria for the validity of the e.m.a. in which the behaviour of $V(k)$ for $k>k_F$ (suitably defined in a certain manner) is also investigated, are such to allow the e.m.a. to hold for very high wave numbers k. However, the ‘ effective mass ’ for high k is not the same as the ‘ effective mass ’ for low k in general, so that this cannot be spoken of as validity of the e.m.a. to high k, except in a very rough manner. The functional dependence of eqn. (7) in the range $0<k<k_F$ is still a necessary condition for the e.m.a. and the conditions derived in § 4 of this paper cannot be relaxed. It is true, however, that M^* is increased by not neglecting the Pauli principle in the intermediate states of eqns. (4) and (5), and that this will therefore lead to an increased maximum density for the range of validity of the e.m.a.

§ 3. EFFECTIVE MASS AND TOTAL ENERGY IN THE LOW DENSITY LIMIT

The chosen configuration, in which each single particle state with wave number $k<k_F$ contains two particles, while all those with $k>k_F$ are empty, corresponds to a gas at the absolute zero of temperature and of density

$$n=\frac{N}{\Omega}=\frac{1}{3\pi^2}k_F^3 \quad . \quad . \quad . \quad . \quad . \quad . \quad . \quad . \quad . \quad (19)$$

where N is the total number of particles and Ω is the volume. Henceforth, the hard sphere radius will be taken as the unit of length, so that $a=1$. ($\hbar=1$ throughout this paper.) For sufficiently low density, i.e. low k_F, and $k<k_F$, it is possible to drop all l values except the first few in eqn. (18), and to expand the remaining Bessel functions in a power series. Let only $l=0$, 1, 2 be retained, and replace

$$\sum_{l=0,1,2}(2l+1)f_l\arctan\left[(-1)^{l+1}\frac{J_{l+1/2}(x)}{J_{-l-1/2}(x)}\right] \text{ by } -x-3x^3+\frac{76}{45}x^5, \qquad (20)$$

then there results

$$\frac{\pi M^* V(k)}{8}=\frac{1}{12}k_F{}^3+\left(\frac{3}{80}k_F{}^5+\frac{1}{16}k_F{}^3k^2\right)$$
$$-\left(\frac{19}{5040}k_F{}^7+\frac{19}{1080}k_F{}^5k^2+\frac{19}{2160}k_F{}^3k^4\right). \quad . \quad . \quad (21)$$

Now the validity of eqn. (11) (or of its Riesenfeld–Watson modification) for the reaction matrix depends on eqn. (7) being satisfied. If this is not so, then the procedure is not self consistent, and a more complicated assumption for the k- dependence of $V(k)$ must be made. Equation (21) shows that in the limit of low densities ($k_Fa \ll 1$), eqn. (7) is indeed well satisfied. To the extent that the terms of degree 7 in k_F, $k(k<k_F)$ on the right-hand side of (21) can be neglected, the effective mass approximation is now completely justified. Hence,

$$\frac{\pi M^* V(k)}{8}=\left(\frac{1}{12}k_F{}^3+\frac{3}{80}k_F{}^5\right)+\frac{1}{16}k_F{}^3k^2. \quad . \quad . \quad . \quad . \quad (22)$$

Define $\sigma=M^*/M$ and $\tau=M/M^*$. Also define $U(k)=\pi M V(k)/8$. Then it follows from definition (8) of effective mass that

$$\tau=1+\frac{16}{\pi k^2}\left\{U(k)-U(0)\right\} \quad . \quad . \quad . \quad . \quad . \quad . \quad (23)$$

or

$$\sigma=1-\frac{16}{\pi k^2}\sigma\left\{U(k)-U(0)\right\}. \quad . \quad . \quad . \quad . \quad . \quad (24)$$

Hence,

$$\sigma=1-\frac{1}{\pi}k_F{}^3=1-3\pi n. \quad . \quad . \quad . \quad . \quad . \quad . \quad . \quad (25)$$

This means that for small densities, the effective mass is slightly less than the real mass. It is interesting to note that if the hard sphere interaction had the p-wave part ($l=1$) suppressed, the result to this order of approximation would have been

$$\sigma=1, \quad . \quad . \quad . \quad . \quad . \quad . \quad . \quad . \quad . \quad . \quad . \quad (26)$$

while if the s-wave part ($l=0$) were suppressed, eqn. (25) would still have been obtained. Hence, the quantity $1-\sigma$ is different from zero at low densities chiefly because of p-wave interaction. The d-wave does not contribute to $1-\sigma$ in the approximation (22), although in the approximation (21), it contributes to the k^4 term in $V(k)$ which causes the e.m.a. to break down. (The limit of validity of the approximation is discussed in § 4.)

The total energy, or the energy per particle **E**, may now be derived in the low density limit.

$$\mathbf{E}=\frac{\int_0^{k_F} k^2\,dk\{k^2/2M+\frac{1}{2}V(k)\}}{\int_0^{k_F} k^2\,dk} \quad . \quad . \quad . \quad . \quad . \quad . \quad . \quad . \quad (27)$$

where the factor $\frac{1}{2}$ in front of $V(k)$ serves to prevent the potential energy between each pair of particles from being counted twice. Equations (27), (7), (8) lead to

$$\mathbf{E}=\tfrac{1}{2}V(0)+\frac{3}{10}\frac{k_F^2}{M}\{1-\tfrac{1}{2}(1-\tau)\}. \qquad (28)$$

It should be noted that the leading term dropped in (25) is of order k_F^5

$$\sigma=1-\frac{1}{\pi}k_F^3+O(k_F^5) \qquad (25)$$

so that (28), (25), and (22) yield the result

$$M\mathbf{E}=\frac{3}{10}k_F^2+\frac{1}{3\pi}k_F^3+\frac{3}{10\pi}k_F^5+\frac{1}{3\pi^2}k_F^6+O(k_F^7). \qquad (29)$$

The neglect of the Pauli principle in intermediate states in the integrals in eqns. (4) and (5) should obviously be least serious in the low density limit. It turns out that if this approximation were not made, the first two terms of eqn. (29), proportional to $n^{2/3}$ and n, would not be changed. This calculation will be contained in a subsequent paper.

§ 4. LIMIT OF VALIDITY OF THE EFFECTIVE MASS APPROXIMATION

For k_F approximately equal to 1·9, the e.m.a. breaks down because $\sigma/k_F^2\{U(k_F)-U(0)\}$ becomes so large (viz. $>\pi/16$) that σ passes through 0 and becomes negative, according to eqn. (24) with $k=k_F$. Clearly, $\sigma>0$ is a necessary condition for validity, since if $\sigma<0$, eqns. (18) and (28) lead to a negative total energy, arising from an interaction which is entirely repulsive. Since $k_F=1{\cdot}9$ corresponds to a density of hard spheres below the density of close packing, the range $k_F>1{\cdot}9$ is not to be considered as unphysical. This absurd result simply means that for $k_F>\sim 1{\cdot}9$, eqn. (7) does not hold at all for $V(k)$, $0\leqslant k\leqslant k_F$, and that

$$V(k)=V(0)+bk^2+b'k^4 \qquad (30)$$

or some other form for $V(k)$ must be guessed, with b, b' then being adjusted in place of M^* in the course of the self consistent calculation.

Even if $\sigma>0$, it is still necessary that the σ obtained from eqn. (23 *b*) be roughly independent of k for $0<k<k_F$. This condition is well satisfied throughout most of the range of k_F for which σ remains >0, as table 1 shows.

Figures 1 and 2 give the effective to actual mass ratio σ and the value of $M\mathbf{E}$ (where $\hbar=1$, $a=1$) for various values of k_F. At the lower end of the range eqns. (25) and (29) are reasonably accurate. The results were calculated by replacing

$$\sum_l (2l+1)f_l \arctan\left[(-1)^{l+1}\frac{J_{l+1/2}(x)}{J_{-l-1/2}(x)}\right]$$

by an odd polynomial in x of degree 9 which gives a good fit over the whole range of x in question. Its coefficients were not obtained from any power series expansion of the arc tangent of the ratio of the two Bessel functions.

Inspection of table 1 shows that for $k_F\leqslant 1{\cdot}6$, the effective mass approximation for hard spheres is reasonably self consistent. For $k_F\geqslant 1{\cdot}9$, it

Fig. 1

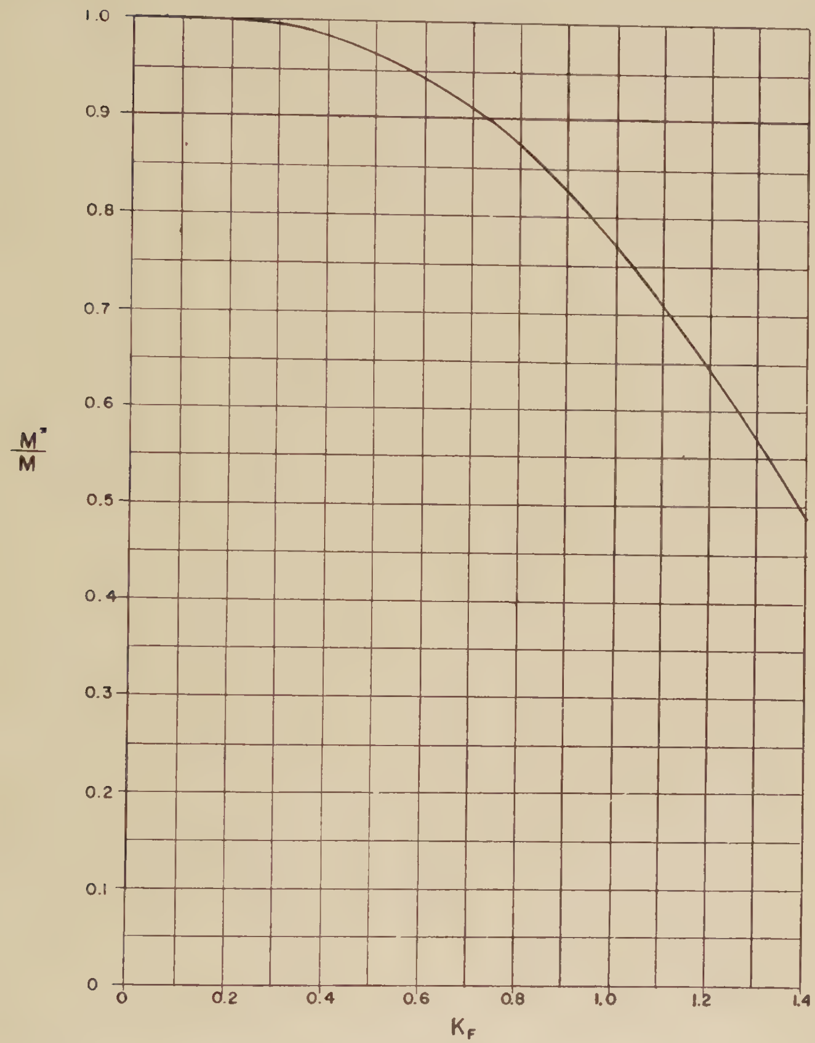

Ratio of the effective mass to the actual mass $\sigma = M^*/M$ as a function of the Fermi wave number k_F.

Table 1. Values of $\sigma(=M^*/M)$ as obtained from eqn. (24) with $k=k_F$ and $k=\frac{1}{2}k_F$ near the limit of validity of e.m.a.

k_F	$k=k_F$	$k=\frac{1}{2}k_F$
1·4	0·490	0·443
1·6	0·317	0·250
1·8	0·116	0·039

is absurd, since σ becomes negative. For a hard sphere core with an attractive potential outside it, as in ^{3}He, the effective mass approximation will be valid to a somewhat higher value of $k_F a$ than for the present case (a=radius of hard core part of the potential).

Fig. 2

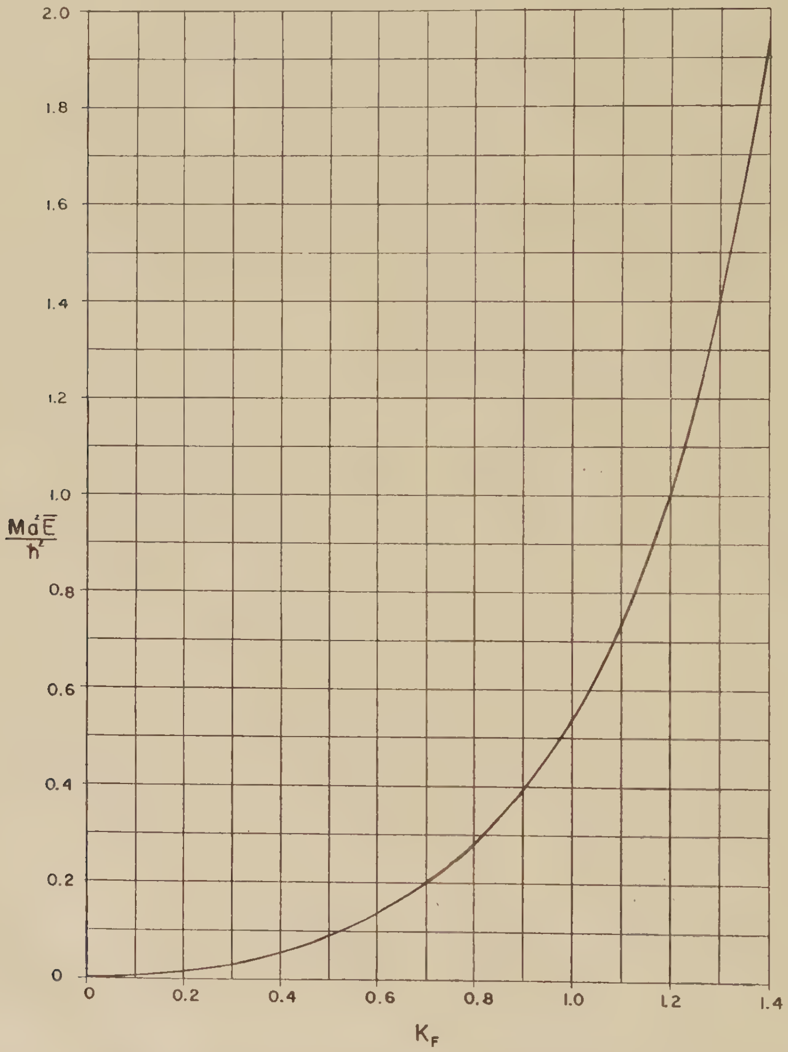

$Ma^2\mathbf{E}/\hbar^2$ ($\mathbf{E}$=energy per particle) as a function of the Fermi wave number k_F

§ 5. SPIN DEPENDENT EFFECTIVE MASS APPROXIMATION

The chosen configuration of § 2 is now replaced by another one, in which each single particles state with wave number $k<k_{F(-)}$ is occupied by two particles of opposite spin; each state with $k_{F(-)}<k<k_{F(+)}$ occupied by

one particle, whose spin is aligned in the same direction for all singly occupied states; while all states with $k > k_{F(+)}$ are empty. We shall refer to the direction of the magnetic moments of the particles in the singly occupied states as the 'up' or 'plus' direction, and to the opposite direction as the 'down' or 'minus' direction.

The energy of the new chosen configuration will now be worked out in the spin dependent effective mass approximation (s.d.e.m.a.) in which the single particle energy of an 'up' particle (one whose magnetic moment points up) is given by

$$E_+(k) = k^2/2M^*(+) + V(+\,;0) \quad . \quad . \quad . \quad . \quad (31\,a)$$

while the energy of a 'down' particle is

$$E_-(k) = k^2/2M^*(-) + V(-\,;0) \quad . \quad . \quad . \quad . \quad (31\,b)$$

$M^*(+)$ and $M^*(-)$ being the two effective masses.

Equation (13) (with the Riesenfeld–Watson modification) must now be generalized to the following form:

$$\begin{aligned} V(+\,;k_i) = &-(2\pi)^{-3}\int_0^{k_{F(+)}}\iint d^3\mathbf{k}_j \frac{4\pi}{M^*(+)k_{ij}} \sum_l^{\text{odd}} 2(2l+1)\,\delta_l(k_{ij}) \\ &-(2\pi)^{-3}\int_0^{k_{F(-)}}\iint d^3\mathbf{k}_j \frac{4\pi}{M_0^*k_{ij}} \sum_l^{\text{all}} (2l+1)\,\delta_l(k_{ij}) \,. \qquad (32\,a) \end{aligned}$$

$$\begin{aligned} V(-\,;k_i) = &-(2\pi)^{-3}\int_0^{k_{F(-)}}\iint d^3\mathbf{k}_j \frac{4\pi}{M^*(-)k_{ij}} \sum_l^{\text{odd}} 2(2l+1)\,\delta_l(k_{ij}) \\ &-(2\pi)^{-3}\int_0^{k_{F(+)}}\iint d^3\mathbf{k}_j \frac{4\pi}{M_0^*k_{ij}} \sum_l^{\text{all}} (2l+1)\,\delta_l(k_{ij}). \quad . \quad (32\,b) \end{aligned}$$

M_0^* is the harmonic mean $2M^*(+)M^*(-)/\{M^*(+)+M^*(-)\}$ of $M^*(+)$ and $M^*(-)$. It is for the second term on the right-hand side of eqn. (32 *a*) that eqn. (15) was derived, since in (32 *a*), $0 < k_i < k_{F(+)}$, so that k_i exceeds $k_{F(-)}$ for some of its range. It then follows from eqns. (14) and (15) that $V(+)$ and $V(-)$ may be written as follows:

If $k < k_{F(-)}$,

$$\begin{aligned} V(\pm\,;k) = &-\frac{8}{\pi M^*(\pm)}\int_0^{1/2(k+k_{F(\pm)})} dx\; x\; P_k(\pm\,;x) \sum_l^{\text{odd}} 2(2l+1)\,\delta_l(x) \\ &-\frac{8}{\pi M_0^*}\int_0^{1/2(k+k_{F(\mp)})} dx\; x\; P_k(\mp\,;x) \sum_l^{\text{all}} (2l+1)\,\delta_l(x). \quad . \quad . \quad (33) \end{aligned}$$

If $k > k_{F(-)}$

$$\begin{aligned} V(+\,;k) = &-\frac{8}{\pi M^*(+)}\int_0^{1/2(k+k_{F(+)})} dx\; x\; P(+\,;k) \sum_l^{\text{odd}} 2(2l+1)\,\delta_l(x) \\ &-\frac{8}{\pi M_0^*}\int_{1/2(k-k_{F(-)})}^{1/2(k+k_{F(-)})} dx\; x\; Q_k(-\,;x) \sum_l^{\text{all}} (2l+1)\,\delta_l(x) \quad . \quad . \quad (34) \end{aligned}$$

where

$$\begin{aligned} P_k(\pm\,;x) &= 2, \text{ when } 0 < x < \tfrac{1}{2}(k_{F(\pm)}-k) \\ &= \{\tfrac{1}{4}k_{F(\pm)}{}^2 - (\tfrac{1}{2}k-x)^2\}/kx \\ &\quad \text{when } \tfrac{1}{2}(k_{F(\pm)}-k) < x < (\tfrac{1}{2}k_{F(\pm)}+k) \quad . \quad . \quad . \quad . \quad (35) \end{aligned}$$

and $Q_k(-\,;x)$ is obtained from $Q_k(x)$ of (17) by replacing k_F by $k_{F(-)}$.

If $n(+)$ and $n(-)$ denote the densities (number of particles per unit volume) of 'up' and 'down' particles respectively, then

$$n(\pm)=\frac{N(\pm)}{\Omega}=\frac{1}{6\pi^2}k_{F(\pm)}{}^3 \qquad (36)$$

and

$$n=\frac{1}{6\pi^2}(k_{F(+)}{}^3+k_{F(-)}{}^3). \qquad (37)$$

§ 6. EFFECTIVE MASSES AND ENERGY IN THE LOW DENSITY LIMIT FOR S.D.E.M.A.

Let the phase shifts in (33), (34) be given by their values for a hard-sphere interaction (of unit radius), and expand up to and including terms in x^3. Then

$$\sum_{l}^{\text{odd}} 2(2l+1)\,\delta_l(x)=-2x^3 \qquad (38\,a)$$

and

$$\sum_{l}^{\text{all}} (2l+1)\,\delta_l(x)=-(x+x^3). \qquad (38\,b)$$

Then eqns. (33), (34) give

$$V(\pm\,;\,k)=\frac{8}{\pi M_0{}^*}\left(\frac{1}{12}k_{F(\mp)}{}^3+\frac{1}{80}k_{F(\mp)}{}^5+\frac{1}{48}k_{F(\mp)}{}^3k^2\right)$$
$$+\frac{8}{\pi M^*(\pm)}\left(\frac{1}{40}k_{F(\pm)}{}^5+\frac{1}{24}k_{F(\pm)}{}^3k^2\right). \qquad (39)$$

Define $\sigma(-)=1/\tau(-)=M^*(-)/M$ and $\sigma(+)=1/\tau(+)=M^*(+)/M$. Then eqns. (31), (39) yield the two simultaneous equations

$$\frac{2}{3\pi}k_{F(\pm)}{}^3+\frac{1}{6\pi}(1+\sigma(\pm)/\sigma(\mp))k_{F(\mp)}{}^3=1-\sigma(\pm) \qquad (40)$$

which have the solutions

$$\sigma_{\pm}=1-\frac{2k_{F(\pm)}{}^3+k_{F(\mp)}{}^3}{3\pi}+O(k_F{}^5). \qquad (41)$$

In eqn. (41), $O(k_F{}^5)$ means that the leading terms dropped in deriving (39) and (40) are of degree 5 in $k_{F(+)}$, $k_{F(-)}$ together. Equation (41) shows that if $n(+)>n(-)$, then $\sigma(+)<\sigma(-)$, i. e. the effective mass of a particle with magnetic moment in the direction of the majority is lower than the 'minority effective mass'.

If $\mathbf{E}$ is the average energy per particle, then

$$M\mathbf{E}=\frac{N(+)}{N}\int_0^{k_{F(+)}}k^2\,dk\,[(k^2/2M)+\tfrac{1}{2}V(+\,;\,k)]\Big/\int_0^{k_{F(+)}}k^2\,dk$$
$$+\frac{N(-)}{N}\int_0^{k_{F(-)}}k^2\,dk\,[(k^2/2M)+\tfrac{1}{2}V(-\,;\,k)]\Big/\int_0^{k_{F(-)}}k^2\,dk. \qquad (42)$$

Equations (42), (36), (39), (41) then yield the following result :

$$M\mathbf{E}=\frac{3}{10}\frac{k_{F(+)}{}^5+k_{F(-)}{}^5}{k_{F(+)}{}^3+k_{F(-)}{}^3}+\frac{2}{3\pi}\frac{k_{F(+)}{}^3k_{F(-)}{}^3}{k_{F(+)}{}^3+k_{F(-)}{}^3}$$

$$+\frac{1}{10\pi}\cdot\frac{1}{k_{F(+)}{}^3+k_{F(-)}{}^3}\{2(k_{F(+)}{}^8+k_{F(-)}{}^8)+(k_{F(+)}{}^3k_{F(-)}{}^5+k_{F(-)}{}^3k_{F(+)}{}^5)\}$$

$$+\frac{1}{3\pi^2}k_{F(+)}{}^3k_{F(-)}{}^3+O(k_F{}^7)\quad . \; . \; . \; . \; . \; . \; . \; . \quad (43)$$

which of course reduces to eqn. (29) when $k_{F(+)}=k_{F(-)}=k_F$.

The first term in (43), which is quadratic in the k_F's, is the contribution of the kinetic energies of the individual particles. The next term, which is cubic in the k_F's, arises from the term in (39) which is cubic in the k_F's, and which comes entirely from the *s*-wave interaction of the hard spheres. By eqn. (37), a fixed density of particles implies that $k_{F(+)}{}^3+k_{F(-)}{}^3$ is fixed. At sufficiently low densities, the first term in (43) dominates the others, and for fixed $k_{F(+)}{}^3+k_{F(-)}{}^3$, it is a minimum if $k_{F(+)}=k_{F(-)}$. Hence, at low densities, the antiferromagnetic configuration, for which as many spins (and therefore, magnetic moments) are in the ' down ' as in the ' up ' direction, has the lowest energy, and is the configuration in which the gas is in equilibrium at temperature $T=0$. For an ideal Fermi–Dirac gas, this is, of course, true for arbitrary density.

At a somewhat higher density, the second term of (43) becomes important. Its effect is to favour inequality of $k_{F(+)}$ and $k_{F(-)}$. The physical interpretation of this is quite simple. This term is the leading term (in powers of $k_{F(+)}$, $k_{F(-)}$) of the energy due to *s*-wave interaction of the hard spheres, which at not too high densities is certainly more important than higher values of l, and it can exist only between a pair of particles with opposite spins, not between a pair with the same spin, in accordance with the Pauli principle. Hence, this interaction tends to line up spins (and so, magnetic moments) of near by particles and to produce ferromagnetism.

Now, fix $k_{F(+)}{}^3+k_{F(-)}{}^3=2\alpha$, and minimize $\psi(y)=M\mathbf{E}(k_{F(+)}{}^3+k_{F(-)}{}^3)$ as a function of $y\equiv\frac{1}{2}(k_{F(+)}{}^3-k_{F(-)}{}^3)$. We shall use (43) for $M\mathbf{E}$, neglecting $O(k_F{}^7)$, and assuming that $|y|\ll\alpha$ for the range of y in question. (Indeed, we know *a priori* that at low enough densities, $y=0$ minimizes $\psi(y)$, and we wish to investigate at what density this ceases to be the only relative extremum.) For this purpose, it is necessary to expand $\psi(y)$ in powers of y^2, up to and including y^4. The result is

$$\psi(y)=\frac{3}{5}\alpha^{5/3}\left(1+\frac{5}{9}\frac{y^2}{\alpha^2}+\frac{5}{243}\frac{y^4}{\alpha^4}\right)+\frac{2}{3\pi}(\alpha^2-y^2)+\frac{3}{5\pi}\alpha^{8/3}\left(1+\frac{10}{9}\frac{y^2}{\alpha^2}\right)$$

$$+\frac{2}{3\pi^2}\alpha^2(\alpha^2-y^2).\quad . \; . \; . \; . \; . \; . \; . \; . \quad (44)$$

For α low enough, $d\psi(y)/dy$ has only one real root, viz. $y=0$, corresponding to the above mentioned minimum. For higher α, $d\psi(y)/dy$ has three, real roots, $y=0$ corresponding to a local maximum in $\psi(y)$ (instability of the antiferromagnetic configuration at $T=0$) and two minima $y=\pm y_0$, where

$$y_0=\alpha\sqrt{\left\{-\frac{27}{2}\left(1-\frac{2}{\pi}\alpha^{1/3}+\frac{2}{\pi}\alpha-\frac{2}{\pi^2}\alpha^{4/3}\right)\right\}} \quad . \quad . \quad . \quad . \quad (45)$$

y_0 becomes real as $\alpha^{1/3}$ becomes greater than $\sim 3{\cdot}0$ which, by § 4, is far beyond the range of validity of the e.m.a. In § 7, the minimum density for ferromagnetism at $T=0$ is calculated without the low density approximation (which (45) shows to be inapplicable), and it turns out that the limiting density is that for which $k_F=1{\cdot}674$ rather than the above estimate $k_F=3{\cdot}0$. This lower value is within the range of validity of the e.m.a., although table 1 shows that the e.m.a. is beginning to fail at a somewhat higher density.

§ 7. MINIMUM DENSITY FOR FERROMAGNETISM AT $T=0$

Define

$$U(\pm\,;\;k)=\frac{\pi M}{8}V(\pm\,;\,k). \quad . \quad . \quad . \quad . \quad . \quad . \quad . \quad (46)$$

Assume that $k_{F(+)}$ and $k_{F(-)}$ are approximately equal, with $k_{F(+)}\geqslant k_{F(-)}$, so that $0\leqslant D\ll C^3$ where

$$k_{F(\pm)}{}^3=C^3\pm D. \quad . \quad . \quad . \quad . \quad . \quad . \quad . \quad . \quad (47)$$

Define

$$d=\frac{D}{C^3}=\frac{k_{F(+)}{}^3-k_{F(-)}{}^3}{k_{F(+)}{}^3+k_{F(-)}{}^3}. \quad . \quad . \quad . \quad . \quad . \quad . \quad . \quad (48)$$

The average energy per particle is to be considered as a function of d for fixed C. It is an even function of d, and since $d\ll 1$, it may be written in the form

$$M\mathbf{E}=\mathbf{A}+\mathbf{B}d^2+O(d^4) \quad . \quad . \quad . \quad . \quad . \quad . \quad . \quad . \quad (49)$$

where **A**, **B** are independent of d but are functions of C. From the discussion of § 6, it follows that **B** is positive for low values of C, while for higher values of C, it becomes negative. In fact, we know from preceding considerations that in the limit of small C, **B** is given by

$$\mathbf{B}=\frac{1}{6}C^2-\frac{1}{3\pi}C^3+\frac{1}{3\pi}C^5-\frac{1}{3\pi^2}C^6+O(C^7) \quad . \quad . \quad . \quad (50)$$

but that this does not hold to a high enough value of C to establish the point where **B** changes its sign and becomes negative. The lowest positive zero of $\mathbf{B}(C)$ gives the density above which ferromagnetism sets in at $T=0$.

The effective masses now depend on d, and one expands the ratios $\tau(\pm)=M/M^*(\pm)$ as follows:

$$\tau(+)=\tau_{00}+d\tau_{+1}+d^2\tau_{+2}+O(d^3) \quad . \quad . \quad . \quad . \quad . \quad (51\,a)$$

$$\tau(-)=\tau_{00}+d\tau_{-1}+d^2\tau_{-2}+O(d^3). \quad . \quad . \quad . \quad . \quad . \quad (51\,b)$$

Furthermore, it follows from (47), (48) that

$$k_{F(\pm)}=C\left\{1\pm\frac{1}{3}d-\frac{1}{9}d^2+O(d^3)\right\}. \qquad (52)$$

Define

$$\Phi(x)=-\sum_{l}^{\text{odd}}2(2l+1)\,\delta_l(x) \qquad (53\,a)$$

and

$$\phi(x)=-\sum_{l}^{\text{all}}(2l+1)\,\delta_l(x). \qquad (53\,b)$$

Substituting the above expressions into eqns. (33) and (34) and keeping in mind that both the integrands and the limits of integration are d-dependent and that only quantities which are of cubic and higher degree in d may be neglected, it turns out that

$$\tau_{+1}=-\tau_{-1} \qquad (54\,a)$$

$$\tau_{+2}=+\tau_{-2}. \qquad (54\,b)$$

Writing τ_1 for τ_{+1} and τ_2 for τ_{+2}, this gives

$$\tau_{+}=\tau_{00}+d\tau_1+d^2\tau_2 \qquad (55\,a)$$

$$\tau_{-}=\tau_{00}-d\tau_1+d^2\tau_2 \qquad (55\,b)$$

$$\tau_0\equiv\tfrac{1}{2}(\tau_{+}+\tau_{-})=\tau_{00}+d^2\tau_2. \qquad (55\,c)$$

Having established eqns. (54), it suffices to deal with the function $U(-\,;k)$. The following results are then obtained :

$$\begin{aligned}\tfrac{1}{2}U(-\,;0)&=\tau_{00}\int_0^{1/2C}dx\,.\,x\{\Phi(x)+\phi(x)\}\\&+d\left[-\tau_1\int_0^{1/2C}dx\,.\,x\Phi(x)-\frac{1}{12}\tau_{00}C^2\{\Phi(\tfrac{1}{2}C)-\phi(\tfrac{1}{2}C)\}\right]\\&+d^2\left[\tau_2\int_0^{1/2C}dx\,.\,x\{\Phi(x)+\phi(x)\}+\frac{1}{12}\tau_1C^2\Phi(\tfrac{1}{2}C)\right.\\&\left.+\tau_{00}\frac{C^2}{72}\{-\Phi(\tfrac{1}{2}C)-\phi(\tfrac{1}{2}C)+\tfrac{1}{2}C\Phi'(\tfrac{1}{2}C)+\tfrac{1}{2}C\phi'(\tfrac{1}{2}C)\}\right], \qquad (56)\end{aligned}$$

$$\begin{aligned}U(-\,;k_{F(-)})&=\tau_{00}\int_0^C dx\,.\,x\left(1-\frac{x}{C}\right).\{\Phi(x)+\phi(x)\}\\&+d\left\{-\frac{1}{3}\tau_{00}\int_0^C dx\frac{x^2\Phi(x)}{C}+\frac{1}{3}\tau_{00}\int_0^C dx\left\{C\phi(x)-\frac{x^2\phi(x)}{C}\right\}\right.\\&\left.-\tau_1\int_0^C dx\left(1-\frac{x}{C}\right)x\Phi(x)\right\}\\&+d^2\left\{\frac{1}{18}\tau_{00}C^2\Phi(C)+\frac{1}{9}\tau_{00}C\int_0^C dx\phi(x)-\frac{2}{9}\frac{\tau_{00}}{C}\int_0^C dx\,x^2\phi(x)\right.\\&-\frac{2}{9}\frac{\tau_{00}}{C}\int_0^C dx\,.\,x^2\Phi(x)+\frac{1}{3}\frac{\tau_1}{C}\int_0^C dx\,.\,x^2\Phi(x)\\&\left.+\tau_2\int_0^C dx\left(1-\frac{x}{C}\right)x\,[\Phi(x)+\phi(x)]\right\}. \qquad (57)\end{aligned}$$

Now, from eqn. (23 *a*), it follows that

$$(\tau_{00}-d\tau_1+d^2\tau_2-1)=\frac{16}{\pi k_{F(-)}{}^2}\{U(-\,;k_{F(-)})-U(-\,;0)\} \qquad (58)$$

which permits the τ_{00}, τ_1, and τ_2 which make the s.d.e.m.a. self-consistent to be deduced. The results are :

$$\tau_{00}=\left\{1-\frac{16}{\pi C^2}(\alpha-2\beta)\right\}^{-1} \quad . \quad . \quad . \quad . \quad . \quad . \quad . \qquad (59)$$

$$\begin{aligned}\tau_1=&\left\{-\frac{\pi C^2}{16}+\gamma-2\nu\right\}^{-1}\left\{-\frac{\pi C^2}{24}\right.\\&\left.+\tau_{00}\left[\frac{\pi C^2}{24}+\frac{1}{3}(\eta-\epsilon)+\frac{1}{6}C^2\Phi(\tfrac{1}{2}C)-\frac{1}{6}C^2\phi(\tfrac{1}{2}C)\right]\right\} \quad . \qquad (60)\end{aligned}$$

$$\begin{aligned}\tau_2=&\left\{\frac{\pi C^2}{16}-\alpha+2\beta\right\}^{-1}\left\{-\frac{\pi C^2}{144}+\tau_1\left[\frac{\epsilon}{3}-\frac{C^2}{6}\Phi(\tfrac{1}{2}C)-\frac{\pi C^2}{24}\right]\right.\\&+\tau_{00}\left[\frac{\pi C^2}{144}+\frac{1}{18}C^2\Phi(C)+\frac{\mu}{9}-\frac{2\epsilon}{9}\right.\\&\left.\left.+\frac{C^2}{36}(\Phi(\tfrac{1}{2}C)+\phi(\tfrac{1}{2}C)-\tfrac{1}{2}C\Phi'(\tfrac{1}{2}C)-\tfrac{1}{2}C\phi'(\tfrac{1}{2}C))\right]\right\} \quad . \quad . \quad . \qquad (61)\end{aligned}$$

where α, β, γ, ϵ, η, μ, ν are the following functions of C. (In eqns. (59), (60), (61), it is understood that the argument of each one is C).

$$\alpha(C)=\int_0^C dx\,.\,x\left(1-\frac{x}{C}\right).\{\Phi(x)+\phi(x)\} \quad . \quad . \quad . \qquad (62\,a)$$

$$\beta(C)=\int_0^{1/2C} dx\,.\,x\{\Phi(x)+\phi(x)\} \quad . \quad . \quad . \quad . \quad . \quad . \quad . \qquad (62\,b)$$

$$\gamma(C)=\int_0^C dx\,.\,x\left(1-\frac{x}{C}\right)\Phi(x) \quad . \quad . \quad . \quad . \quad . \quad . \quad . \qquad (62\,c)$$

$$\epsilon(C)=\frac{1}{C}\int_0^C dx\,.\,x^2\Phi(x) \quad . \quad . \quad . \quad . \quad . \quad . \quad . \quad . \quad . \qquad (62\,d)$$

$$\eta(C)=\int_0^C dx\,.\,x\left(\frac{C}{x}-\frac{x}{C}\right)\phi(x) \quad . \quad . \quad . \quad . \quad . \quad . \quad . \qquad (62\,e)$$

$$\mu(C)=\int_0^C dx\,.\,x\left(\frac{C}{x}-\frac{2x}{C}\right)\phi(x) \quad . \quad . \quad . \quad . \quad . \quad . \qquad (62\,f)$$

$$\nu(C)=\int_0^{1/2C} dx\,.\,x\Phi(x) \quad . \quad . \quad . \quad . \quad . \quad . \quad . \quad . \quad . \quad . \qquad (62\,g)$$

A and **B** of eqn. (49) then have these values :

$$\mathbf{A}=\frac{3}{10}C^2+\frac{8}{\pi}\tau_{00}\beta+\frac{3}{20}C^2(\tau_{00}-1) \quad . \quad . \quad . \quad . \quad . \quad . \quad . \qquad (63)$$

$$\mathbf{B}=\frac{1}{6}C^2+\frac{4}{\pi}\{U_{-2}(0)-U_{-1}(0)\}+\frac{3}{20}C^2\left\{\tau_2+\frac{5}{3}\tau_1+\frac{5}{9}(\tau_{00}-1)\right\} \quad . \qquad (64)$$

where
$$U_{-1}(0)=-2\tau_1\nu-\frac{1}{6}\tau_{00}C^2\{\Phi(\tfrac{1}{2}C)-\phi(\tfrac{1}{2}C)\}. \quad . \quad . \quad . \qquad (65\,a)$$

$$U_{-2}(0)=2\tau_2\beta+\frac{1}{6}\tau_1C^2\Phi(\tfrac{1}{2}C)$$
$$+\frac{1}{72}C^2\tau_{00}\{-2\Phi(\tfrac{1}{2}C)-2\phi(\tfrac{1}{2}C)+C\Phi'(\tfrac{1}{2}C)+C\phi'(\tfrac{1}{2}C)\}. \quad . \qquad (65\,b)$$

For a hard sphere interaction, the following are good approximations for Φ and ϕ over the range $0\leqslant x\leqslant 2$

$$\Phi(x)=2x^3-0{\cdot}9628x^5+0{\cdot}2900x^7-0{\cdot}03199x^9 \quad . \quad . \qquad (66\,a)$$
$$\phi(x)=x+0{\cdot}8603x^3-0{\cdot}1420x^5+0{\cdot}01545x^7. \quad . \quad . \quad . \qquad (66\,b)$$

Fig. 3

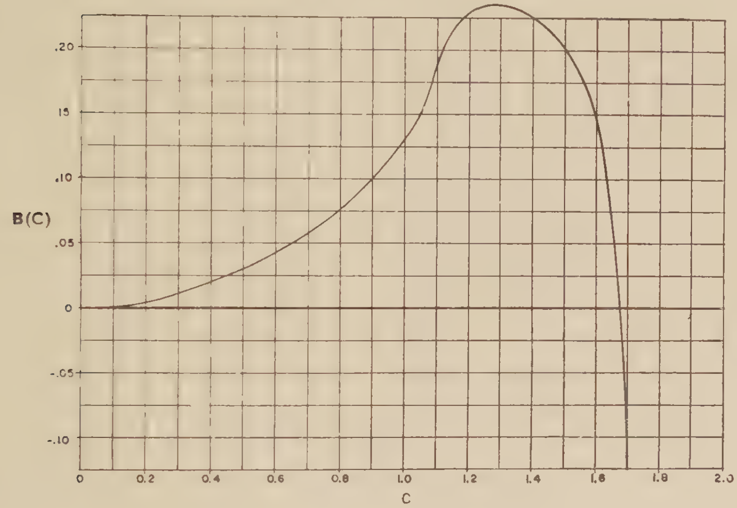

B(C) as a function of C, where **B** is defined by eqn. (49).

The function **B**(C) is plotted in fig. 3, and has a zero at $C=1{\cdot}674$. Since this is still somewhat within the range of validity of the e.m.a., it is concluded that at absolute zero, a gas of Fermi–Dirac particles of spin $\frac{1}{2}$, interacting by a hard sphere potential of radius a, becomes ferromagnetic if the density

$$n\geqslant\frac{(1{\cdot}674)^3}{3\pi^2}a^{-3}. \quad . \quad . \quad . \quad . \quad . \quad . \quad . \quad . \qquad (67)$$

§ 8. ENERGY IN THE FERROMAGNETIC REGION OF DENSITY

Equations (42), (36), and (31) lead to the following expression for the energy per particle **E** in the s.d.e.m.a.

$$M\mathbf{E}=\frac{3}{10}\cdot\frac{{k_{F(+)}}^5+{k_{F(-)}}^5}{{k_{F(+)}}^3+{k_{F(-)}}^3}+\frac{4}{\pi}\cdot\frac{{k_{F(+)}}^3U(+\,;0)+{k_{F(-)}}^3U(-\,;0)}{{k_{F(+)}}^3+{k_{F(-)}}^3}$$
$$+\frac{3}{20}\cdot\frac{{k_{F(+)}}^5\{\tau(+)-1\}+{k_{F(-)}}^5\{\tau(-)-1\}}{{k_{F(+)}}^3+{k_{F(-)}}^3}. \quad . \quad . \quad . \quad . \quad . \quad . \qquad (68)$$

For C fixed at a value slightly greater than 1·674, $M\mathbf{E}$ as an even function of d has a local maximum at $d=0$ and local minima at $d=\pm d_0$ where $d_0 \ll 1$. As C becomes larger, d_0 increases towards 1. At a value of C above that for which $d_0=1$, the local minima disappear, and $d=\pm 1$ become absolute minima. It is only this latter case, for which $\mathbf{E}$ has its minima at $d=\pm 1$, which corresponds to the familiar kind of ferromagnetism. The behaviour in the other case is of an intermediate sort, in which the energy is lowered as $|d|$ is increased and thus the magnetization tends to be increased, provided $0<|d|<d_0$ (ferromagnetic behaviour) while for $d_0<|d|<1$, the energy is lowered as $|d|$ is decreased, and thus the magnetization tends to be decreased (antiferromagnetic behaviour). This will be referred to as ' intermediate ferromagnetism '.

Table 2

C	d	$M\mathbf{E}$	$\tau(+)$	$\tau(-)$
1·40	0	1·9257	2·0391	2·0391
1·40	0·2	1·9348	2·0435	2·0193
1·60	0	4·2379	3·1522	3·1522
1·60	0·2	4·2439	3·1406	3·1270
1·68	0	6·3771	4·1519	4·1519
1·68	0·05	6·3770	4·1524	4·1477
1·68	0·2	6·3752	4·1320	4·1101
1·68	0·5	6·3623	3·9990	3·8975
1·68	1·0	6·4160	3·5316	——
1·75	0	10·106	5·8764	5·8764
1·75	0·5	9·871	5·5484	5·4002
1·75	0·75	9·470	5·0614	4·7154
1·75	1·0	8·949	4·3948	——

Table 2 gives the value of the energy per particle $\mathbf{E}$ and of the reciprocal effective mass ratios $\tau(+)=M/M^*(+)$ and $\tau(-)=M/M^*(-)$ for various values of C and d. It is seen that for $C<1{\cdot}674$ (C fixed), $\mathbf{E}$ increases as $|d|$ increases, while for C slightly above 1·674, $\mathbf{E}$ has a local maximum at $d=0$, reaches minima at certain values $d=\pm \mathrm{d}_0$, and increases as $|d|$ increases from d_0 to 1. For somewhat larger C, $\mathbf{E}$ is a monotonic decreasing function of $|d|$.

Since the densities for which ' intermediate ferromagnetism ' and ferromagnetism occur lie near the limit of validity of the s.d.e.m.a., a detailed study of this phenomenon must use a more complicated wave number dependence for $V(+\,;\,k)$, $V(-\,;\,k)$, and must also exclude the occupied states for the intermediate states in the integrals of eqns. (4) and (5).

The most obvious application of these results to an actual physical system is a study of the paramagnetic susceptibility of ^{3}He, and an investigation as to whether or not ^{3}He becomes ferromagnetic at a sufficiently low temperature. L. Goldstein and M. Goldstein (1950) have concluded that at $T=0$, the antiferromagnetic configuration ($d=0$) is more stable than the totally ferromagnetic one ($d=\pm 1$). Their derivation involves the use of a different set of approximations from those of this paper, viz. the use of plane waves, neglect of spatial correlations between the atoms, and the use of two types of semi-empirical interatomic potentials with cut-offs at physically plausible values to avoid divergencies. Furthermore, they do not investigate 'intermediate ferromagnetism' at $T=0$. The attractive part of the ^{3}He interaction increases the minimum density at which $d=0$ is most stable with respect to its value in the hard sphere case (taking the same radius for the hard sphere part of the ^{3}He interaction as in the pure hard sphere case).

A gross overestimate for the Curie temperature of a gas of hard sphere fermions is given by

$$kT_{\text{curie}}=-2\mathbf{B}\frac{\hbar^2}{Ma^2} \quad . \quad . \quad . \quad . \quad . \quad . \quad . \quad (69)$$

where $\mathbf{B}$ is the function of C defined in eqn. (49). For $M=5{\cdot}0\times 10^{-24}$ g and $a=2{\cdot}6\times 10^{-8}$ cm, this overestimate becomes

$$T_{\text{curie}}=-\mathbf{B}\times 4{\cdot}8^{\circ}\text{K}. \quad . \quad . \quad . \quad . \quad . \quad . \quad . \quad . \quad (70)$$

Equations (69) and (70) were derived on the extremely crude assumption that even for $T>0$, all the filled wave numbers for 'up' particles lie below all the empty ones in each member of the canonical ensemble, and similarly for the 'down' particles. However, it was, of course, assumed that the number of 'up' and 'down' particles in a member of the ensemble differs, in general, from the numbers at $T=0$.

ACKNOWLEDGMENTS

The author is deeply grateful to Dr. W. Wada for several very interesting and enlightening discussions on Brueckner theory. He also wishes to thank the Hand Computing section of the National Bureau of Standards Computational Laboratory under Miss R. Zucker for their invaluable aid in carrying out most of the computations on which the results are based.

REFERENCES

BETHE, H. A., 1956, *Phys. Rev.*, **103,** 1353.
BRUECKNER, K. A., 1955 a, *Phys. Rev.*, **97,** 1353 ; 1955 b, *Ibid.*, **100,** 36.
BRUECKNER, K. A., and LEVINSON, C. A., 1955, *Phys. Rev.*, **97,** 1344 ; see also other references given in § I of Bethe (1956).
GOLDSTEIN, L., and GOLDSTEIN, M., 1950, *J. Chem. Phys.*, **18,** 538.
SKYRME, T. H. R., 1956, to be published.

CORRESPONDENCE

The Effect of Free Electrons on Lattice Conduction at High Temperatures†

By R. Stratton
Metropolitan Vickers Electrical Co. Ltd., Manchester, 17

[Received December 4, 1956]

The thermal conductivity of a semiconductor is equal to the sum of two parts which are due to the transport of energy by current carriers (free electrons or holes) and thermal lattice vibrations (phonons) respectively. The lattice contribution will be controlled by inter-phonon, phonon–lattice defect and phonon–electron (or hole) scattering. The last process has been considered by Ziman (1956) for lattice temperatures (T) below the Debye characteristic temperature (θ)‡. We will give a simple extension to the theory for the high temperature range ($T>\theta$).

Now a simple argument indicates that whereas at low temperatures phonon–electron collisions may be important, this will not be the case at high temperatures. Thus according to Ziman (eqn. (7)) it follows from the conservation of energy that the minimum wave number k_0 of an electron which is capable of scattering a phonon with wave number p (emission or absorption) is given by

$$k_0=\left|\tfrac{1}{2}p-m^*v/\hbar\right| \quad . \quad . \quad . \quad . \quad . \quad . \quad . \quad . \quad (1)$$

where m^* is the effective mass of the electron and v is the velocity of the phonon. This leads to a minimum electron energy

$$E_0=\frac{\hbar^2k_0^2}{2m^*}=\frac{\hbar^2\omega^2}{8m^*v^2}+\tfrac{1}{2}m^*v^2-\tfrac{1}{2}\hbar\omega \quad . \quad . \quad . \quad . \quad . \quad (2)$$

where $\omega=p/v$ is the angular frequency of the phonon. Now when $T<\theta$, most of the phonons have an energy of about $2kT$ so that

$$E_0\approx\frac{kT}{2}\left[\frac{kT}{m^*v^2}-1+\frac{m^*v^2}{kT}\right]. \quad . \quad . \quad . \quad . \quad . \quad . \quad . \quad (3)$$

It follows that when $T\sim m^*v^2/k(\sim 1°\mathrm{K})$ most of the electrons are capable of scattering the phonons. With increasing T only the higher energy electrons will come into the picture until finally, when T is greater than θ and the most important phonon energy is $k\theta$, the minimum electron energy required becomes

---

† Communicated by the Author.

‡ The restriction on the temperature is implied in Ziman's paper (eqn. (19)) since the integration over the lattice frequencies in the expansion for the mean free path is extended to an infinite upper limit which is only permissible if $T<\theta$.

$$\bar{E}_0=(k\theta/8m^*v^2)k\theta \quad . \quad . \quad . \quad . \quad . \quad . \quad . \quad . \quad (4)$$

which is of the order of 1 electron volt.

It will thus be expected that electron–phonon scattering is relatively unimportant at high temperatures contrary to the results of ter Haar and Neaves (1956) who have however not taken account of the fact that a minimum energy E_0 for scattering exists. (This will be referred to in detail after eqn. (10).)

The detailed calculation for the thermal conductivity can be carried out by taking over Ziman's expression for the phonon relaxation time τ_p (eqn. (9) in Ziman's paper and corrigendum) applied to the case of high temperatures, i.e.

$$\frac{1}{\tau(\omega)}=\frac{C^2m^{*3}v}{4\pi\hbar^4\rho}\cdot\frac{kT}{\frac{1}{2}m^*v^2}\cdot\frac{1}{1+\exp\left[-\zeta/kT+\hbar^2\omega^2/8m^*v^2\right]} \quad . \quad . \quad (5)$$

Here ζ is the arbitrary Fermi energy of the electron gas, ρ is the mass density of the lattice and C is an electron–lattice interaction constant whose magnitude is of the order of a few electron volts.

Substituting for $\tau(\omega)$ into the expression for the thermal conductivity (cf. Klemens (1951), eqn. (24) for the general expression) namely

$$\kappa=\frac{k}{6\pi^2}\int_0^{k\theta/\hbar}\sum_j\frac{\tau_j(\omega)}{v_j}\,\omega^2d\omega \quad . \quad . \quad . \quad . \quad . \quad . \quad (6)$$

if $T\gg\theta$ where $j=1$, refers to the longitudinal direction of polarization, $j=2$ and 3 to the transverse, gives

$$\kappa=\frac{k^3\hbar\rho\theta^2}{6\pi m^{*2}}\sum_j\frac{1}{C_j^{\,2}}\left[1+\exp\left(-\frac{\zeta}{kT}\right)\left\{\frac{\exp(\bar{E}_0/kT)-1}{(\bar{E}_0/kT)}\right\}\right]. \quad . \quad (7)$$

If $(\zeta-\bar{E}_0)/kT\gg1$, then κ is a constant in agreement with the result for metals given by Wilson (1953, eqn. 9.82.2) in the temperature range $T\gg\theta$.

For a semiconductor, provided that $(\bar{E}_0-\zeta)/kT\gg1$, eqn. (7) can be reduced to

$$\kappa\simeq\frac{k^3\hbar\rho\theta^2}{6\pi m^{*2}}\sum\frac{1}{C_j^{\,2}}\frac{\exp\{(\bar{E}_0-\zeta)/kT\}}{(\bar{E}_0/kT)}. \quad . \quad . \quad . \quad . \quad . \quad (8)$$

The unknown quantities C_j can be eliminated from eqn. (8) by introducing the expression for the electron mobility (cf. Wilson (1953), eqns. 9.36.3 and 9.36.4)

$$\mu=\frac{4}{3}\frac{e}{(2\pi m^*kT)^{1/2}}\cdot\frac{\rho\delta^2\hbar^2k\theta^2}{4\pi(6\pi^2)^{2/3}m^{*2}C^2T} \quad . \quad . \quad . \quad . \quad . \quad (9)$$

where δ is the lattice constant and $C^2=C_1^{\,2}+C_2^{\,2}+C_3^{\,2}$. Now in the elementary theory only C_1 (longitudinal waves) is non-vanishing which would make κ infinite since transverse waves (C_2 and C_3) are not scattered.

A more exact discussion however (cf. Wilson 1953, p. 279) indicates that there will always be some interaction between the transverse waves and electrons; it has been suggested (Makinson 1938) that it is better to assume that $C_1 \gtrsim C_2 \gtrsim C_3$.

From eqns. (8) and (9)

$$\kappa = 4{\cdot}7 \times 10^{-23} \left(\frac{m^*}{m}\right)^{1/2} \frac{\mu T^{3/2}}{\delta^2} \sum_j \frac{C^2}{C_j^2} \frac{\exp\{(\bar{E}_0 - \zeta)/kT\}}{\bar{E}_0/kT} \quad . \quad . \quad (10)$$

cals/sec cm°K

where μ is in practical units ($\mathrm{cm}^2 V^{-1} \mathrm{sec}^{-1}$), m is the free electron mass and if $C_1 = C_2 = C_3$ then $\Sigma C^2/C_j^2 = 9$. The result by ter Haar and Neaves (1956, eqn. (171)) differs from the above by the factor $(\bar{E}_0/kT)^{-1} \exp(\bar{E}_0/kT)$ and applies only to non-degenerate semiconductors. The omitted factor is however a very large quantity so that the thermal resistance ($1/\kappa$) due to electron phonon collisions is very small compared to the experimental values (of the order of several cm sec°c/cals for covalent semiconductors at room temperature) which must therefore be explained in terms of the other phonon scattering mechanisms.

ACKNOWLEDGMENTS

The author wishes to thank Mr. R. P. Chasmar for discussions, Dr. Willis Jackson, F.R.S., M.I.E.E., Director of Research and Education and Mr. B. G. Churcher, M.Sc., M.I.E.E., Manager of the Research Department, Metropolitan-Vickers Electrical Co. Ltd., for permission to publish this letter.

REFERENCES

HAAR, D. TER, and NEAVES, A., 1956, *Advances in Physics*, **5**, 241.
KLEMENS, P. G., 1951, *Proc. Roy. Soc.* **A208**, 108.
MAKINSON, R. E. B., 1938, *Camb. Phil. Soc. Proc.*, **34**, 474.
WILSON, A. H., 1953, *The Theory of Metals* (Cambridge: University Press).
ZIMAN, J. M., 1956, *Phil. Mag.*, **1**, 191 (see also Corrigendum, *Phil. Mag.*, **2**).

REVIEWS OF BOOKS

The Life of Arthur Stanley Eddington. By A. Vibert Douglas. (London and New York : Thomas Nelson & Sons Ltd., 1956.) [Pp. xiv +208.] Price 25*s*.

This admirably written biography gives an account, with a minimum of technicalities, of the work of one of the most distinguished astronomers and astrophysicists of his age and draws a portrait of an attractive personality.

Born in 1882, Eddington entered Trinity College, Cambridge, as a Scholar in 1902 and became a Fellow of the College in 1907. From 1906 to 1913 he was Chief Assistant to the Astronomer Royal at Greenwich, and from 1913 to 1944—the year of his death—Plumian Professor of Astronomy at Cambridge. From 1914 he combined with his Professorship the Directorship of the University Observatory. He was elected to a Fellowship of the Royal Society in 1914, was knighted in 1930 and was awarded the O.M. in 1938.

His first original work was on the motion and distribution of stars, and in 1914 he published his book entitled " Stellar Movements and the Structure of the Universe ".

Shortly after this, Eddington was " led to make a close scrutiny " of Einstein's theory of relativity ; the results of this study were published in a " Report on the Relativity Theory of Gravitation " (1918). This was followed five years later by his " great, now classical, exposition ", " The Mathematical Theory of Relativity ".

His skill as a practical astronomer and his grasp of the principles of relativity made inevitable his inclusion among the team of observers sent to Sobral and Principe for the solar eclipse of 1919. One of the objects of the expedition was to test the Einstein theory of the gravitational deflection of light, the Einstein value of the deflection being double that calculated on the classical theory. Mr. Douglas tells the story with a keen sense of drama :

" In Dyson's study at Greenwich on the last evening before sailing, he and Eddington were discussing the amount of deflection calculated on the classical Newtonian theory and the Einstein value, about twice as great, which Eddington fully expected to obtain. Cottingham who was to accompany Eddington asked ' What will it mean if we get double the Einstein deflection ? ' to which Sir Frank replied ' Then Eddington will go mad and you will have to come home alone '. Three months later at Principe, when he had made his first plate reduction, Eddington turned to his companion with the words, ' Cottingham, you won't have to go home alone '."

From relativity Eddington returned to stellar physics. His book on the " Internal Constitution of the Stars " was published in 1926 and, says Mr. Douglas, " immediately became and has remained the standard treatise on this new field of astrophysics which he himself had so largely opened up and developed ".

During the last years of his life Eddington occupied himself with the preparation of a work on " Fundamental Theory ", left unfinished at his death. Here he brought together relativity and quantum theory—and especially Dirac's work in the latter field—and endeavoured to derive from theoretical premises numerical values for the natural constants. Of this work, full of mathematical and other difficulties, Douglas remarks that while most physicists have " dismissed it from serious consideration ", others have found in it starting points for further researches. " Unfinished it stands as a challenge to future manipulators of the mathematical symbolism of physics . . .".

A bibliography lists 13 books written by Eddington and nearly 160 papers communicated to learned societies and other publications. C.F.M.

Thermal Power from Nuclear Reactors. By A. S. THOMPSON and O. E. RODGERS. (Chapman and Hall.) Price $7.25.

THE authors of this new book state that their main object is to present an analysis of the engineering of nuclear reactors, with special emphasis on the thermal aspects of reactor design. This is undoubtedly an aim to be recommended, since though there are now many excellent books on nuclear reactor science, there has long been a need for an adequate work dealing with the special problems of heat transfer and heat removal.

The first two chapters are presented as an introduction to the required reactor physics and reactor theory, and give such background as is necessary for an understanding of the principles involved in the nuclear physics design of reactors. The interactions of the elementary particles, diffusion theory and the calculation of critical mass are discussed, and a particularly interesting treatment of the numerical solution of the reactor equations is also presented. In the following chapter an excellent analysis is given of reactor kinetics, in which the interdependence of reactor power and temperature, through the temperature coefficients, is well brought out. The authors show that a satisfactory solution to such problems is equally dependent on an adequate calculation of component temperature variations and neutron flux changes.

After rather brief treatment of reactor shielding problems and desirable reactor material properties, the remainder of the book is devoted to thermal aspects of reactor design. This part opens with a most useful chapter dealing with thermal stress problems which arise in reactor design. This is a subject rather neglected in previous reactor engineering text books, and it is pleasing to see the authors developing working theories and showing how they may be applied in various examples. Certain heat conduction solutions are also given in this section, as being necessary for calculation of the temperature distributions giving rise to thermal stress. In following chapters the calculation of pressure losses, the working heat transfer correlations and boiling heat transfer are dealt with. It is felt that some discussion on the necessity for considering compressible flow with gas cooling and with heat addition could usefully have been added, and also that the conditions for application of the heat transfer correlations should have been made clearer and emphasised. There is now considerable information available on boiling heat transfer and although it is a rather specialised topic, more of this might perhaps have been usefully included.

The book concludes with a chapter on thermal power cycles giving the fundamentals of both steam and gas turbine cycle analysis.

Considering the book as a whole, it is felt that it should be a very useful introduction to the special problems of reactor engineering, especially to those working in other engineering fields who would like a link up with their well established practices.

D.V.W.

[*The Editors do not hold themselves responsible for the views expressed by their correspondents.*]

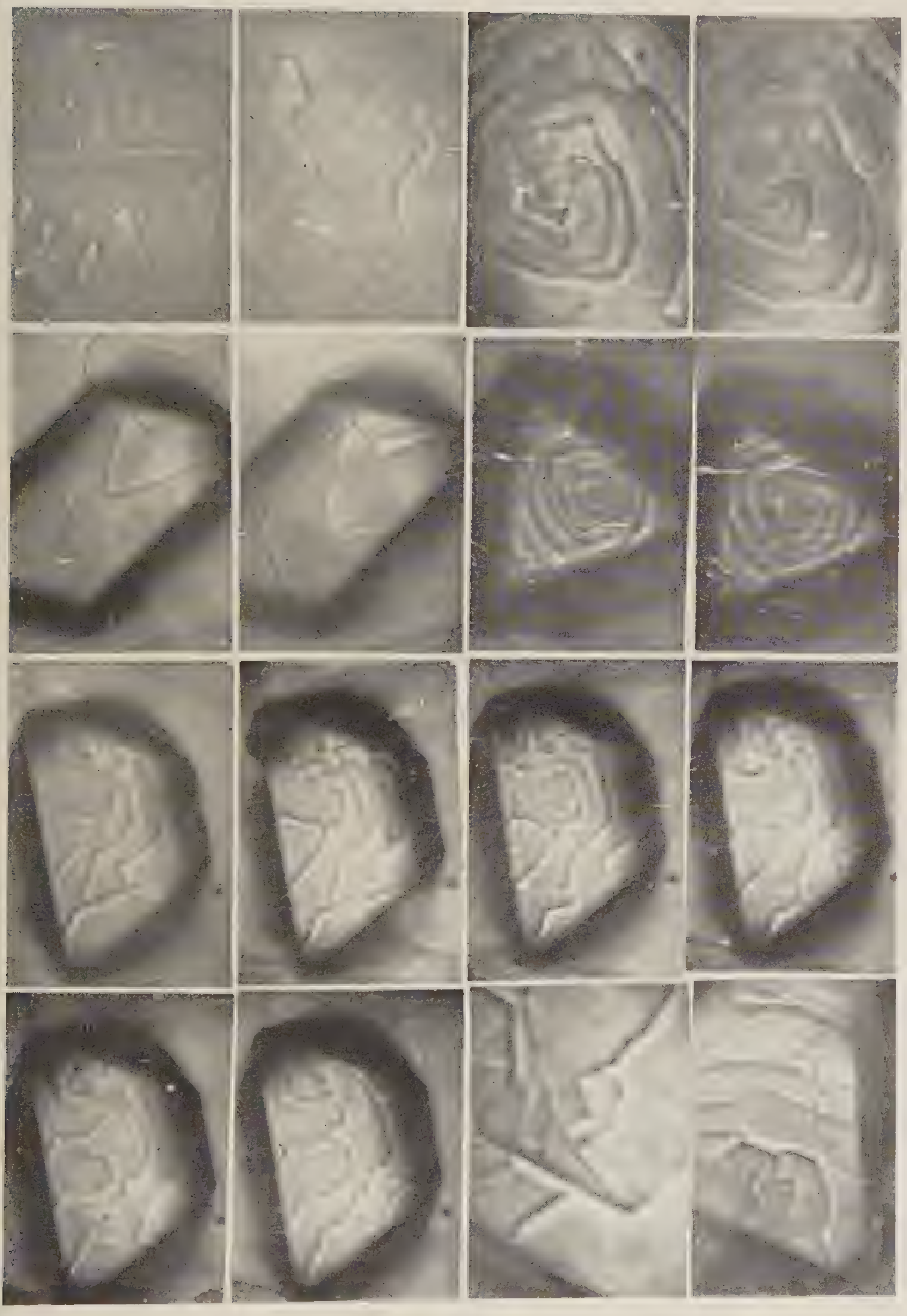

First row : Figs. 1, 2, 3, 4.
Second row : Figs. 5, 6, 7, 8.
Third row : Figs. 9, 10, 11, 12.
Fourth row : Figs. 13, 14, 15, 16.

Order of magnification given in the text.

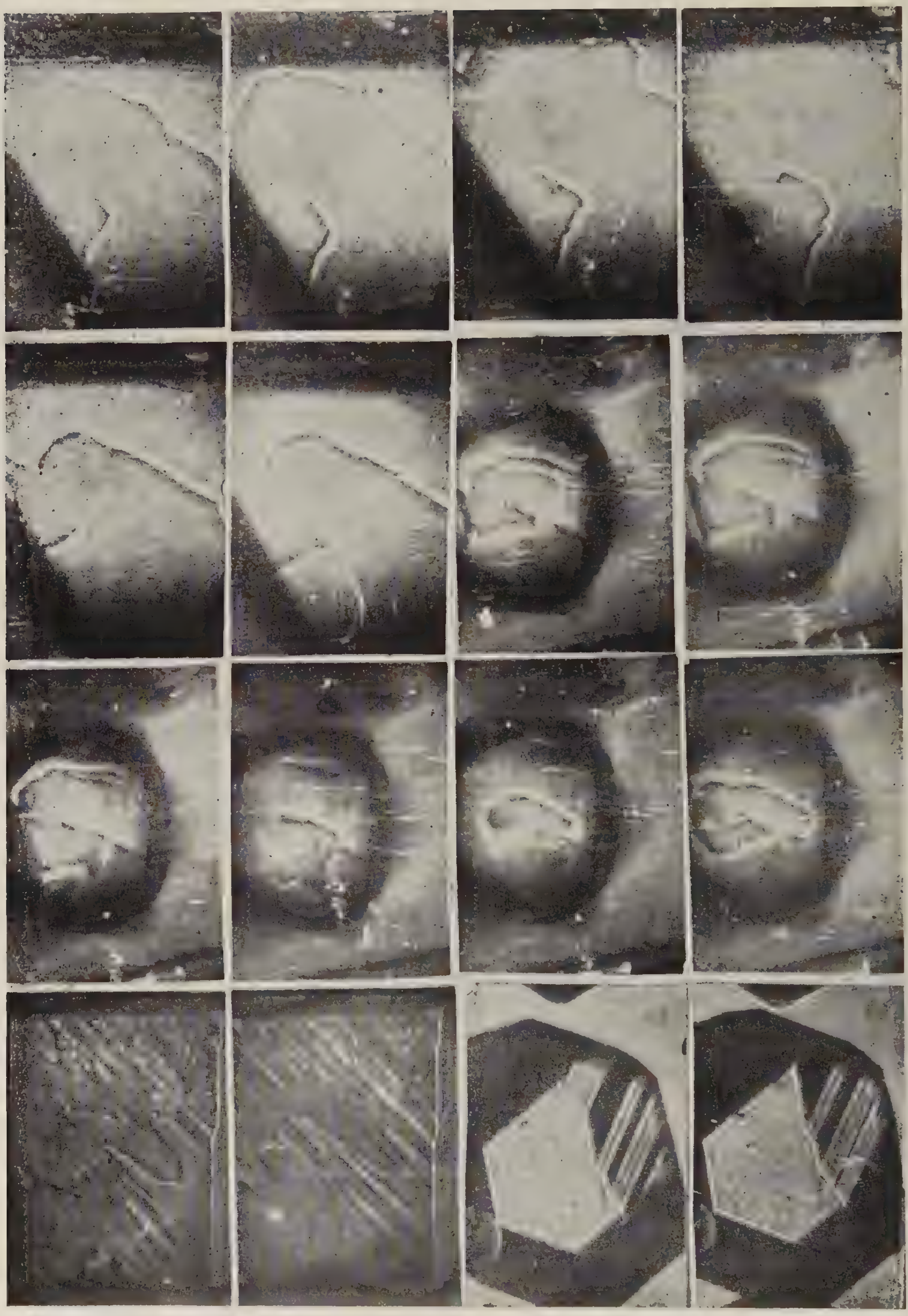

First row: Figs. 17, 18, 19, 20.
Second row: Figs. 21, 22, 23, 24.
Third row: Figs. 25, 26, 27, 28.
Fourth row: Figs. 29, 30, 31, 32.

Order of magnification given in the text.

Fig. 5

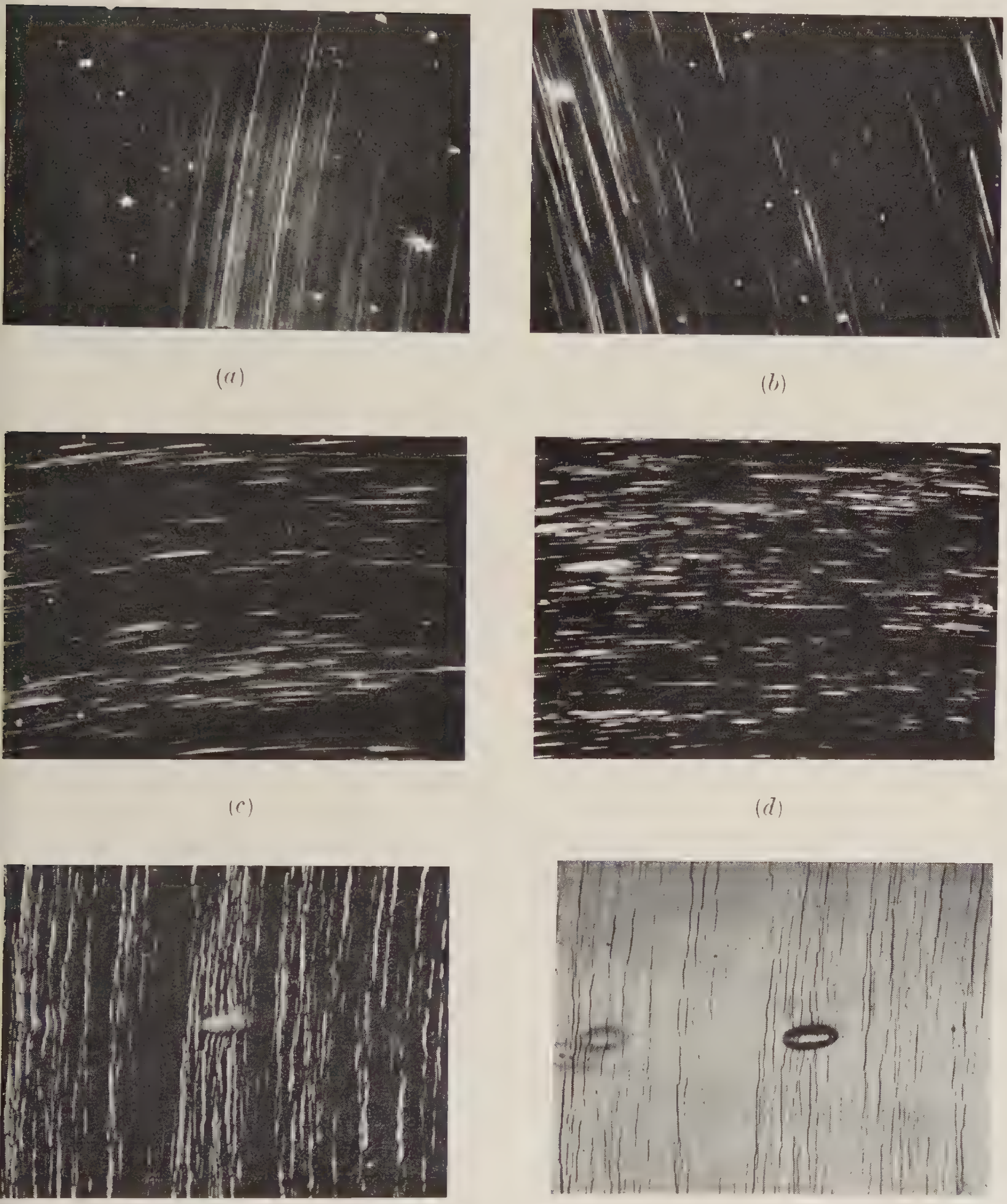

(*a*) (*b*)

(*c*) (*d*)

(*e*) (*f*)

Slip-lines on a copper crystal deformed at room temperature by additional shear strains $\Delta\epsilon=0{\cdot}05$ after various prestrains ϵ. (*a*) prestrain $\epsilon=0$; (*b*) $\epsilon=0{\cdot}1$; (*c*) $\epsilon=0{\cdot}2$; (*d*) $\epsilon=0{\cdot}3$; (*e*) $\epsilon=0{\cdot}6$; (*f*) $\epsilon=0{\cdot}6$ (*a–e*) dark field illumination; (*f*) bright field illumination, same site as (*e*). All photographs ×225.

Fig. 9

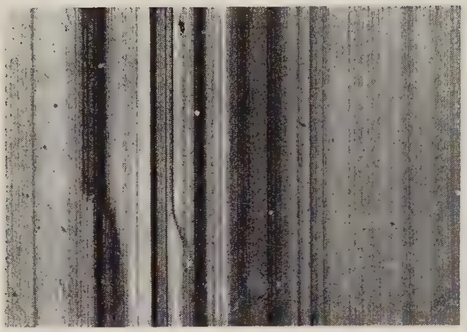

Slip markings on the top surface of an aluminium crystal deformed at room temperature showing a typical slip band.
Shear strain $\epsilon=0{\cdot}3$. Electron micrograph ×7500.

Fig. 10

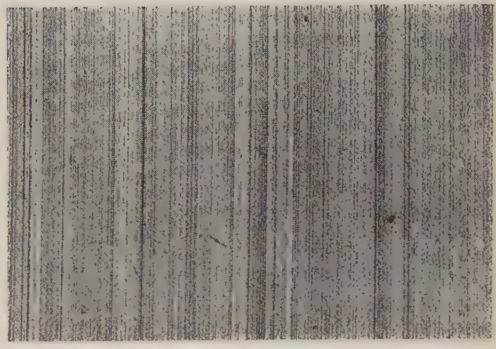

Slip markings on the top surface of a copper crystal deformed at room temperature. No clustering of slip-lines into bands. Shear strain $\epsilon=0{\cdot}3$. Electron micrograph ×7500.

Fig. 11

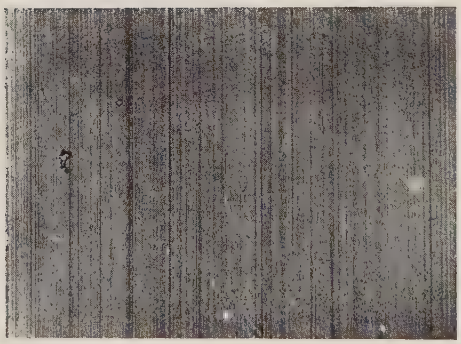

Slip line pattern of an aluminium crystal deformed at 90°K in stage II. Prestrained up to a flow-stress $\tau=0{\cdot}5$ kp/mm^2, polished, strained in addition up to a flow-stress $\tau=1{\cdot}3$ kp/mm^2 corresponding to a strain increment $\Delta\epsilon=0{\cdot}07$. Electron micrograph × 7500.

Fig. 12

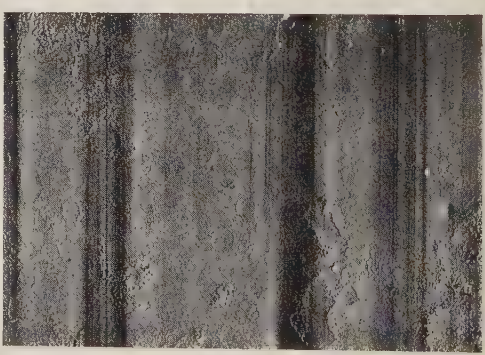

Clustering of slip lines into bands on an aluminium crystal deformed at 90°K in stage III. Prestrained $\epsilon=0{\cdot}3$, polished, and strained in addition by $\Delta\epsilon=0{\cdot}10$. Electron micrograph × 7500.

Fig. 13

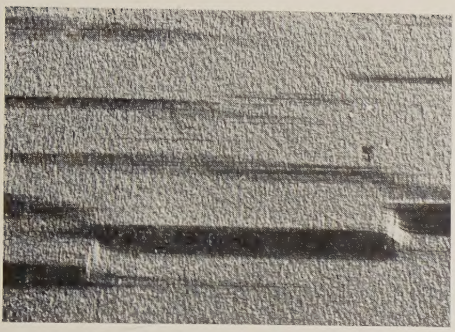

Fig. 14

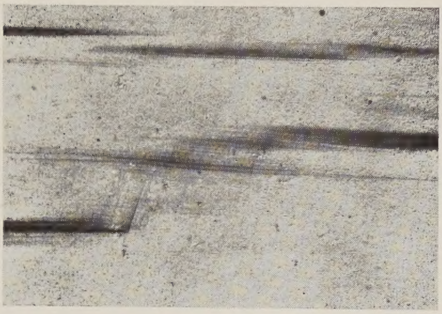

Fig. 15

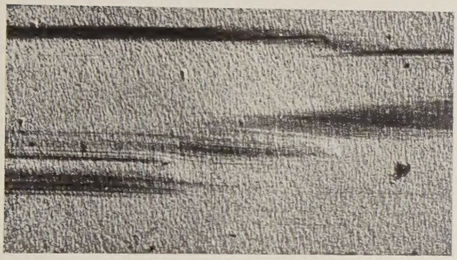

Fig. 16

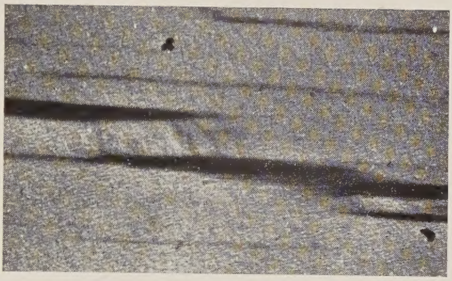

Electron micrographs of fragmented slip-bands on the surface of a copper crystal prestrained $\epsilon=0{\cdot}6$ at room-temperature. Additional strain after polishing $\Delta\epsilon=0{\cdot}05$, ×9000. Same crystal as figs. 5 (*e*) and (*f*).

Fig. 18

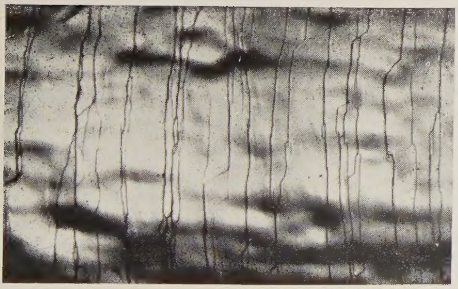

Aluminium crystal, prestrained at 90°K $\epsilon=0{\cdot}35$, polished, and work-softened at room temperature. Bright field illumination, ×90.

Fig. 19

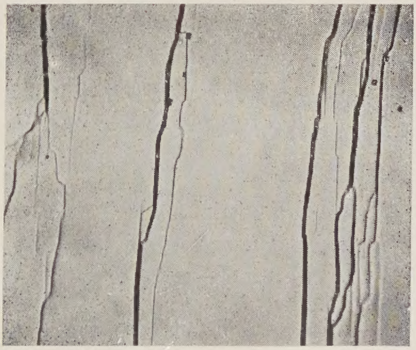

Same site as fig. 18, ×345.

Fig. 20

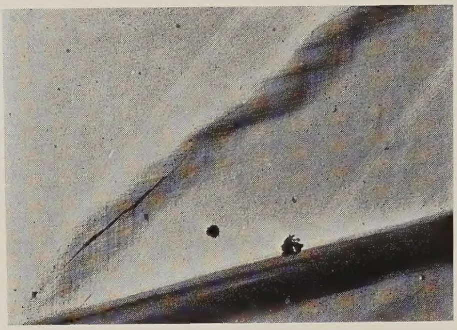

Same crystal as figs. 18 and 19, electron micrograph, ×5000.

Fig. 21

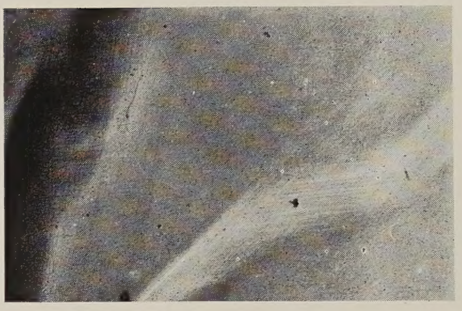

Same crystal as figs. 18, 19, 20, showing traces of the primary slip plane, the conjugate slip plane, and the cross slip plane, ×5000.

Fig. 22

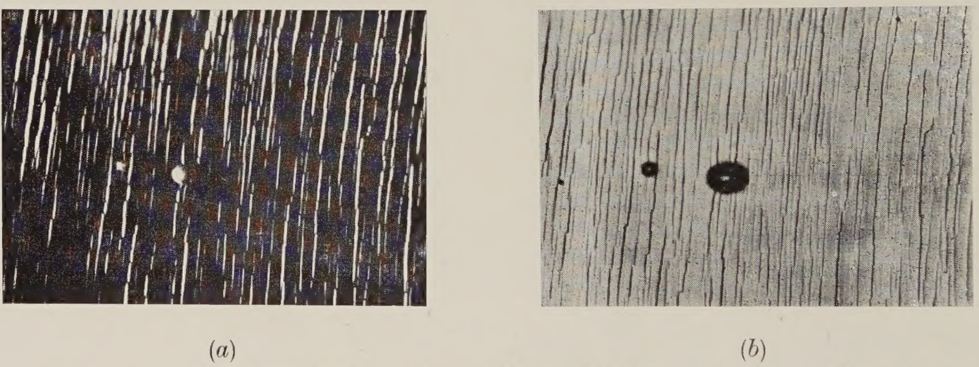

(*a*) (*b*)

Copper crystal, prestrained $\epsilon=0\cdot6$ at 90°K, polished, and work-softened at 300°C, ×200. (*a*) Dark field illumination ; (*b*) Same site in bright field illumination.

Fig. 23

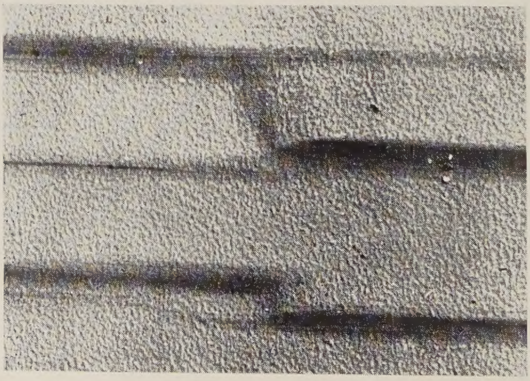

Same crystal as fig. 22, electron micrograph, ×8000.

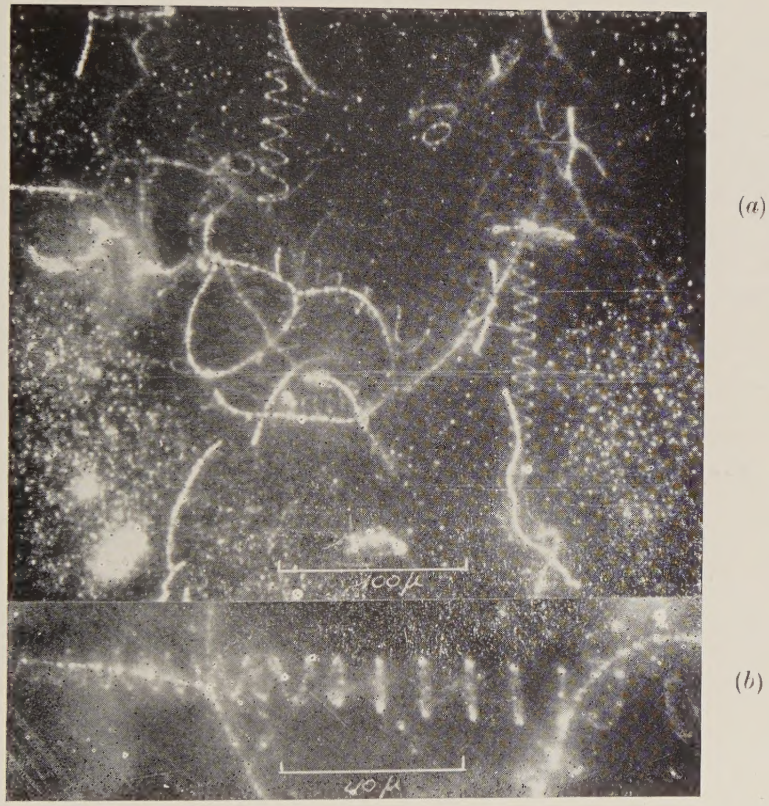

(*a*) General view of helical dislocations.
(*b*) Helical dislocation with closed loops.